COLLAGEN HYDROGELS FOR REGENERATIVE MEDICINE

JUSTINA PUPKAITE

Thesis submitted to

the University of Ottawa

in partial fulfillment of the requirements for the
PhD degree in Cellular and Molecular Medicine

and

Linköping University

in partial fulfillment of the requirements for the
PhD degree in Medical Science

as part of a cotutelle doctoral program

Department of Cellular and Molecular Medicine
Faculty of Medicine
University of Ottawa

Department of Clinical and Experimental Medicine
Linköping University

Table of Contents

Abstract

The need for regenerative therapies to repair damaged or deteriorated organs and tissues, such as heart, skin, and cornea, is rising due to donor shortage and aging of the world's population. Many proposed regenerative therapeutic approaches include a combination of cells, bioactive compounds, and hydrogels. Although collagen hydrogels have shown a lot of promise in regenerative medicine research, there are still challenges in their design and application strategies. Therefore, this thesis describes the development of novel collagen hydrogel designs for improved use in tissue bonding, cell delivery, and myocardial infarction therapy applications.

Firstly, a visible-light crosslinked collagen hydrogel for tissue photobonding was developed. Methacrylated collagen hydrogel was crosslinked using the photoinitiator rose Bengal and visible light. The properties of the resulting hydrogel were tunable by changing the hydrogel composition. Biomimetic and *ex vivo* skin models were used to demonstrate the ability of the hydrogel to bond tissues whose edges are separated. Additionally, using the hydrogel led to less scarring compared to traditional sutures in a mouse skin incision model.

Secondly, collagen was modified with thiol groups to design a hydrogel crosslinked using the thiol-Michael addition click reaction for cell encapsulation and delivery. The hydrogels demonstrated excellent shear-thinning and self-healing properties, allowing for injection after the crosslinking was complete. Additionally, the hydrogels showed minimal swelling and maintained their shape in an aqueous buffer for a prolonged period. Cell encapsulation and delivery using the hydrogels was demonstrated *in vitro* with mesenchymal stromal cells and endothelial cells.

Thirdly, recombinant human collagen III hydrogels were prepared by crosslinking the collagen with EDC and NHS. The hydrogels contained either 1% or 2% collagen. Therapeutic strategies for these hydrogels were investigated, including the timing and dosage of the

treatment, in a mouse MI model. Comparing 1% hydrogel injection at a single early time point (3 h) and three time points (3 h, 7 and 14 days) post-MI revealed improved cardiac function, reduced scar size and inflammation, and increased vascularization in the single injection group. Additionally, increasing the collagen III dose to 2% in the hydrogel at a single early time point (3 h) injection did not confer any additional functional improvement compared to 1% and resulted in scar size and vascular density comparable to control (PBS injection).

In summary, this work contributes to the development of collagen hydrogel therapies for regenerative medicine by presenting a visible-light crosslinked collagen hydrogel for tissue bonding, a novel click-crosslinked collagen hydrogel with excellent shear-thinning properties for cell delivery, and the use of a recombinant human collagen III hydrogel in post-MI therapy, highlighting the importance of optimizing the timing and dosage of biomaterial therapies.

List of Publications and Contribution Statement

This thesis is based on the following papers, referred to in the text by their roman numerals. My contributions and those of my co-authors are specified below for each manuscript. I am the sole author of this thesis. My supervisor Dr. Erik Suuronen provided guidance and feedback throughout the writing process.

I **Justina Pupkaite**, Manuel Ahumada, Sarah McLaughlin, Maha Temkit, Sura Alaziz, Richard Seymour, Marc Ruel, Irene Kochevar, May Griffith, Erik J. Suuronen, Emilio I. Alarcon

Collagen-based photoactive agent for tissue bonding

ACS Appl. Matter. Interfaces, 9, 9265–9270 (2017)

Dr. Erik Suuronen and Dr. Emilio Alarcon developed the concept and provided guidance and supervision throughout the work. I developed and tested the hydrogel formulations (absorbance, mechanical properties, degradation, swelling, and thermal stability tests), with help from Dr. Manuel Ahumada and Maha Temkit. All animal procedures were approved by the University of Ottawa Animal Care Committee (protocol number HI-2714-R2 A1) and were performed by Richard Seymour. Sarah McLaughlin and Sura Alaziz carried out histological data collection and analysis. Dr. Marc Ruel, Dr. Irene Kochevar, and Dr. May Griffith provided scientific and clinical input and feedback. The manuscript was written through contributions of all authors.

II **Justina Pupkaite**, Jenny Rosenquist, Jöns Hilborn, Ayan Samanta

Injectable shape-holding collagen hydrogel for cell encapsulation and delivery crosslinked using thiol-Michael addition click reaction

Biomacromolecules, 20, 3475–3484 (2019)

Dr. Ayan Samanta and I conceived the idea for the paper and designed the experiments. While being trained by Dr. Samanta I performed the initial material synthesis and characterization and subsequently I carried out the material synthesis, characterization, and *in vitro* tests and analysis, with the exception of long-term swelling, long-term self-healing tests, time-sweep rheology, and part of shear-thinning tests (which were performed by Jenny Rosenquist). I wrote the initial draft of the methods, results, discussion, and conclusion and contributed to the introduction and editing of the whole manuscript, which was done through contributions of all authors. Dr. Jöns Hilborn provided scientific input and guidance.

III **Justina Pupkaite***, Veronika Sedlakova*, Cagla Eren Cimenci, Marc Ruel, Emilio I. Alarcon, Erik J. Suuronen

Effect of dose and timing of delivery in human recombinant collagen III hydrogel therapy for treating myocardial infarction

Manuscript

*Authors contributed equally

The idea and experimental plan was developed by Dr. Suuronen, Dr. Alarcon, Dr. Veronika Sedlakova, and me. All animal procedures were approved by the University of Ottawa Animal Care Committee (protocol number HI-2039-R4 A2). Dr. Sedlakova optimized and prepared the biomaterial for the animal experiments. I performed the intramyocardial injections, the collection and analysis of echocardiography data, with assistance from Dr. Sedlakova and Cagla Eren Cimenci, except cardiac strain analysis which was carried out by Dr. Sedlakova. Tissue harvest was performed by Dr. Sedlakova, Ms. Eren Cimenci, and me. I performed the Masson's

Trichrome staining and data analysis with guidance by Ms. Eren Cimenci. Dr. Sedlakova and I performed the immunohistochemical staining and data analysis. I performed the statistical analysis of all the data. Dr. Suuronen, Dr. Alarcon, and Dr. Marc Ruel provided guidance and input throughout the work. Dr. Sedlakova and I wrote the initial manuscript, which was edited through contributions of all authors.

Additional publications that are not included in this thesis:

Christopher D. McTiernan, **Justina Pupkaite**, Irene E. Kochevar, Erik J. Suuronen, Emilio I. Alarcon

Recent advances in the design of light-activated tissue repair

Photochemistry 46 (eds S. Protti and A. Albini), 265–280 (Royal Society of Chemistry) (2019)

Jenny Rosenquist, **Justina Pupkaite**, Jöns Hilborn, Ayan Samanta

Injectable self-healing collagen hydrogel using covalent crosslinking – a click approach

Manuscript

Acknowledgements

I want to thank my co-supervisor Dr. May Griffith for the opportunity to undertake a PhD in a cotutelle program and carry out my work in Canada and Sweden. I am also grateful to my co-supervisor Dr. Peter Påhlsson for his help in the final stages of my studies. And most of all, I would like to thank my supervisor Dr. Erik Suuronen for his guidance throughout.

I would also like to gratefully acknowledge my Thesis Advisory Committee members: Dr. Emilio Alarcon, Dr. Darryl Davis, and Dr. Maxwell Hincke.

I am grateful to the members, past and present, of the BEaTS research group at the University of Ottawa Heart Institute, especially Cagla Eren Cimenci, Dr. Veronika Sedlakova, Danielle Giroux, and Madison Bak for excellent team work and friendship.

I would also like to thank the Polymer Chemistry Department at Uppsala University who graciously hosted me while I worked on Paper II. I would like to thank Dr. Jöns Hilborn for his mentorship and guidance. I am especially grateful to Dr. Ayan Samanta for his support, friendship, and training in organic chemistry.

Finally, I would like to thank everyone who provided moral and emotional support during my studies, especially my parents Zita and Kestutis, Dr. Egle Jakubaviciute, Tanja Kosenko, Dr. Julija Lasinskaite, and Dr. Samantha Sarkar.

List of Figures

List of Tables

List of Schemes

List of Abbreviations

BDDGE – 4-Butanediol diglycidyl ether

BMSC – bone marrow stromal cell

BS – breaking strain

CAC – circulating angiogenic cell

Cryo-SEM – scanning electron cryo-microscopy

CS – chondroitin sulfate

DC – direct current

DSC – differential scanning calorimetry

DTNB – 5,5′-Dithiobis(2-nitrobenzoic acid)

ECM – extracellular matrix

EDC – 1-ethyl-3-(3-dimethylaminopropyl) carbodiimide

FT-IR – Fourier Transform-Infrared

G′ – storage modulus

G″ – loss modulus

GAG – glycosaminoglycan

GFOGER – glycine-phenylalanine-hydroxyproline-glycine-glutamic acid-arginine

H&E – hematoxylin & eosin stain

HA – hyaluronic acid

HUVEC – human umbilical vein endothelial cell

IKVAV – isoleucine-lysine-valine-alanine-valine

IR – infrared

LAD – left anterior descending coronary artery

LED – light emitting diode

LVEDV – left ventricular end-diastolic volume

LVEF – left ventricular ejection fraction

LVESV – left ventricular end-systolic volume

LVR – linear viscoelastic region

MAA – methacryl-anhydride

MC – methacrylated collagen

MI – myocardial infarction

MMP – matrix metalloproteinase

MSC – mesenchymal stem cell

NHS – N-hydroxysuccinimide

NIPAAm – poly(N-isopropylacrylamide)

NMR – nuclear magnetic resonance

PBS – phosphate buffered saline

PEG – polyethylene glycol

PFA – paraformaldehyde

PLL – poly-L-lysine

PVA – polyvinyl alcohol

RB – rose Bengal

RGD – arginine-glycine-asparagine

rHCIII – recombinant human collagen type III

ROS – reactive oxygen species

SD – standard deviation

SEM – standard error of the mean

UV – ultraviolet

YM – Young's modulus

α-SMA – α smooth muscle actin

1 General Introduction

1.1 Preface

Progress in biomedical research over the years has found successful treatments for many conditions, diseases, and types of trauma. However, many challenges remain, and new ones arise as the world's population ages. Many of these challenges concern the need to repair or replace organs and tissues damaged by trauma, disease, or deteriorated by age. For example, surgical methods are used to repair spinal traumas, but damage to the neural tissue of the spinal cord is generally permanent because the connections between nerve cells are not regenerated. Often, the only way to help patients whose corneas were damaged by trauma or disease is to replace them, but there are not enough donor corneas available. After myocardial infarction (MI), different types of interventions may be used to restore blood flow supplying the myocardium, but the heart may still not recover and deteriorate to heart failure.

To solve these problems, extensive research efforts are devoted in the fields of regenerative medicine and tissue engineering. Strategies involving various combinations of cells, biomaterials, and bioactive molecules are being investigated to induce or augment tissue repair and regeneration. Therapeutic cells may be expected to integrate into the damaged tissue, thus helping repair it, or to exert paracrine effects that induce reparative responses in endogenous cells. Similarly, bioactive molecules are meant to activate regenerative processes. Biomaterials may provide adhesion sites for therapeutic and endogenous cells, sustained release of bioactive molecules, and may also have a signaling role themselves.

In light of these challenging problems and the different approaches to solving them, the focus of this thesis is the development of collagen hydrogels for cardiovascular applications, as cardiovascular disease is a rising problem in the aging population and is one of the main causes

of death worldwide. Collagen was chosen because it has shown promise as a biomaterial in regenerative medicine, but collagen hydrogel design and application strategies require further investigation and improvement in areas such as cell-friendly crosslinking methods, tunable mechanical properties, and injectability, to enhance their performance in regenerative applications. The work presented in this thesis proposes possible solutions to these challenges.

1.2 Hydrogel Design for Regenerative Medicine

Hydrogels are a natural choice for many regenerative medicine applications due to their crosslinked 3D network structure, which may contain up to 98% water, mimicking the native extracellular matrix (ECM). As such, hydrogels are being developed for cell and drug delivery or to use as bioactive agents facilitating healing and tissue regeneration after trauma or disease. There are hydrogel designs reported for the treatment of trauma and diseases of the cardiovascular system, the nervous system, cartilage, bone, skin, and cornea, to name a few[1–5].

When developing a therapeutic hydrogel for regenerative medicine applications, several aspects should be considered. In particular, the choice of polymer, crosslinking method, physical and biological properties of the hydrogel, and their characterization should be factored in with regard to the intended application (Figure 1.1). Fortunately, the concept of a hydrogel allows for great flexibility in designing a material that fits the requirements for a particular application. Hydrogels may be prepared using synthetic or natural polymers, or a combination of both. The crosslinked 3D network may be created using different chemical reactions or physical interactions. As each material and crosslinking method possesses characteristics that may be advantageous or disadvantageous depending on the intended application, a universal hydrogel design is likely not possible; rather it needs to be tailored to each specific biomedical situation.

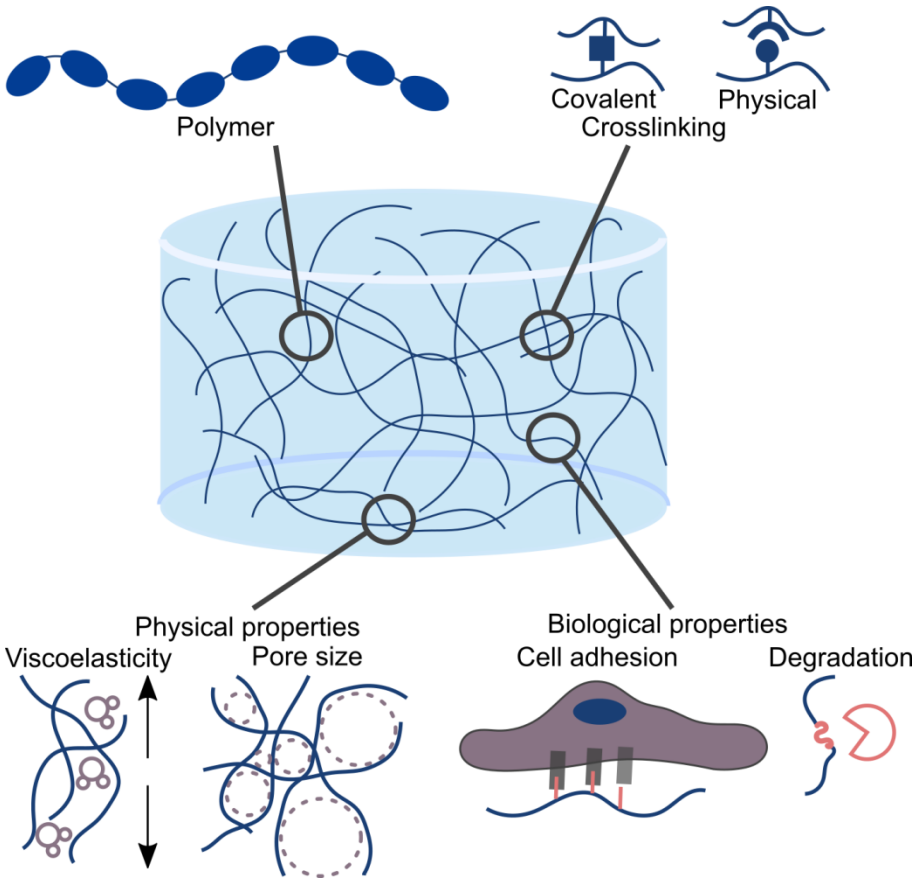

Figure 1.1. Key factors to consider in the design of hydrogels for biomedical applications.

1.2.1 Materials: Natural versus Synthetic Polymers

Since natural and synthetic polymers possess such distinctive properties, either type may be optimal, depending on the requirements for the hydrogel design. Sometimes a combination of both types of polymers can help capture the desired qualities of both while reducing the drawbacks.

Synthetic polymers, such as polyethylene glycol (PEG), polyvinyl alcohol (PVA), polyacrylamide, and polyacrylic acid, have simple repeating units, controlled architecture, are reliably reproducible, and can be easily synthesized with different functional groups allowing for different crosslinking methods[6–8]. Additionally, synthetic polymer hydrogels have a wide range of achievable mechanical properties. However, in general, synthetic polymers have low innate biodegradability, i.e., they are very slowly degraded inside the body. Therefore, if degradation is desired, the hydrogel design needs to incorporate components that can be cleaved by enzymes, hydrolysis, or other means, such as matrix metalloproteinase (MMP)-cleavable peptide sequences[9] and ester bonds[8,10]. Furthermore, toxicity and immune response to synthetic materials and their degradation products is also a concern. For example, polylactic acid is degraded via hydrolytic, enzymatic, and oxidative mechanisms releasing lactic acid, which reduces pH, causes inflammation, and may damage the surrounding tissue, although these processes can be ameliorated through different chemical modifications and additional components incorporated into the hydrogel[11]. Importantly, synthetic polymers intrinsically do not possess adhesive ligands or enzyme-cleavable domains, unless they are composed of or incorporate synthetic peptides[6]. On the one hand, this is a significant drawback if cell attachment and tissue integration is the goal. On the other hand, this may also be an opportunity to incorporate only the desired amount of specific peptide or enzyme-cleavable sequences via chemical modification. However, this

introduces an added level of complexity in the hydrogel preparation but still fails to recapitulate the full complexity of a protein molecule. Nonetheless, in some cases, such design may be the optimal compromise between the advantages of synthetic polymer hydrogels and biological activity required. For instance, a hydrogel containing arginine-glycine-asparagine (RGD)-PEG and matrix metalloproteinase (MMP)-cleavable PEG was used to guide vascular sprouting[12]. In another report, MMP-cleavable PEG was injected into the heart after MI, leading to improved function, which was further enhanced by the co-delivery of a pro-angiogenic factor and therapeutic cells with the hydrogel[13].

Natural polymers commonly used for hydrogel preparation can be divided into two categories: proteins (collagen[14], fibrin[15], etc.) and polysaccharides (hyaluronic acid [HA][16], alginate[17], chitosan[18], etc.). Since they are present in the natural ECM of different tissues and organs, these polymers are more suitable to mimic the structural and biological properties of ECM required in regenerative medicine applications, compared to synthetic polymers. Proteins generally have cell adhesion sites, whereas polysaccharides typically do not (although some cells express CD44, a transmembrane protein that binds to HA[19]). Two of the major drawbacks of natural polymers as biomaterials are their narrow range of mechanical properties and the challenges they pose in handling and chemical modification. Additionally, even though natural polymers have been well established for use in regenerative medicine, the use of xenogeneic materials may raise host response concerns[20]. However, while any type of foreign material introduced into the body may elicit a response, the quality of this reaction determines whether the outcome is negative (such as fibrous capsule formation[21]) or positive (improved regeneration of treated tissue[22,23]).

Many natural polymers in their native state form hydrogels via non-covalent interactions at mild conditions, for example, collagen and fibrin through protein-protein interactions[15,24], alginate through interaction with calcium ions[17], which generally result in hydrogels with lower elastic or storage modulus than covalently crosslinked materials but allow for simple hydrogel preparation procedures under physiological conditions. However, some natural polymers, such as HA, chitosan, and collagen, also contain free amine or hydroxyl functional groups that can participate in a number of chemical reactions. These reactions can be used to crosslink the molecules covalently or to modify the molecules with different functional groups. For example, one of the most established collagen and gelatin modifications is methacrylation[25,26]. Methacrylated collagen II, crosslinked through a photoinitiated reaction, has been used in cartilage tissue engineering applications[27]. In recent years, different HA modifications, such as furan and cyclooctyne, have been reported and used in hydrogel formation through bio-orthogonal click reactions with multi-arm PEG-maleimide[28] and PEG-azide[29], respectively.

The advantageous characteristics of both synthetic and natural polymer hydrogels are often combined through the mixing of both types of materials in one hydrogel design (composite hydrogels[30]). The synthetic component may help achieve desired physical characteristics and slower degradation, while the natural polymer conveys the bioactive effect. For example, a hydrogel composed of collagen, PEG, and PVA showed improved mechanical properties, gelation characteristics and stabilized the system during freeze-drying[31]. Chitosan and difunctional dibenzaldehyde-PEG were used to prepare a self-healing hydrogel crosslinked through Schiff base formation under mild conditions which showed promise as a treatment for nerve tissue repair[32].

1.2.2 Crosslinking Methods

The method of crosslinking is another way to manipulate the properties of the resulting hydrogel. Hydrogel networks may be formed via physical interactions or chemical (covalent) bonds. As mentioned in the previous section, physical hydrogels tend to have weaker mechanical properties, although due to the transient nature of physical bonds they are more dynamic and may be easier to prepare under physiological conditions with fewer toxicity concerns. Polymer networks in physical hydrogels may be formed via hydrogen bonds, hydrophobic association, and other physical interactions[33,34].

Compared to physical hydrogels, covalent crosslinking can generally achieve more stable hydrogels with better mechanical properties. In the case of natural polymers crosslinked this way, it may also be hypothesized that the additional covalent bonds, not found in native polymers, will slow their enzymatic degradation because such bonds would likely not be recognized by enzyme active sites. Although chemical crosslinks may be formed via amino acids that are part of cell-adhesive domains, reducing cell-hydrogel interaction[35], depending on the application, this may be an acceptable loss in preparing a more stable hydrogel. There exists a variety of methods to produce covalently crosslinked hydrogels, such as chemical-initiator-mediated reactions, photo-crosslinking, and click chemistry.

Chemical initiators are commonly used to crosslink natural polymers, such as collagen, which contain carboxyl or amine groups. Historically, dialdehydes, namely glutaraldehyde, have been used to crosslink decellularized xenogeneic tissue scaffolds for use as bioprostheses, such as in valve replacement[36]. However, glutaraldehyde is cytotoxic, and its removal may be challenging and, if not achieved completely, may lead to cytotoxicity and detrimental host response to the biomaterial[37–39]. Another type of commonly used chemical initiators are

carbodiimides, such as 1-ethyl-3-(3-dimethylaminopropyl) carbodiimide (EDC, often used in conjunction with N-hydroxysuccinimide [NHS]), which crosslink carboxyl groups with amine groups, thus making this a convenient method to crosslink polymers containing both of these functional groups[40]. Chemical crosslinkers often present toxicity concerns, and there are reports of the toxic effects of EDC through DNA damage *in vitro*[41]. However, hydrogel crosslinking using EDC and NHS is generally considered to be safe because EDC and NHS molecules themselves are not incorporated in the crosslinks and are hydrolyzed and washed out[40,42]. Collagen hydrogels crosslinked using this method have been used *in vitro* and *in vivo*, and no significant cytotoxicity was observed[43–45].

Photo-crosslinking may be achieved in a few different ways, including non-specific crosslinking of proteins in the presence of photo-initiator[46,47] and activation of functional groups, such as methacrylate, thiol, and norbornene, with or without a photo-initiator[48–50]. Although ultraviolet (UV) light has been commonly used, it has very low tissue penetration depth and is known to damage DNA and proteins, prompting the development of visible- and infrared (IR)-spectrum activated alternatives that would overcome these issues. The alternative approaches include compounds such as rose Bengal (RB)[46,47], eosin[50], upconversion nanoparticles[51], and multi-photon excitation strategies[52]. Importantly, photo-crosslinking offers control over the hydrogel formation both in time and space as long as the hydrogel is protected from light.

Click chemistry reactions have gained a lot of interest in search of biocompatible crosslinking methods since they are defined as selective reactions that can be performed under mild aqueous conditions and without the generation of undesirable by-products[53]. Additionally, click reactions may be quite slow compared to the other covalent crosslinking methods described since they can take hours to completely crosslink the hydrogels, giving more time to manipulate

the hydrogel before crosslinking is complete[54]. Although many different click reactions have been reported, for hydrogel design a few types are commonly used, such as azide-alkyne cycloaddition, Diels-Alder, thiol-ene, and thiol-Michael addition reaction[55,56]. Azide-alkyne cycloaddition may be copper-catalyzed or strain-promoted. Due to concerns regarding possible copper toxicity, the strain-promoted method may be favorable; however, copper also has anti-microbial and osteogenic properties, and collagen scaffolds have been used with success to locally deliver copper and enhance angiogenesis and bone formation in a chick embryo model[57]. A strain-promoted azide-alkyne crosslinking method has been applied in hydrogels for various cell encapsulation and delivery applications, including cartilage tissue regeneration and complex 3D systems for *in vitro* cell studies[58–60]. The thiol-Michael addition reaction is a reaction between a thiol (nucleophile) and an electron-deficient C=C bond (electrophile) in α,β-unsaturated carbonyl compounds, such as maleimides, vinyl sulfones, and acrylates[61]. It is important to note that the high reactivity of thiol groups and the presence of thiol groups in proteins may compromise the bio-orthogonal characteristic of thiol-Michael addition reaction[54,61]. However, manipulating the reactivity of the hydrogel components may help increase the selectivity and, consequently, the bio-orthogonal character of this reaction[61,62]. Hydrogel crosslinking using thiol-Michael addition in the presence of proteins and cells has been demonstrated, preserving encapsulated protein activity, cell viability, and stem cell differentiation potential[63–67].

1.2.3 Hydrogel Characteristics for Biomedical Applications

In designing a hydrogel for biomedical use, each specific application requires that the hydrogel possess a certain set of physical and biological properties. Physical properties include

viscoelasticity, shear-thinning, self-healing, and thermal characteristics. From the biological standpoint, the hydrogels need to be non-toxic. In addition, consideration may be needed regarding their biodegradability properties, their ability to provide sufficient space for cells and the appropriate cell attachment sites or other signaling factors in order to elicit the desired biological response (broadly defined as biocompatibility[2,68]) (Figure 1.2).

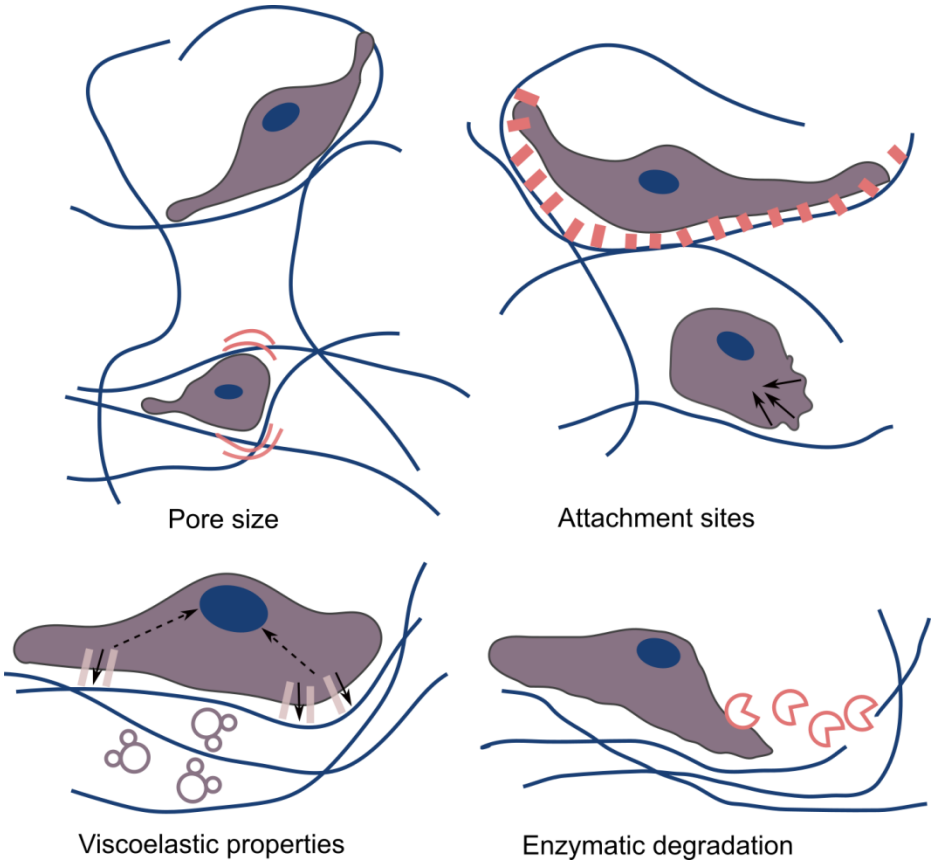

Figure 1.2. Key hydrogel characteristics that affect cell interaction with the material.

It is important to note that the physical properties of the environment affect cell behavior and differentiation. The effects of substrate stiffness have been widely investigated on different cell types in different conditions *in vitro*. For instance, cardiomyocytes were shown to maintain beating on substrates matching the measured stiffness of healthy myocardium, whereas substrates of higher stiffness (matching MI scar) were not able to sustain the beating of the cells[69]. Stem cell behavior on different substrates is of particular interest to regenerative medicine and tissue engineering applications, which often involve the use of stem and progenitor cells in combination with hydrogels. Tuning the elastic modulus of a polyacrylamide hydrogel from low (1 kPa) to medium (10–20 kPa) to high (100 kPa) was shown to guide neurogenic, myogenic, and osteogenic mesenchymal stem cell (MSC) differentiation, respectively[70,71]. In a more specific case, mouse bone marrow $CD34^+$ cells were guided toward endothelial lineage on a substrate whose stiffness corresponded to that of the myocardium 1–2 weeks post-MI[72]. However, it is worth noting that the 2D cell culture environment may not be entirely reflective of *in vivo* conditions, where cells are embedded in a 3D matrix. Development of 3D *in vitro* systems may be more complicated if the hydrogels need to be crosslinked in the presence of cells using bio-orthogonal reactions, i.e., avoiding cross-reaction with cell surface elements. Nonetheless, alginate, hyaluronic acid, and gelatin hydrogels have been used to show that neural stem and progenitor cell differentiation into neurons could be enhanced in very soft hydrogels matching brain stiffness, while somewhat stiffer hydrogels (matching spinal cord stiffness) led to increased astrocyte differentiation[73–75]. Therefore, when choosing a hydrogel for the regeneration of different tissues, the mechanical properties of the tissue should be taken into account.

Often, only the elastic properties of the hydrogel are reported[69–73,76–78]. However, in addition to elastic solid properties (storage modulus, G′) hydrogels also have viscous fluid

properties (loss modulus, G″). This means that during hydrogel deformation part of the energy is dissipated as heat, creating a non-linear (time-dependent) response to applied stress[79]. Thus, hydrogel response to deformation is arguably best determined through measuring the complex viscoelastic properties, especially given that the viscous characteristics of the environment have also been shown to affect cells. For instance, MSC differentiation into smooth muscle cells was enhanced on substrates with a more pronounced viscous character (G″ = 130 Pa compared to 1 Pa), when maintaining the same storage modulus (~5 kPa)[80]. Similarly, improved MSC osteogenic differentiation was demonstrated using stiffness-matched (G′ ~ 20 kPa) hydrogels with fast stress-relaxation (more pronounced viscous character) both *in vitro* and *in vivo*[81,82].

For applications such as corneal replacement[76,83,84] or bone defect repair[82], a hydrogel may be delivered as a solid implant, but often it is desirable to have a hydrogel system that can be injected through a needle in a minimally invasive procedure, such as for nerve[85,86] or cardiac tissue regeneration[3]. This can be achieved by designing a hydrogel system that remains uncrosslinked until the injection is complete, either due to slow gelation reaction or due to the reaction being activated only once inside the body. However, the crosslinking reaction needs to be carefully optimized because the hydrogel being crosslinked too slowly may lead to material loss from the injection site, while the reaction being too fast may result in the hydrogel becoming solid inside the catheter or needle before reaching the injection site[87]. Alternatively, a hydrogel may be designed to possess shear-thinning (sometimes also referred to as self-healing) properties, allowing it to be injected and recover its mechanical properties afterward. Such hydrogels may be designed employing a number of dynamic covalent bonds and non-covalent interactions, such as disulfide bonds and guest-host interactions[32,88].

In tissue regeneration applications, hydrogels are generally intended for cell infiltration or encapsulation. Therefore, the hydrogel pores should be of sufficient size to allow for the desired cellular and tissue response (cell survival, migration, tissue formation, etc.). Unfortunately, accurate measurement of pore size and determination of optimal values is challenging due to discrepancies between methods and possible hydrogel deformation during measurement[89–91]. Study designs may also fail to capture the desired cell behavior (e.g., initial cell attachment and survival versus growth and infiltration into the scaffold) leading to conflicting reports[92].

However, physical properties are not the only characteristics that determine cell response to hydrogels. On the fundamental hydrogel design level, it should be non-toxic, to allow for cell survival. Depending on the requirements of the application (e.g., the hydrogel needs to be crosslinked in the presence of cells versus implanting it after crosslinking), the toxicity of hydrogel precursors, crosslinking reaction, fully crosslinked hydrogel, and degradation products may have to be evaluated.

Additionally, cells possess a variety of cell-surface proteins which facilitate cell interaction with the environment. Different integrins mediate cell adhesion and signaling pathways by binding to different peptide sequences (RGD, GFOGER, IKVAV, etc.) present on ECM proteins (fibronectin, collagens, laminins, etc.), which in turn affects cellular processes[93,94]. These biological interactions can be harnessed in hydrogel design to induce desired cellular responses. For instance, a collagen hydrogel was shown to enhance the angiogenic potential of circulating angiogenic cells (CAC) through an integrin-dependent mechanism[95]. RGD-functionalized agarose hydrogels used to encapsulate articular chondrocytes increased their chondrogenesis-related gene expression, compared to agarose hydrogels which did not contain the RGD sequence[96]. Human monocytic cells (THP-1) preferably differentiated into M2 (pro-

healing) macrophages when embedded in gelatin hydrogels, while PEG hydrogels induced M1 (pro-inflammatory) macrophage commitment, and the effects of the gelatin hydrogel were showed to be integrin-dependent[77].

Since hydrogels are often intended as a temporary scaffold for regenerating tissue, meant to be integrated into or replaced by the cell-deposited ECM, optimal hydrogel biodegradation characteristics need to be evaluated. Methods involving the use of enzyme solutions[97,98] or other conditions (such as reducing[99] or oxidizing agents [100,101]) *in vitro* are more convenient in terms of replication and precision, but, naturally, they do not entirely reflect the complexity of *in vivo* environment. However, they may be useful in determining possible key degradation mechanisms which may affect the hydrogel *in vivo*[100,101]. Evaluation of biodegradation is perhaps more relevant for natural polymer-based hydrogels as they are susceptible to the enzymes present in tissues and may be degraded too fast to convey any benefit to the regenerating tissue[102]. However, synthetic polymer hydrogels with enzyme-cleavable or hydrolysis-susceptible components merit evaluation for the same reason as well. Although hydrogel degradation *in vivo* is arguably of greatest interest, it is more difficult to measure and track. Different labeling methods can be employed to visualize the hydrogel either *in vivo* or in tissue sections using fluorescent or magnetic resonance imaging[87,103–106].

Furthermore, enzymatic degradation properties of hydrogels may affect the behavior of encapsulated or infiltrating cells. Although the integrity of the hydrogel is important to provide an adhesive environment for cells and sustain their engraftment[104], a specific rate of hydrogel degradation by cell-secreted enzymes (mostly MMPs) may be necessary to induce cell spreading and tissue formation. For instance, cardiac progenitor cells were encapsulated in HA hydrogels containing cell-adhesive RGD peptides and peptide sequences cleaved by different MMPs at

different rates; in addition to greater survival and proliferation, the cells had a higher rate of endothelial differentiation in hydrogels containing a slowly cleaved peptide sequence[107]. In another study, dextran-PEG hydrogels which showed faster degradation by inflammatory cells, led to improved angiogenesis and healing in a third-degree burn model compared to a more slowly degraded counterpart[78].

Finally, and crucially, relevant models are needed to determine whether the characteristics and effects of the hydrogel observed *in vitro* translate into the desired outcomes *in vivo*, such as improved healing and function of the damaged tissues. The following three studies are examples demonstrating how the beneficial effects of hydrogels observed on cells *in vitro* corresponded to improved outcomes *in vivo*. Fast-relaxing hydrogels, optimized for osteogenic differentiation of MSCs *in vitro*, were used to encapsulate MSCs, implanted in a bone defect site and led to improved bone healing[82]. A collagen hydrogel, which enhanced the angiogenic potential of CACs *in vitro*, was used to deliver encapsulated CACs into ischemic myocardium, resulting in improved cardiac function[95]. Finally, a soft methacrylated gelatin hydrogel, which led to neuronal differentiation of induced neural stem cells *in vitro*, also improved recovery in spinal cord injury model[75].

The following sections will discuss hydrogel application strategies in models of cardiovascular applications, focusing on three categories: therapeutic cell delivery, bioactive ECM mimics to aid endogenous repair mechanisms, and tissue adhesives.

1.3 Hydrogels for Cardiovascular Applications

1.3.1 Injectable Hydrogels for Cell Delivery

Since the regenerative capacity of the heart is minimal, cell therapy appeared as a promising solution for treating MI and heart failure by replacing the cells that are lost. However, the exciting pre-clinical data did not translate to the same success in clinical trials, where, upon meta-analysis of different types of therapies, a slight or no improvement in cardiac function with cell therapy was observed[108–110]. However, cell retention at the delivery site is known to be poor, and the cells are exposed to the same damaging environment as the endogenous cells. Additionally, the paracrine mechanisms through which cell therapy leads to improved functional and pathological outcomes are complex and not completely understood[111,112]. Nonetheless, the efficacy of cell therapy might be improved by protecting the therapeutic cells from the destructive environment and enhancing their retention, thus prolonging the therapeutic effects.

One cell protection strategy is to deliver them inside a hydrogel. Indeed, a number of pre-clinical studies show that delivering therapeutic cells in hydrogels results in improved treatment efficacy in animal MI models compared to cell delivery in solution[113–117]. Interestingly, a wide variety of hydrogels appear to be suitable for this purpose: reported designs include fibrinogen[113], synthetic self-assembling peptides[114], polycaprolactone-based synthetic polymer hydrogel containing trapped collagen[115], PEG crosslinked with MMP-cleavable peptide and covalently attached heparin[116], and a composite hydrogel crosslinked using EDC and containing synthetic dendrimers, collagen, and pro-survival peptides[117]. The common factor in these hydrogels appears to be cell-adhesive sites, suggesting that perhaps this is the key feature required. This is supported by data showing that the beneficial effects of collagen matrix on CACs *in vitro* and *in vivo* require cell-matrix interaction[95].

Despite the promising results using bioactive hydrogels, further improvements to encapsulated cell therapy may be possible. For example, since conduction is compromised in the infarct region, introducing a conductive hydrogel may help electrical signals travel between cells, helping establish cellular connections and thus improving cardiac function[118]. Additionally, even though hydrogel encapsulation is meant to protect cells during injection as well as afterward, it has been shown that typical hydrogels (injectable only while uncrosslinked) may not provide adequate protection from shear forces during injection[119,120]. It has been postulated that the protective effect occurs if the hydrogel can undergo reversible gel-sol transition when sheared (i.e., it is shear-thinning) because during injection only some of the bonds are broken to enable injection, while the rest of the hydrogel remains in the gel state protecting the cells from shear forces. Furthermore, such shear-thinning systems would eliminate injection timing constraints as they remain injectable after crosslinking is complete. In a recent report, delivery of endothelial progenitor cells inside an HA hydrogel crosslinked using guest-host interaction between cyclodextrin and adamantane in a rat MI model improved cardiac function compared to cell delivery in solution (unfortunately, a hydrogel without shear-thinning properties was not used for comparison)[121].

1.3.2 Acellular Injectable Hydrogel-Based Therapies for Heart Disease

Despite the potential of cell-based therapies for cardiovascular diseases, the transplantation of live cells presents a number of challenges, such as impaired regenerative potential of autologous cell transplants, immune reactions, as well as logistic issues of preparing, storing, and transporting cells[122]. Therefore, the development of alternative acellular treatment strategies is of interest. Two promising biomaterial-based approaches are patches[123–125] and

injectable hydrogels. Although minimally invasive strategies for patch application are possible, injectable hydrogels are generally more suitable for minimally invasive application[1] and are the focus of this thesis. Hydrogel therapy may be beneficial in both acute (MI) and chronic (heart failure) ischemia cases. However, since it is possible to identify patients who are at risk of negative remodeling and heart failure early after MI, the development of preventative therapies would help improve clinical outcomes, in addition to reducing healthcare costs[126,127].

In one of the first uses of biomaterial therapy for cardiovascular diseases, fibrin glue was injected into the ischemic tissue in a rat MI model[128]. Importantly, the outcome (preservation of fractional shortening and myocardial thickness) was similar between the group that received only fibrin treatment and the group that received cells encapsulated in the fibrin glue; suggesting that an acellular treatment can be as effective as a cell therapy approach.

Currently, the mechanism of action of bioactive hydrogel therapy for MI is thought to be two-fold. Firstly, a hydrogel injected into the myocardium (or on top of the myocardium) has a bulking effect on the thinning heart wall. An injected hydrogel can increase the thickness of the myocardium, thus reducing the stress experienced by the heart wall, especially at the infarct border, and preventing ventricular dilation[129]. Secondly, hydrogels containing bioactive components, such as collagen or growth factors, have been shown to exert anti-inflammatory, anti-apoptotic, and pro-angiogenic effects on the injured heart, thus also reducing the spread of fibrosis and improving function[130–132] (Figure 1.3).

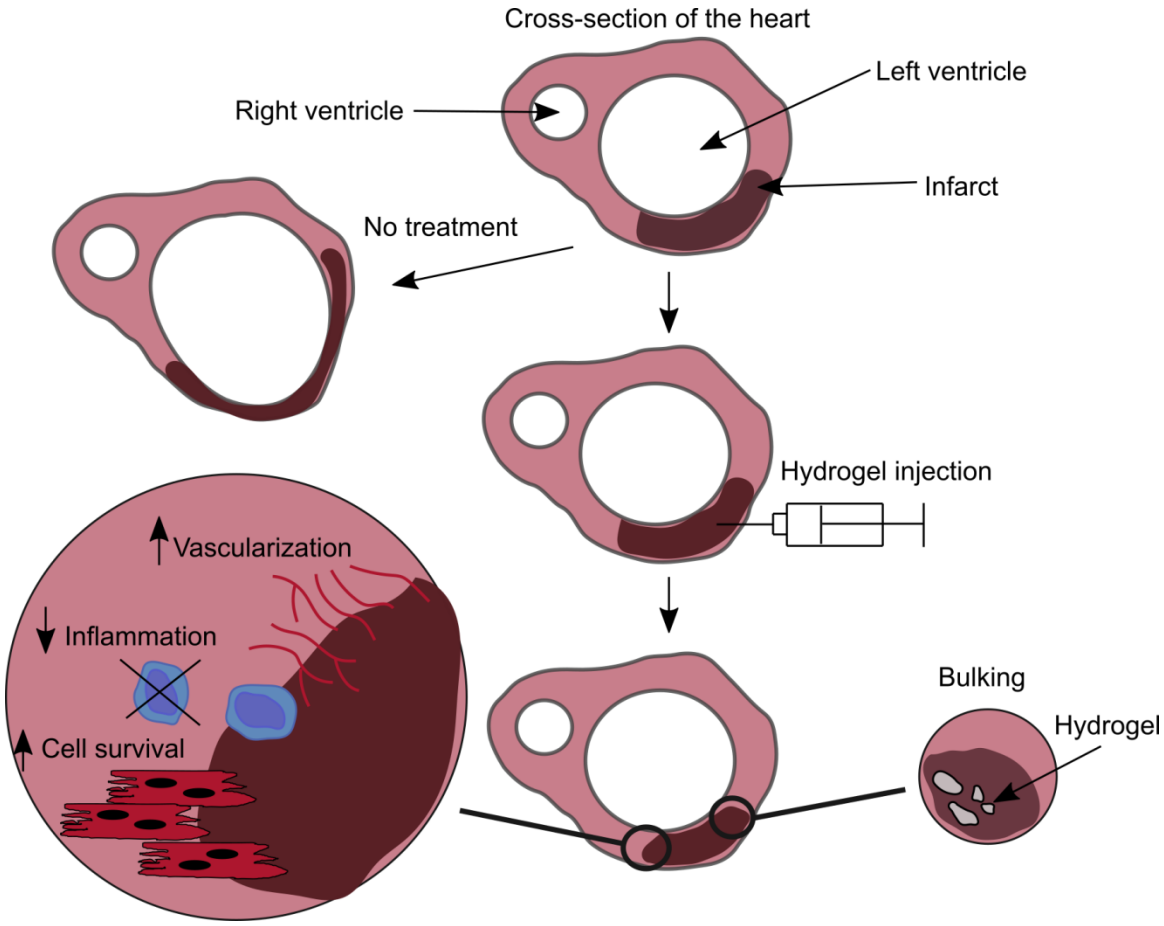

Figure 1.3. The mechanism of action of hydrogel therapy for myocardial infarction.

Injectable hydrogel designs proposed for cardiac applications include natural (alginate[133,134], collagen[95,130], HA[87,135,136]), synthetic (acrylamide[106,137], PEG[105]), and composite (PEG-HA[138,139], PEG-fibrinogen[140,141]) materials. Due to the many differences between studies, such as animal model parameters and the delivery of different growth factors inside the hydrogels, it is difficult to evaluate the comparative effectiveness of hydrogel designs and what properties may be desirable. Nonetheless, one of the commonly expressed concerns regarding natural polymer-based materials is their fast degradation. An acrylamide hydrogel was shown to be present in the scar for up to 10 weeks after injection[106]. However, an HA-based hydrogel crosslinked through guest-host interaction and click chemistry was retained in the heart 4 weeks after injection, showing that it is possible to develop natural-polymer hydrogels with slower degradation kinetics[87].

Another obstacle in the search for the optimal hydrogel therapy is the difference between the timing of treatment in the reported studies. After an ischemic event, the affected tissue undergoes a series of changes which lead to the formation of a mature scar[142]. Thus, a hydrogel injected at different time points after MI encounters a different environment and cells at the delivery site, which, depending on the hydrogel properties (e.g., embedded bioactive molecules or susceptibility to MMPs), may lead to different outcomes. However, very few reported studies investigated the optimal timing for the delivery of the biomaterial treatment. For rodent MI models, the hydrogel is usually injected once: immediately (within a few hours)[87,135–137,139–141] or within 1 week[95,132,143] post-MI. The rationale for the particular choice is usually not reported, although in most cases the hydrogel is injected during an open-chest procedure; therefore, treatment delivery shortly after MI induction (before closing the chest) reduces the number of highly invasive procedures the animals have to undergo. The few studies that have investigated

the timing of hydrogel delivery have used acrylamide[106], MMP-cleavable PEG[105], alginate[144], HA[138], and collagen[130] hydrogels in rat and mouse MI models. Interestingly, the optimal delivery time for collagen was found to be within a few hours after MI (during the inflammatory phase), while the acrylamide and PEG hydrogels led to best outcomes if injected 3–7 days post-MI (during the proliferative phase). The two remaining studies (alginate and HA) did not investigate early time points, but their findings show that the benefits of hydrogel therapy are diminished when injected into a mature scar (1 and 2 months post-MI). Collectively, these studies show that hydrogel therapy timing is a factor that affects treatment outcomes and should be considered when designing a strategy for hydrogel therapy post-MI.

1.3.3 Tissue-Adhesive Hydrogels

Tissue adhesives are of interest for cardiovascular applications in several areas, including closure of surgical incisions and tissue damaged by trauma[145] and attachment of cardiac patches and other devices[124].

Currently, most common wound or incision closure methods in clinical practice are sutures and staples, with a few cyanoacrylate and fibrin glues approved for clinical use as well. However, sutures and staples fail to provide an immediate seal of the wound or incision, in addition to risking additional trauma and scarring. They may also pose a challenge in minimally invasive procedures. Cyanoacrylate and fibrin glues can provide an immediate seal, but their adhesiveness or flexibility are often insufficient[146]. Additionally, despite being approved for human use, some cyanoacrylate glues are cytotoxic[147].

Therefore, there is a need for alternative tissue sealant and adhesive materials that can overcome these limitations. Hydrogels present a suitable system for developing tissue adhesives

since they can be prepared using a wide variety of materials and crosslinking methods, resulting in a system with desired gelation, mechanical, biological, swelling, and tissue-adhesive properties. Additionally, a hydrogel can fill gaps in tissues, enabling the closure of uneven wounds[148].

Due to the need for quick-acting adhesives that can be safely crosslinked *in situ*, hydrogels for this purpose are often based on photo-activated, click chemistry reactions, and mussel-inspired systems containing catechol functional groups. Reported photo-activated hydrogels include phenol-modified gelatin[149], phenol-chitosan[150], and methacrylated tropoelastin[145], all crosslinked using UV or blue light within 30 s. The rate of click chemistry reactions is a concern when creating fast-gelling systems, but a hydrogel composed of chitosan-maleimide and dithiol-PEG was shown to gel within 25 s[151]. Mussel-inspired adhesive hydrogels are commonly intended for skin wound applications (as dressing)[152,153] but have also been proposed for internal use[154]. For the latter application, a stable yet fast gelling hydrogel is required; therefore, in the reported study, Fe^{3+} ions were introduced in a dopamine-modified gelatin system to induce a rapid catechol-mediated crosslinking, while genipin was used to produce stable crosslinks at a slower rate. Although these results are promising, further research efforts are dedicated to addressing issues such as development of multifunctional adhesive hydrogels, excessive swelling, and the use of short-wavelength light[155].

2 Rationale, Hypotheses, and Aims

Prompted by the need for novel regenerative therapies, hydrogel development and application has yielded a lot of promising pre-clinical results using a wide variety of different material designs. However, there are still many aspects that require additional development, both in terms of biomaterial design and application approaches. For example, collagen I has gathered a lot of attention as it comprises most of the ECM network, leading to the development of many collagen-based hydrogels. Many of these hydrogels were shown to improve tissue regeneration and repair. However, due to the large size and complex structure of the molecule, it remains challenging to modify and crosslink collagen I using biocompatible methods, as well as manipulate its mechanical properties. On the other hand, with efforts focused on developing new collagen I hydrogel designs, other aspects of the hydrogel therapy that might help increase efficacy and other types of collagen are neglected. Therefore, the overall goal of this work was to develop novel collagen hydrogel designs and application strategies in order to offer possible solutions and insight into some of the issues concerning collagen hydrogel use for regenerative medicine applications. Specifically,

I aimed to test the following hypotheses (corresponding to Papers I – III):

I. Application of a collagen hydrogel crosslinked with visible light will result in improved skin wound healing compared to traditional sutures;
II. Injectable collagen hydrogel crosslinked with an orthogonal reaction will be suitable for cell encapsulation and delivery;
III. Delivering collagen hydrogel into the myocardium at 3 time-points post-MI will result in improved cardiac function compared to a single time-point injection.

The experimental aims to test the hypotheses were as follows:

I. Design a collagen hydrogel crosslinked using visible light for tissue bonding applications;
II. Design an injectable collagen hydrogel crosslinked using non-toxic chemistry that is suitable for cell encapsulation and delivery;
III. Investigate whether collagen hydrogel delivered to the myocardium at 3 time-points post-MI results in improved cardiac function compared to a single time-point delivery.

3 Paper I. Collagen-Based Photoactive Agent for Tissue Bonding

Reprinted with permission from:

J. Pupkaite, M. Ahumada, S. Mclaughlin, M. Temkit, S. Alaziz, R. Seymour, M. Ruel, I. Kochevar, M. Griffith, E.J. Suuronen, E.I. Alarcon. Collagen-based photoactive agent for tissue bonding. ACS Appl. Matter. Interfaces, 9, 9265–9270 (2017).

Abstract

Using a combination of methacrylated collagen and the photosensitizer rose Bengal, a new light-activated biomimetic material for tissue sutureless bonding was developed. This formulation was crosslinked using green light. *In vivo* tests in mice demonstrate the suitability of the material for sutureless wound closure.

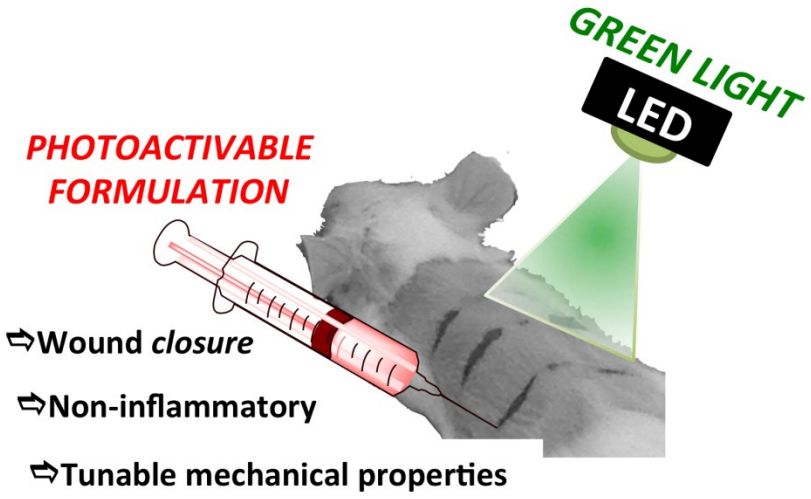

Table of contents figure of Paper I.

The design of new technologies for solving critical problems in the clinic must comprise realistically translatable approaches. Engineered biomaterials have contributed significantly to recent advances in the medical sciences, where they are being implemented as tissue scaffolds, fillings, and prosthetics[156–159]. Surgical suturing has evolved over the last century from the use of silk and catgut stitches to more advanced and biodegradable materials. However, excessive scarring post suturing remains an issue[160–163]. Furthermore, stitches are not always suitable, for which the choices for suturing are reduced to sutureless glue-like products, which close the tissue gap by chemically bonding the edges of the incision or wound[164]. Although sutureless materials are currently available for clinical use, they are limited in their ability to modulate the biomechanical properties of the glued tissue. Additionally, these products typically have very short gelation times (<30 s), which can present a challenge for the surgeon[165,166]. Thus, developing a new material able to provide some extent of control over the mechanical properties of the repaired tissue, with appropriate consideration given to the timing/spatial control required for its application, would present a significant advance for wound repair.

Light-activated tissue bonding using biomaterials activated by visible light in the presence of photosensitizers offers numerous advantages for tissue repair over surgical suturing, such as reduced inflammation and minimal scarring[164,167–170]. However, a current limitation for using light-activated tissue bonding in the clinic is that the sides of the wound must be placed in tight contact, since proteins must be in close proximity for being chemically activated by the photosensitizer and ultimately allowing the protein−protein crosslinking to occur. Thus, in the present contribution, we report *in vitro* and *in vivo* findings for the development of a new generation of light-activated tissue bonding materials that will overcome the limitations, such as tissue gaps, of using standalone photosensitizers for tissue repair. Our deliverables harnessed the

visible photosensitizing properties of rose Bengal (RB) for promoting *in situ* crosslinking, and tissue bonding, when embedded within a mixture of methacrylate-modified type I collagen and positively charged amines. These materials possess attractive and promising properties for future clinical translation in tissue photobonding.

When designing new tissue photobonding technology, an important consideration is the cost-effectiveness of the illumination source used to initiate the crosslinking of the formulation, which confers the bonding of the tissue. Therefore, we chose an LED as the basis for the illumination system (Figure 3.1a). A 523 nm high-power LED was mounted onto a heat dissipation fan (to prevent LED overheating). Light from the LED was collimated with a reflective cylinder surface and aimed onto the sample. Samples were irradiated at 220 mW/cm^2 power for increasing times, up to 10 min, to establish the minimum time needed to achieve crosslinking of the material.

Collagen, the most abundant protein in skin dermal extracellular matrix was chosen as the primary component for a scaffold to fill the wound and facilitate RB-initiated tissue bonding. However, initial attempts to crosslink unmodified collagen in the presence of the photosensitizer RB were unsuccessful. Therefore, the protein was modified to introduce methacrylate moieties to yield methacrylated collagen (MC). Then, hydrogel assembly is triggered upon activation of the methacrylate moieties mediated by rose Bengal excited states[a], which lead to hydrogel formation. Mixing RB and MC resulted in a viscous intensely pink solution, whose color gradually faded as the reaction proceeded (Figure 3.1b).

The photochemistry of rose Bengal and related spectrum changes have been previously investigated in different contexts, such as in the presence of albumin. Both type I (radical-initiated) and type II (singlet-oxygen-mediated) mechanisms were found to be implicated in the

[a] Hydrogels were not formed in the absence of light or when irradiation was performed without rose Bengal.

quenching process depending on the conditions[171]. Additionally, RB is known to form dimers and oligomers in solution, which are believed to be photochemically inactive and are readily formed in the presence of proteins like collagen[172]. The monomer spectrophotometric absorption maximum is centered at 550−555 nm, whereas the aggregates absorb at shorter wavelengths[172]. In this regard, to elucidate the possible link between the bleaching of the samples during illumination and the formation of reactive oxygen species (ROS) or free radicals under our study conditions, different additives were incorporated into the core formulation of MC and RB, and the changes of the RB absorbance with increasing duration of illumination were monitored (MC does not absorb in the visible range of RB absorption).

Adding the singlet oxygen quencher, sodium azide, to the mixture had no effect on the degradation rate of the RB monomer (maximum absorption at ≈554 nm), but it slowed down the formation of the band centered at 450 nm, which is presumed to reflect the formation of oxidation products (Figure 3.1c). Amines, such as the natural amino acid arginine, can quench the triplet excited state of RB, leading to the formation of free radicals[173], which can be involved in the degradation of the photosensitizer. Introducing arginine to the mixture accelerated the degradation rate of the monomer by a factor of 2, whereas the final absorbance of the photoproduct was reduced by approximately 30% compared to the basic formulation (MC and RB). In both the azide and arginine experiments, hydrogels were formed after illumination, indicating that crosslinking of the collagen had occurred. Interestingly, the formulations prepared using poly-L-arginine did not form a hydrogel even after 30 min of illumination (not shown). This could be a consequence of the formation of more stable reactive intermediates for the arginine chains that bears two sets of nitrogen moieties per amino acid, which in turn might lead to a lower crosslinking yield. Thus, we tested another polyamine, poly-L-lysine (PLL), which

resulted in hydrogel formation, while reducing both the degradation rate of the monomer and the formation of oxidation product by a factor of ≥100 (Figure 3.1c). ^{1}H NMR was performed to detect the presence of the different components in the material formed by the mixture of MC-RB and PLL (Figure 3.1d). A qualitative comparison of the methacrylate ^{1}H NMR spectra shown in Figure S3.1 points toward a decrease in the signal intensity of the methacrylate protons after irradiation. Interestingly, the remaining population of methacrylate after irradiation did not show any toxic effect in our *in vivo* model (see below). Furthermore, infrared spectra for the samples demonstrate the presence and preservation of the functional groups of collagen in the assembled polymer (Figure 3.1d). A simplified mechanism that summarizes the main steps involved in the crosslinking of our materials is shown in Scheme 3.1.

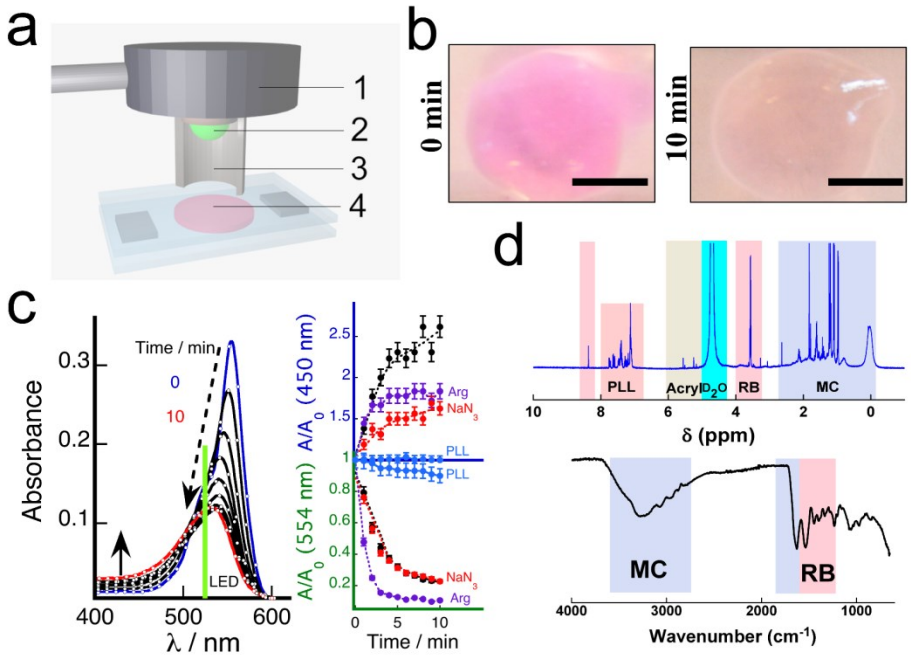

Figure 3.1. (a) Schematic representation for the illumination setup used in our study: (1) cooling fan, (2) 523 nm LED, (3) collimator, and (4) methacrylated collagen (MC) and rose Bengal (RB) mixture between two glass slides; 1.0% MC and 25 μM RB were used for preparation of the parental solution; a 523 nm LED was used for photo-crosslinking using 220 mW/cm^2 with a 10 min irradiation; (b) representative images for MC and RB formulation before (left) and after 10 min of illumination (right); scale bars = 2.5 mm; (c) left: temporal changes in absorption spectra for the methacrylated collagen (MC) and rose Bengal (RB) formulation; LED emission wavelength is shown as the rectangular green bar in the plot; right: changes in absorption intensities at 450 and 554 nm for MC-RB formulations containing arginine (10 mM, Arg), sodium azide (10 mM, NaN_3), or poly-L-lysine (0.025%, PLL); error bars correspond to the standard deviation (n = 3); (d) representative measurements of ^{1}H NMR (top) and FT-IR (bottom) for the MC-RB formulation containing 0.025% poly-L-lysine (PLL) measured after 10 min irradiation with our LED system.

Scheme 3.1. Simplified Representation for the Proposed Rose Bengal (RB) Mediated Photobonding Mechanism Observed in This Work[a]

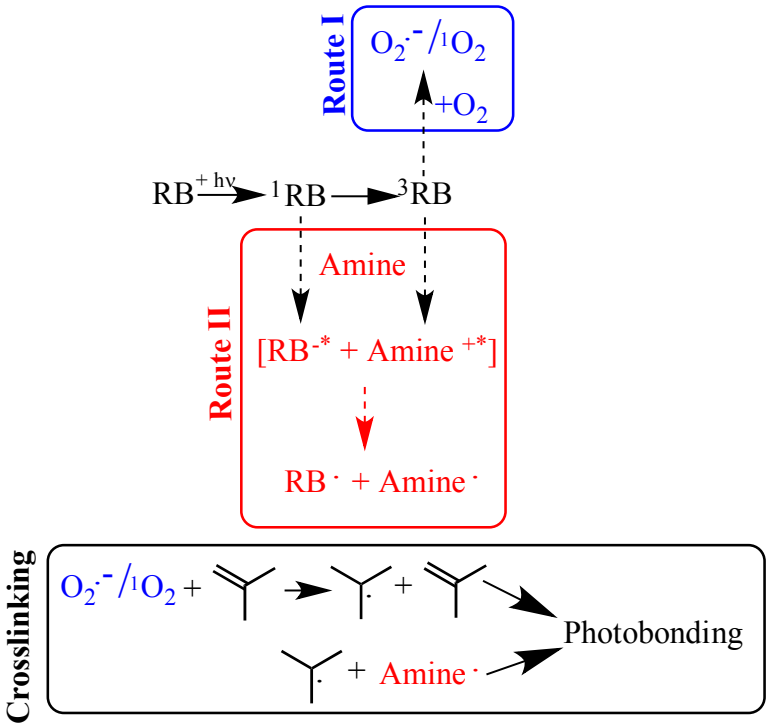

[a]Overall, upon light excitation of the dye, excited states are formed that can either act as energy (triplet) or electron (singlet or triplet) to amines and/or oxygen. Route I: Corresponds to the oxygen pathway where the formation of either singlet oxygen and/or anion radical superoxide is a possibility. Route II: Amine-mediated electron transfer mechanism observed upon deactivation of rose Bengal excited states. Ultimately, the formation of those reactive intermediates leads to the matrix crosslinking (bottom) which allows tissue photobonding.

Stability at physiological temperatures is one of the essential features that a hydrogel with potential for medical use should possess. Therefore, the denaturation temperatures of the hydrogels were measured by differential scanning calorimetry (Figure 3.2a). Unmodified collagen hydrogels (irradiated under the same experimental conditions) were denatured at <40 °C meaning they were not stable enough to be used at physiological temperatures. The MC-RB formulation matrices displayed denaturation temperature of ~52 °C, approximately 12 °C higher than the unmodified collagen gels and greater than the normal range of physiological temperatures. Introducing arginine or poly-L-lysine to the formulation resulted in no significant changes in the denaturation temperatures. This data illustrates that light-mediated crosslinking of MC takes place upon green light irradiation in the presence of a photosensitizer.

Other important features of hydrogels intended for *in vivo* use are their swelling and enzymatic degradation properties. To this end, we assessed these properties using *in vitro* experiments designed to mimic *in vivo* conditions. First, the swelling behavior of the hydrogels was investigated by incubating them in 0.9% NaCl (saline) solution at 37 °C. MC and MC/PLL gels exhibited a reduction in wet mass (Figure 3.2b), which was also observed for samples prepared with arginine (not shown). Interestingly, the weight of all hydrogel formulations was reduced to a third of the original weight, but the hydrogels made with PLL took 20× longer to reach a steady mass state than the basic formulation. Reduction in wet weight could be attributed to the reorganization of the collagen fibers within the hydrogel upon their evolution to a less hydrophilic structure. This is delayed when PLL is incorporated, probably due to its cationic structure[174]. Enzymatic degradability of the hydrogels was then assessed *in vitro* using type I collagenase (Figure 3.2c). Interestingly, the presence of arginine decreased the degradation rate of the matrix compared to the mixture containing only MC and RB, while the addition of 0.025%

PLL reduced the degradation rate by 5 times. This effect is no longer observed at higher concentrations of PLL, which can be attributed to a loss in the intrinsic nature of an interpenetrating network formed between MC and PLL. Note that these differences cannot be linked to differences in the material pore size, because hydrogels prepared using arginine exhibited similar degradation behavior, despite having significantly different pore sizes (Figure 3.2d), whereas the gel made using 0.025% PLL showed similar pore sizes compared to the MC-RB samples.

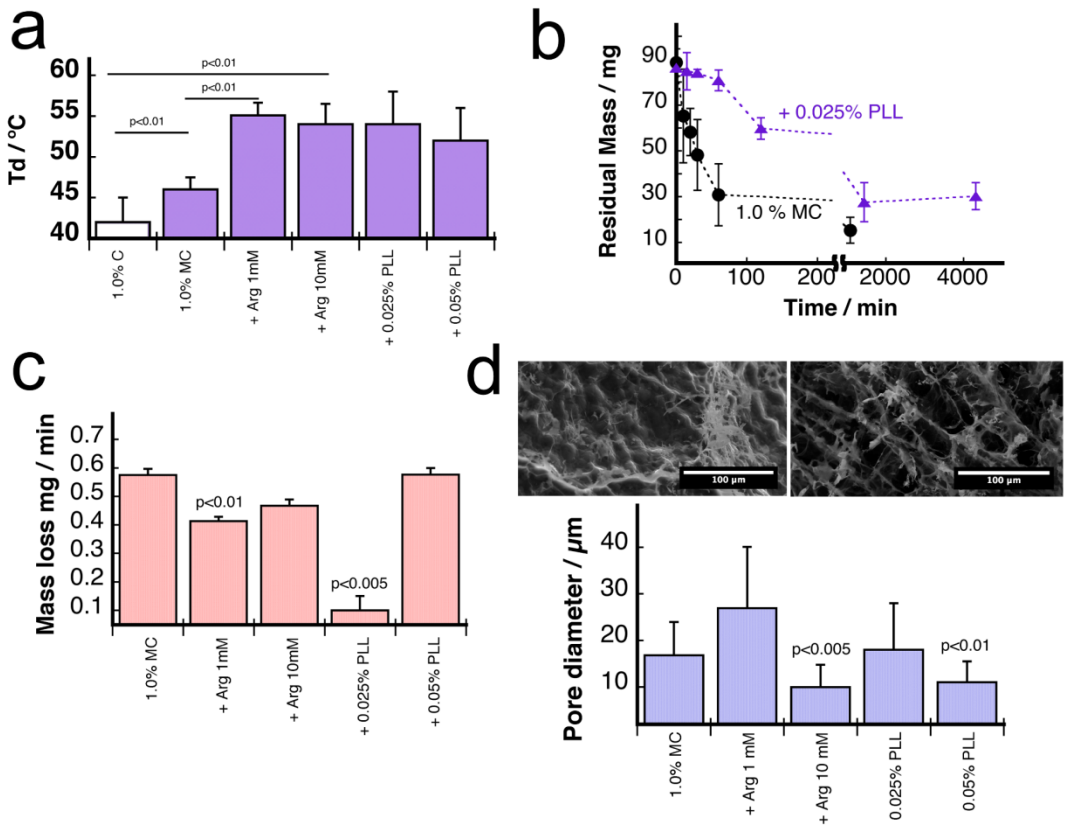

Figure 3.2. Physical properties of MC-RB hydrogels (25 µM RB and 1.0% MC): (a) denaturation temperature of different formulations; (b) changes in wet mass of hydrogels incubated at 37 °C in saline solution; (c) enzymatic degradation of hydrogels mediated by type I collagenase (5 U/mL) measured at 37 °C; (d) top: representative cryo-SEM images of MC-RB hydrogels without (left) and with (right) 0.025% poly-L-lysine (PLL); bottom: average pore size measured for the different collagen hydrogels prepared in our study. Error bars are standard deviations (n = 3); *p* values included in the plots were calculated by t tests (two-tailed, non-paired data).

To evaluate whether the proposed formulations could serve as tissue bonding agents, we carried out photobonding experiments using a biomimetic material and *ex vivo* mouse skin (Figure 3.3). An unmodified collagen (10% w/w) hydrogel crosslinked using 1,4-butanediol diglycidyl ether[175], was used as a biomimetic material and 2 pieces of this material were successfully photobonded using different RB and MC formulations, with or without additional components (Figure 3.3a). Notably, a reestablishment of the mechanical properties (Young's modulus and breaking strain) was observed for the basic formulation (RB and MC), with the materials containing arginine exhibiting similar properties. However, the formulation containing 0.025% PLL had a significantly higher breaking strain than the MC-RB or the one containing arginine. The effect of PLL on material strength disappeared when PLL concentration was increased to 0.05%. Those differences can be explained if one considers the formation of interpenetrating networks between the protein and PLL, see bottom of Scheme 3.1, which seems to find an optimal molar ratio at values of PLL of 0.025%. Thus, doubling the PLL concentration might result in reducing the PLL-collagen crosslinking, which translates in decreasing the interpenetrating network abundance, and consequently losing elasticity. Regardless of the polypeptide concentration, Young's modulus of PLL-containing formulations was significantly lower than the intact hydrogel control.

Next, we used pieces of mouse skin to test the *ex vivo* performance of the MC-RB or the MC-RB + 0.025% PLL formulations (Figure 3.3b). Upon irradiation, both formulations resulted in a much lower Young's modulus compared to the intact skin control, which can be due to the lack of cellular and structural components present in skin. While the MC-RB formulation resulted in lower breaking strain compared to control, the breaking strain of the sample irradiated using the PLL formulation was similar to that of the intact skin control.

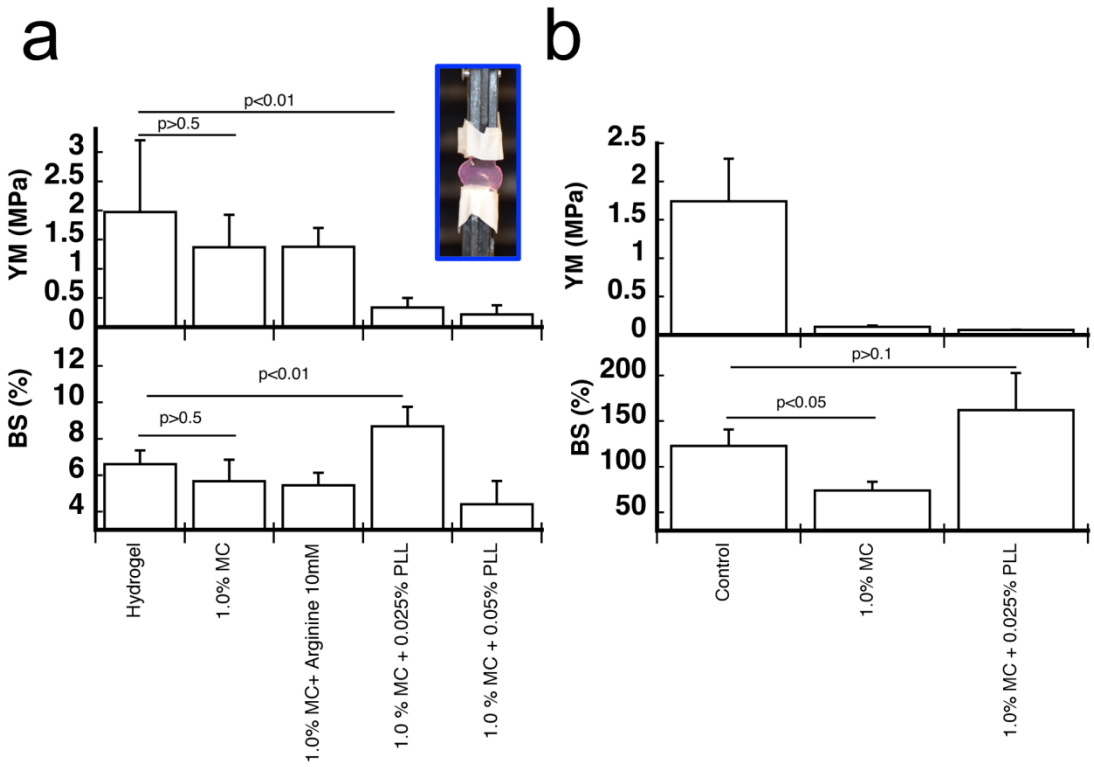

Figure 3.3. Mechanical properties: Young's modulus (YM in MPa) and breaking strain (BS in %), of irradiated hydrogels and *ex vivo* mouse skin: (a) two collagen hydrogel pieces were photobonded using different formulations of the photoactive agent; hydrogel refers to intact gel; inset: representative image of irradiated photobonded hydrogel pieces loaded onto the mechanical tester; (b) two pieces of mouse skin photobonded together *ex vivo* using different hydrogel formulations (without and with 0.025% PLL), control corresponds to intact mouse skin. Error bars are standard deviations (n = 4); *p* values calculated by two-tail t tests.

Finally, to evaluate the *in vivo* performance of our materials, the mechanical properties and tissue response of mouse skin wounds treated with different formulations were assessed. Traditional sutures were used as control. For the incisions that received the collagen formulations, a thin layer of the material was applied within the wounded tissue, and any excess in the area was physically removed. This was followed by irradiation with the same LED system used in the *ex vivo* assays (220 mW/cm^2 for 10 min). As the gels containing arginine did not show any difference in the mechanical properties *in vitro* (Figure 3.3a), we tested only the original formulation (MC-RB) and the one containing 0.025% PLL. Figure 3.4a, left, shows a representative image for the mouse skin wounds at day 0. The physical appearance of the wounds after 5 days showed that wounds receiving either hydrogel formulation closely resemble nonwounded skin, whereas the sutured group showed signs of erythema suggesting inflammation (Figure 3.4a, right). Interestingly, Young's modulus of tissues bonded with the MC-RB formulation was significantly lower than those obtained with sutures, whereas the breaking strain of photobonded tissue was similar to that of the sutured control (Figure 3.4b). However, when using the formulation containing PLL, mechanical properties similar to that of tissue treated with sutures were obtained after 5 days. Histology analysis for the tissues harvested after 5 days of treatment showed no significant differences in the epithelial thickness for the tissues treated with either MC formulation when compared to the suture group ($p > 0.1$). However, the group treated with sutures appeared to have a more disorganized fibrous-looking underlying dermis invaded by erythrocytes/monocytes (Figure 3.4c).

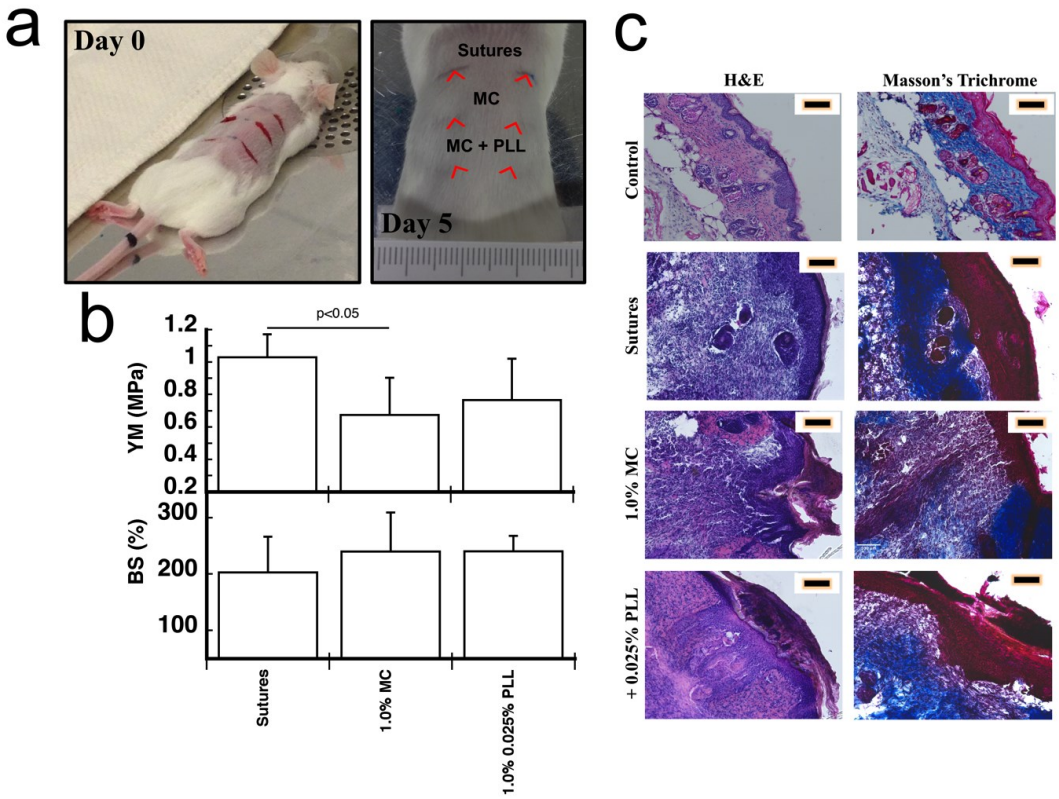

Figure 3.4. *In vivo* assessment of tissue photobonding using MC-RB and MC-RB-PLL formulations: (a) left: representative image of the surgical incisions made on the mouse's back skin before treatment; right: representative image of the skin incisions 5 days after receiving different treatments as indicated in the figure; (b) mechanical properties (Young's modulus, YM, and breaking strain, BS) of the tissue bonded with the MC formulations or with sutures harvested 5 days post-treatment; error bars correspond to standard deviation (n = 6); *p* values calculated from two-tailed t test; (c) representative H&E and Masson's Trichrome stained sections of the skin wound 5 days post-treatment; control represents healthy mouse skin; note the presence of an abundance of erythrocytes/monocytes in a more disorganized fibrous underlying dermal layer of the sutured wound, which appears less substantial in the photobonded hydrogel treatments; scale bars correspond to 100 μm in all cases.

In summary, we have prepared a new material for sutureless wound closure, which is activated using green light. Further, by simply incorporating poly-L-lysine, we improved the mechanical properties of the resulting bonded tissues/materials. Finally, *in vivo* experiments demonstrated the suitability of this new technology for future clinical use as a viable alternative to surgical stitching.

Acknowledgements

This work was made possible by funding from the Natural Sciences and Engineering Research Council (NSERC) to E.I.A. and E.J.S., RGPIN- 2015-0632 and 342107, and initial funding to M.G. from AFA Försäkring, Sweden. E.I.A. also thanks UOHI start-up grant 1255. E.I.A. and I.K. thank the Burroughs Wellcome Fund for a Travel Grant. The authors thank Dr. Godwin Dogbevia for his assistance in tissue sectioning. E.I.A. thanks Mr. Michel Grenier from University of Ottawa for his help in building the LED system used in this study.

Supporting Information

Materials and Methods

Materials

Rose Bengal (RB) dye (4,5,6,7-tetrachloro-2',4',5',7'-tetraiodofluorescein <99%), L-arginine, sodium azide (NaN_3), 4-Butanediol diglycidyl ether (BDDGE), PBS tablets, methacryl-anhydride (MAA), and 0.1% poly-L-lysine (PLL) solution were purchased from Sigma-Aldrich (Canada). Collagenase type I was purchased from ThermoFisher Scientific (Canada). Porcine type I collagen was purchased from Nippon Ham (Japan). Milli-Q water was used for all experiments.

Methacrylated Collagen Preparation

Methacrylated collagen (MC) was prepared as described previously[26]. Briefly, collagen was dissolved in water (0.5% w/V), and the pH was adjusted to approximately 10–11 by adding 2 M NaOH. MAA was then added drop-by-drop at a molar ratio of 10:1 (MAA:Lys residues). The whole procedure was performed while stirring and maintaining pH ≈ 10. The reaction mixture was dialyzed in 12–14 kDa cut-off dialysis tubing against water (pH = 10, 0.05 mg/mL NaN_3 was added to prevent bacterial growth) for three days and lyophilized.

Hydrogel Preparation

The following hydrogel formulations were prepared for testing: 1) 1% MC, 25 μM RB; 2) 1% MC, 25 μM RB, 1 mM Arg; 3) 1% MC, 25 μM RB, 10 mM Arg; 4) 1% MC, 25 μM RB, 10 mM NaN_3; 5) 1% MC, 25 μM RB, 0.025% PLL; and 6) 1% MC, 25 μM RB, 0.05% PLL. Note that lower concentrations of PLL lead to materials with similar properties to the parental formulation, no amine added, while concentrations higher than 0.05% produces materials with reduced stability in buffer (not shown).

Hydrogel formulations were prepared following a general w/w protocol, where the final mixture had 5× the initial weight of the 5% w/w MC solution, yielding a final MC concentration of 1%. In this way, the mixed quantities in weight were: 1× 5% w/w MC solution, 2.5× RB solution and 1.5× water and the solution of either Arg, NaN_3 or PLL. Arg and NaN_3 were chosen as a radical-supplying molecule and a singlet oxygen quencher, respectively, to test the role of free radicals and singlet oxygen in the RB-mediated crosslinking process. Hydrogels were prepared using a syringe mixing system described previously[176]. 5% MC solution was loaded into the system. The calculated amount of water was then injected followed by thorough mixing. Depending on the formulation, the added water may have also contained the required amount of 100 mM LArg, 100 mM NaN_3 or 0.1% PLL to yield final concentrations of 1 mM Arg, 10 mM Arg, 10 mM NaN_3, 0.025% PLL or 0.05% PLL. The rest of the procedure until illumination was carried out in minimal light conditions. A 50 μM RB solution was added in 4 or 5 injections, mixing thoroughly after each injection to yield final concentrations of 25 μM and 1% MC. The syringe with the uncrosslinked mixture was centrifuged at 4000 rpm for 2 min to remove air bubbles from the solution. Then, 1 mm-thick gels were cast between glass plates. The crosslinking of the gels was performed using a custom-made illumination system (Figure 3.1a). The distance between the LED (λ_{em} = 523nm) and a gel was 3.5 cm; a plastic layer was used to prevent the sample from overheating. The LED was supplied by a DC power supply whose current and a voltage was set to 0.6 A and 14.0 V, respectively, to achieve the full power of LED emission (220 mW/cm^2). Gels were illuminated for 10 min using 1 LED at full power.

Differential Scanning Calorimetry (DSC)

For DSC analysis, crosslinked gels were washed with PBS and kept in PBS at 4 °C until further use. The glass transition temperature (T_g) of the hydrogels was measured using a Q2000

differential scanning calorimeter (TA Instruments, USA). Heating scans were recorded in the range of 8 to 80 °C at a scan rate of 5 °C/min. T_g was measured at the onset of the endothermic peak. The reported values correspond to the average of three independent samples.

Swelling Properties

To measure swelling, the gels were tested immediately after illumination by incubating them in pre-heated 0.9% NaCl solution at 37 °C. At each pre-determined time point, the gels were removed from solution (at room temperature) and their surface was blotted to remove excess liquid. The gels were weighed and then returned to incubation conditions.

Absorption Spectra

The samples were loaded between two microscope slides separated by 1 mm spacers and the absorption spectra were measured at room temperature using a Libra Biochrom spectrophotometer (USA). A microscope slide was used as blank.

Enzymatic Degradation in vitro

The gels were washed with PBS at room temperature, cut into pieces of similar weight and shape and incubated in Tris-HCl buffer (pH = 7.4) for 1 h at 37 °C. They were removed from the solution and weighed after carefully blotting away excess liquid. The gels were incubated in preheated collagenase solution (5 U/mL in Tris-HCl buffer) at 37 °C. At each time point the gels were removed from the solution, carefully blotted, weighed and put back into a fresh preheated collagenase solution.

NMR and FT-IR Measurements

Gels (before and after irradiation) were dried under vacuum. Between 5 to 10 mg of the dry gels were dissolved in 0.7 mL of D_2O, and ^{1}H-NMR spectra measured using a Bruker AVIII 600 MHz NMR spectrometer (USA). FT-IR the spectra were measured on a Nicolet 6700 FT-IR

spectrometer equipped with a Smart iTR diamond ATR (Thermo Scientific, USA), and 250 scans were averaged.

Mechanical Properties of the Photobonded Hydrogels

To mimic the bonding of 2 tissue borders, BDDGE-crosslinked collagen hydrogels[175] were photobonded with the MC-RB hydrogel, and tensile stretch tests were performed on an Instron Universal Mechanical Materials Tester (Model 3342, USA), using a setup similar to that previously described by our group[177]. Briefly, the BDDGE hydrogels were cut into strips of 1.5 mm × 0.5 mm and then cut in half. The two pieces were separated by ~1 mm; the gap was filled with uncrosslinked RB gel, covered with a glass slide and illuminated for 10 min at 220 mW/cm^2 power using the setup described above. The bonded samples were loaded onto the Instron tester and stretched to breaking point. Uncut (intact) BDDGE gels were used as the control. All experiments were performed in triplicate. See Scheme S3.1 for a diagram of the experimental setup.

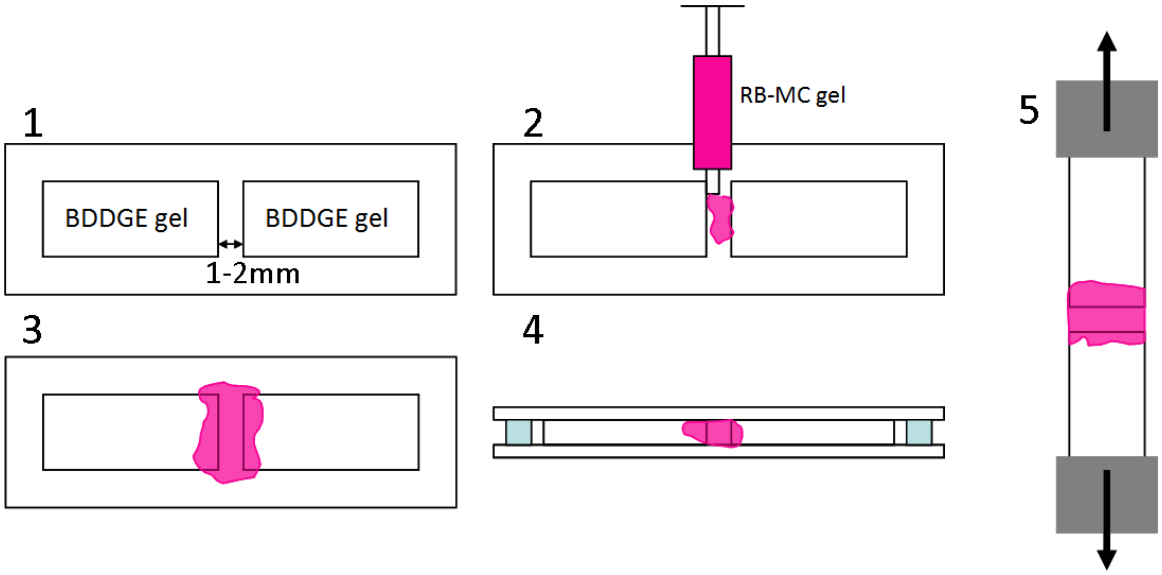

Scheme S3.1. Schematic of the main steps for measuring the mechanical properties of the photoactive RB-collagen hydrogels used to bond 2 BDDGE hydrogels together. Two pieces of a BDDGE gel are placed 1-2 mm apart on a glass slide (1), the gap between BDDGE gel pieces is filled with RB-collagen gel (2-3), covered with a second glass slide (4) and illuminated. The resulting photobonded gel is loaded onto Instron mechanical tester and stretched to breaking point (5).

Measurement of Mechanical Properties of Mouse Skin Photobonded ex Vivo

All animal studies were conducted with ethical approval from the University of Ottawa Animal Care Committee and in compliance with the National Institutes of Health Guide for the Use of Laboratory Animals. Full-thickness skin samples were harvested from 8-week old female C57 mice after sacrifice. Skin pieces (approx. 10 mm × 5 mm) were cut and placed on a glass slide separated by ~1 mm. These skin pieces were subjected to the same MC-RB photobonding procedure as described above for the BDDGE hydrogel, and then *ex vivo* tensile stretch tests were performed using the Instron Universal Mechanical Tester. The bonded samples were stretched until the breaking point. Intact mouse skin was used as the control and pulled until the skin was released from the clamps (breaking point could not be reached with the equipment used). All experiments were performed in triplicate.

In Vivo Assessment of Photobonding and Wound Healing

Eight week old female C57 mice were anesthetized with 2.5% isoflurane and the hair was shaved from the dorsal surgical area. Three pairs of 9-mm-long dorsal skin wounds per mouse were made using a surgical blade (10 mm between incisions, n = 6 mice, Figure 3.4). Incisions and treatments performed were the same for all the mice: the upper pair of wounds was sutured (2 single interrupted suture stitches, 6/0 Surgipro suture, Johnson & Johnson, USA); the middle pair was treated with the 1% MC/25 μM RB formulation (MC/RB), and the bottom pair was treated with the 1% MC/25 μM RB/0.025% PLL formulation (MC/RB/PLL). Formulations for the treatments were prepared as described above and applied using a syringe and spatula to spread the gel uniformly (~0.2 mL/wound). Control mice were shaved but did not receive any incisions or treatment. The mice were sacrificed 5 days following the treatment and full

thickness skin samples of each treated area (approx. 10 mm × 5 mm) was harvested from each mouse. Skin samples were submitted to mechanical testing (n = 8) and histology (n = 4).

Measurement of Mechanical Properties of Mouse Skin Photobonded in Vivo

Tensile stretch tests were performed on the harvested mouse skin samples after *in vivo* treatments, immediately after their harvest from sacrificed mice. Skin samples were collected and loaded onto an Instron Universal Mechanical Tester so that the incision was positioned between the clamps of the instrument and perpendicular to the direction of stretching. The samples were then stretched to breaking point.

Histology Analysis of Photobonded Tissue

Skin samples were harvested and fixed in OCT. Then, slides with 10 μm tissue sections were prepared using a cryostat device (Microm HM550 Cryostat, Thermofisher). The sections were fixed with 4% paraformaldehyde (PFA) for 1 h and then thoroughly rinsed with milli-Q water. Samples were then subjected to Masson's Trichrome or hematoxylin & eosin staining. Images of the stained sections were taken using an Axio Imager microscope (Zeiss). The thickness of epithelium layer was calculated using ImageJ software, with 3 samples randomly selected for each treatment group and the thickness calculated from three measurements in the center and edges of the wound site. No statistically significant difference was observed between groups (data not shown).

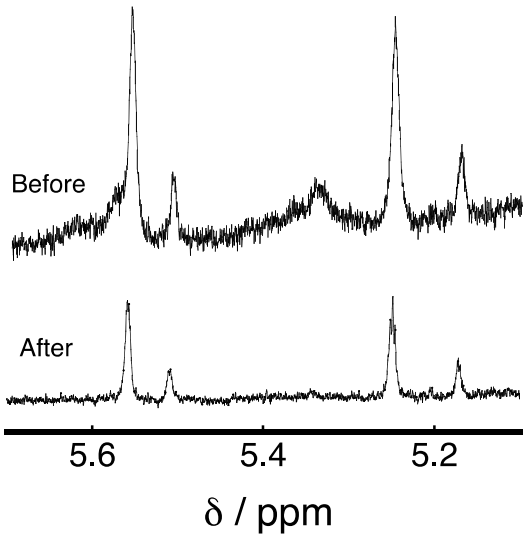

Figure S3.1. Representative ^{1}H-NMR spectra for the photoactivable collagen-rose Bengal formulation containing 0.025% PLL measured before, top, and after, bottom, 10 min irradiation. Total solid content was matched for both experiments and plots scale Y-axis are the same.

4 Paper II. Injectable Shape-Holding Collagen Hydrogel for Cell Encapsulation and Delivery Cross-linked Using Thiol-Michael Addition Click Reaction

Reprinted with permission from:

J. Pupkaite, J. Rosenquist, J. Hilborn, A. Samanta. Injectable shape-holding collagen hydrogel for cell encapsulation and delivery crosslinked using thiol-Michael addition click reaction. Biomacromolecules, 20, 3475–3484 (2019).

Abstract

Injectable hydrogels based on extracellular matrix-derived polymers show much promise in the field of tissue engineering and regenerative medicine. However, the hydrogels reported to date have at least one characteristic that limits their potential for clinical use, such as excessive swelling, complicated and potentially toxic crosslinking process, or lack of shear-thinning and self-healing properties. We hypothesized that a collagen hydrogel crosslinked using thiol-Michael addition click reaction would be able to overcome these limitations. To this end, collagen was modified to introduce thiol groups, and hydrogels were prepared by crosslinking with 8-arm polyethylene glycol-maleimide. Rheological measurements on the hydrogels revealed excellent shear-thinning and self-healing properties. Additionally, only minimal swelling (6%) was observed over a period of 1 month in an aqueous buffer solution. Finally, tests using mesenchymal stromal cells and endothelial cells showed that the hydrogels are cell-compatible and suitable for cell encapsulation and delivery. Thus, the reported thiolated collagen hydrogel crosslinked using thiol-Michael addition click reaction overcomes most of the challenges in the injectable hydrogel design and is an excellent candidate for cell delivery in regenerative medicine and tissue engineering applications. The hydrogel reported here is the first example of a self-healing hydrogel containing covalent crosslinks.

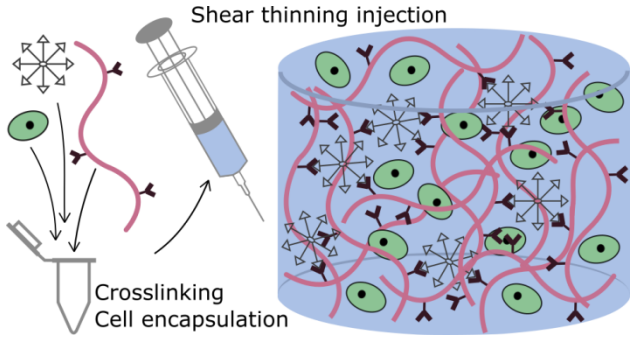

Table of contents figure of Paper II.

Introduction

The development and application of injectable hydrogels has become one of the major research directions in tissue engineering and regenerative medicine in recent years[178]. Such materials are attractive candidates for clinical translation because they can be applied during a minimally invasive surgery. Because of their high water content and tissue-like viscoelastic properties, they are highly suitable for the delivery of therapeutic cells or bioactive factors that promote tissue regeneration[179–181]. Such hydrogels are often prepared using extracellular matrix (ECM)-derived polymers. Although ECM-derived polymers are large, functionally complex, and difficult to modify, their inherent *in vivo* biodegradability is a unique advantage in regenerative medicine applications[182].

One of the major challenges in developing injectable hydrogels for potential clinical application is tuning the onset of crosslinking and the gelation kinetics to accommodate the time frames of surgical procedures[3]. Previously, we developed several injectable hydrogels based on various ECM-derived glycosaminoglycans (GAGs) that have proven to be efficacious in bone regeneration[183–186]. Many of these hydrogels were prepared using bio-orthogonal crosslinking reactions and therefore, non-toxic. Much effort was dedicated to fine-tune the gelation kinetics to match the injection time window in order to achieve a homogeneous hydrogel filling of the void or the tissue defect with no bolus formation post-injection. We observed that delayed injection of a hyaluronic acid-based quick gelling system resulted in the injection of a crushed gel[187]. Hence, we and others have developed shear-thinning/self-healing hyaluronic acid-based hydrogel systems which allow injection to be performed at the gel state, and the injection time window is thus decoupled from the gelling kinetics[87,188–192].

Nonetheless, a major disadvantage of GAG-based hydrogels is that they swell and hence do not hold their shape when stored in aqueous conditions[193–195]. Furthermore, these hydrogels lack cell-adhesive motifs and therefore do not provide an *in vivo*-like niche for cells, thus often requiring additional functionalization with bioactive peptides in order to be used for cell encapsulation[196–199]. However, hydrogels based on collagen, the most abundant polymer in the ECM, provide focal adhesion sites, as well as proliferation and migration signals for cells without additional functionalization[182]. We and others have developed several collagen-based hydrogels that have proven to be efficacious in patching large corneal perforation, corneal regeneration, and for cell encapsulation[5,26,200,201].

The most common approaches to chemically crosslink native collagen molecules are to employ carbodiimide-[40,202], diglycidyl-[203], or dialdehyde[204]-based crosslinkers to crosslink the native pendant functional groups of the protein, or use enzymes[205]. However, such crosslinking chemistries are often toxic to cells because of the involved reagents[39,41], immune-incompatible because of the use of enzymes of non-mammalian origin[206], or suffer from slow reaction kinetics. Alternatively, collagen molecules may be modified to introduce functional groups that can undergo reactions orthogonal to the encapsulated cells, making the gelation process non-toxic. To this end, methacrylamide-modified collagen has been developed enabling hydrogel fabrication by UV-initiated radical polymerization of the methacryl functionalities[207,208]. However, in order to achieve desirable cell viability and mechanical properties, such hydrogels require fastidious fine-tuning of several parameters, including the degree of collagen modification, the photo-initiator concentration, and UV irradiation dose depending on the total polymer concentration in the gel. Moreover, the low tissue penetration depth of UV light further limits the use of such hydrogels *in vivo*.

One approach to circumvent these issues could be to introduce collagen modifications that undergo bio-orthogonal reactions without UV irradiation, as mentioned earlier for other ECM-derived polymers. However, modifying collagens is challenging because of the presence of both strong electrophilic and nucleophilic functional groups on the same polymer, thus, very few such modifications have been reported so far. We previously investigated the potential of Michael addition reaction between methacrylamide collagen and a multifunctional polyethylene glycol (PEG) thiol to form hydrogels for cell encapsulation and observed that such thiol-Michael addition reaction is nontoxic[26], a finding also demonstrated by others[64,104,209,210]. However, these hydrogels are not injectable or self-healing, in addition to being inhomogeneous, suffering from slow kinetics of the crosslinking reaction and requiring basic pH or added catalyst for crosslinking to take place[26]. Furthermore, similar to GAG-based hydrogels, collagen-based injectable hydrogels reported to date undergo swelling and do not hold their shape in an aqueous environment[193–195,210]. Thus, after *in vivo* injection, these hydrogels undergo undesirable expansion because of water absorption, increasing their volume beyond the limits of the original void and causing the hydrogel to push the surrounding tissue[193,211].

Here, we report a novel thiol-modified collagen and investigate its suitability to form injectable hydrogels after crosslinking through a Michael addition reaction with a multifunctional PEG-maleimide. The mechanical properties of these hydrogels can be adjusted by varying preparation parameters. Importantly, the hydrogels reported in this paper overcome all the challenges discussed above and possess key properties desirable in an injectable hydrogel: they are shear-thinning/self-healing and thus injectable in the gel state, but exhibit no swelling in an aqueous buffer even for a prolonged period of time. Moreover, the reported hydrogel is the

first example of a self-healing material that contains covalent crosslinks. We also demonstrate cell survival after encapsulation and injection using these hydrogels.

Experimental Section

Materials

5,5′-Dithiobis(2-nitrobenzoic acid) (DTNB), 8-arm 10 kDa PEG-maleimide, phosphate buffered saline (PBS) powder, γ-thiobutyrolactone, Trizma base powder, glutathione, collagenase from *Clostridium histolyticum* were purchased from Sigma-Aldrich (Sweden). Porcine type I collagen (NMP collagen PS) was purchased from Nordic Biolabs (Sweden).

Methods

Synthesis of Thiol-Collagen

Collagen was dissolved in water (0.5% w/v). The pH was adjusted to 10 with NaOH (2 M). γ-Thiobutyrolactone (10 molar equivalents with respect to lysine and arginine amines, based on 114 amines from lysine and arginine combined per collagen molecule) was mixed with an equal volume of dimethyl sulfoxide and added to the collagen solution while stirring. After adjusting the pH to 10, the reaction mixture was stirred overnight, and then the pH was adjusted to 4.5 with HCl (5 M), dialyzed against water (pH 4.5) for 3 days, and lyophilized. Stock solution (10% w/w) was prepared in water and kept at 4 °C.

Ellman's Assay

To determine the degree of thiol modification, the absorbance of a solution containing thiol-collagen (0.05%) and DTNB (0.4 mg/mL) in PBS (flushed with argon) was measured at 412 nm.

Hydrogel Preparation

A syringe mixing system described previously[176] was used to prepare the hydrogels by mixing thiol-collagen stock solution (10% w/w), water, and 8-arm 10 kDa PEG-maleimide solution. The amounts of all of the components were calculated in such a way as to yield the desired final concentration of thiol-collagen (2%) and the desired ratio between thiol and maleimide groups (1:1, 1:10, 1:20, or 1:40). The gels were cast as 0.5 mm-thick sheets, cured overnight in a humid atmosphere and stored in PBS at room temperature.

Rheological Measurements

Viscoelastic properties of the hydrogels were measured using a Discovery Hybrid Rheometer 2 (TA Instruments, Sollentuna, Sweden) at 25 °C. Storage modulus (G′), loss modulus (G″), and tan δ were calculated from frequency sweep experiments (0.1−25 Hz at oscillation strain of 0.267%) performed on hydrogel discs using 8 mm stainless steel parallel plate geometry under axial load of 300 mN. The linear viscoelastic region (LVR) limit was calculated from amplitude sweep measurements (increasing oscillation strain up to 30% at 1 Hz oscillation frequency) performed same as above. The LVR limit was defined as the oscillation strain value after which $(y_{i+1} - y_i)/y_i > 0.01$, where y_i and y_{i+1} are two adjacent G′ values. The properties of hydrogels containing different thiol/maleimide ratios were compared using one-way ANOVA, followed by Tukey's test (n = 3 independent samples); reported as average ± standard deviation (SD). The significance value was set at $p < 0.05$. To evaluate strain recovery of thiol-collagen hydrogel and mouse heart, G′ was measured under alternating low and high oscillation strain conditions (low strain = 1%, high strain = 12%) at 25 °C and 1 Hz oscillation frequency using 8 mm diameter stainless steel parallel plate geometry. For this experiment, fully crosslinked hydrogels (6 months after preparation) were used. To evaluate the injectability of the hydrogels, viscosity under continuous flow was measured with the increasing shear rate (from

0.01 to 30 s^{-1}) using 20 mm stainless steel parallel plate geometry on hydrogels cast directly on the rheometer plate immediately and 5 h after mixing all the hydrogel components. To evaluate the shear-thinning and self-healing properties of the hydrogels, the hydrogels were extruded directly on the rheometer plate from a syringe immediately, 5, and 16 h after mixing all the hydrogel components and the viscosity was measured under continuous flow conditions switching the shear rate between 0.01 and 10 s^{-1} every 60 s, using 20 mm stainless steel parallel plate geometry. To evaluate the long-term shear-thinning and self-healing properties of the hydrogels, fully crosslinked hydrogels (stored in PBS for over 2 years), were subjected to continuous flow conditions with alternating low and high shear rates as described above.

Differential Scanning Calorimetry (DSC)

A Q2000 differential scanning calorimeter (TA Instruments, USA) was used to record heating scans from 8 to 80 °C (heating rate of 5 °C/min). Denaturation temperature was recorded after linear integration of the endothermic peaks (n = 3 independent samples), reported as the average of all hydrogel formulations ± SD (n = 4 formulations).

Enzymatic Degradation in Vitro

Hydrogels were cut into 8 mm-diameter discs and incubated for 1 h in Tris-HCl buffer (pH 7.4) at 37 °C. Excess liquid was removed and the hydrogels were weighed. After that, they were placed in preheated Tris-HCl buffer containing $CaCl_2$ (5 mM) and collagenase (5 U/mL) and incubated at 37 °C. At each time point, the gels were weighed and placed into a fresh preheated collagenase solution.

Degradation under Reducing Conditions in Vitro

For weight measurements, hydrogel discs (8 mm diameter) were placed in PBS at 37 °C for 30 min, weighed, and then placed in glutathione solution (10 mM in PBS) at 37 °C. At each

time point, hydrogels were weighed and placed into fresh glutathione solution. For G′ measurements, baseline G′ of hydrogel discs (8 mm diameter) was determined from frequency sweep rheology at an oscillation strain of 0.267% as described above. The discs were placed in glutathione solution (10 mM in PBS) at 37 °C. At each time point, G′ of the hydrogels was measured. Reported are G′ values at 1.1 Hz. Glutathione solution was periodically refreshed.

Hydrogel Swelling

The hydrogels were cut into 8 mm-diameter discs, blotted with filter paper, weighed, and incubated in PBS (pH 7.4) at 37 °C. At each time point, the hydrogels were weighed and placed back into the PBS.

Cell Culture

All cell cultures were maintained in the cell culture incubator (37 °C, 5% CO_2). The mouse bone marrow stromal cell line (BMSC, W20-17, ATCC, USA) was maintained in Dulbecco's modified Eagle medium with glucose (4.5 g/L, Gibco, USA), supplemented with fetal bovine serum (10%) and penicillin−streptomycin (1%). Human umbilical vein endothelial cells (HUVEC, Gibco, USA) were maintained in complete M200 medium (Gibco, USA) with penicillin−streptomycin (1%).

Cell Injection

Thiol-collagen hydrogels were prepared according to the same protocol as mentioned above, with the final thiol-collagen concentration of 1% and the thiol/maleimide ratio of 1:20. Cells were suspended in a minimal amount of cell growth medium. Cells (either BMSC or HUVEC) were mixed into the hydrogel by gentle pipetting to yield the final cell concentration in the hydrogel of 35 000 cells/50 μL and 70 000 cells/50 μL, respectively, and transferred into a syringe. Cell-carrying hydrogels were extruded through a 27-gauge needle (at the approximate

rate 20 μL/s) onto thin bottom μ-slides and incubated for 1 h in a cell incubator, followed by cell viability evaluation. Cells suspended in PBS were used as control.

Hydrogel 3D Cell Culture

Hydrogels carrying either BMSC or HUVEC were prepared according to the same protocol as for the cell injection experiment. The cell-carrying hydrogels were cast into thin-bottom μ-slides and cured for 30 min at 37 °C in cell culture incubator. Afterward, the appropriate cell growth medium was added. Cell viability was measured after 24 h, 48 h, and 4 days in culture (n = 4).

Cell Viability Determination

Cell viability was measured using the LIVE/DEAD Viability/Cytotoxicity Kit (Invitrogen, Thermofisher, Sweden). Growth medium was aspirated and the gels were washed with PBS (this step was omitted for the cell injection experiments). Calcein AM and ethidium homodimer-1 stock solutions were diluted with PBS ×3000 and ×500, respectively, added to the slides with the hydrogels, and incubated (37 °C, 30 min). The solution was aspirated and the hydrogels were washed with PBS. Hank's balanced salt solution (no calcium, no magnesium, no phenol red) was added to fully submerge the hydrogels. The cells were imaged using a Zeiss LSM700 confocal microscope (Germany), 3 images per well were taken, and all cells were counted in each image. Cells that stained both red and green were not counted as live cells.

Results and Discussion

Synthesis of Thiol-Functionalized Collagen and Hydrogel Formation

We sought to design a collagen-based injectable and shape-holding hydrogel system for cell delivery, whose injection time window is decoupled from gelling kinetics to allow easy

handling and reproducible gel characteristics upon use. Specifically, we aimed to overcome several challenges in injectable hydrogel design and develop a hydrogel system that has the following characteristics: (1) is prepared using cell-compatible crosslinking chemistry allowing efficient cell encapsulation, (2) shows minimal swelling, and (3) exhibits shear-thinning/self-healing behavior. We hypothesized that a Michael addition reaction between thiol and maleimide functional groups would be suitable for this purpose.

Because collagen lacks thiol functional groups, it needs to be modified in order to be able to participate in thiol-Michael addition reactions. Collagen was functionalized employing the nucleophilicity of the ε-amino group of the lysine side chain[212,213]. As the pK_a of this amine is 10.5, the reaction was carried out at pH 10 by the nucleophilic ring opening of γ-thiobutyrolactone by the ε-amino group (Figure 4.1a) resulting in a thiol-functionalized collagen. The degree of modification was assessed by Ellman's assay and was found to be 10% with respect to the ε-amino groups in collagen. To demonstrate hydrogel formation via thiol-Michael addition click reaction, aqueous solutions of thiol-collagen and 8-arm PEG-maleimide (Figure 4.1b) were mixed together at pH 6−7. Crosslinking was confirmed qualitatively by lifting the hydrogel from the mould (Figure 4.1c). Additionally, the viscoelastic behavior of the hydrogels was analyzed using rheology (Figure S4.1). Moreover, DSC on crosslinked hydrogels revealed a denaturation temperature of 49.9 ± 0.7 °C (Figure S4.2), which is far above the denaturation temperature of collagen physical gel[214], thereby confirming covalent crosslinking.

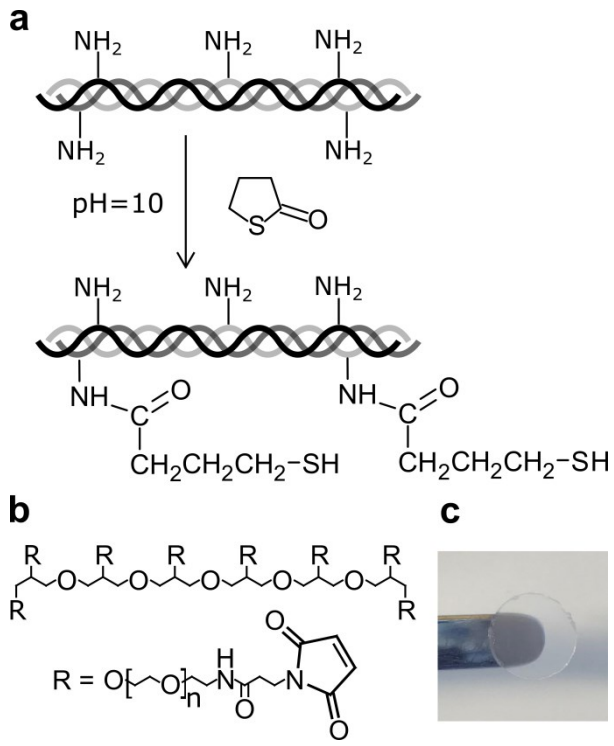

Figure 4.1. (a) Thiol-collagen synthesis scheme; (b) 8-arm PEG-maleimide used in this study; (c) photograph of demoulded hydrogel (t-c-h20, Table 4.1).

Table 4.1. Thiol-collagen hydrogel formulations used in this study.

Thiol-collagen hydrogel	Thiol: maleimide ratio	Collagen concentration		PEG-maleimide concentration		Thiol concentration (μM)[a]	Maleimide concentration (μM)
		%	μM	%	μM		
t-c-h1	1:1	2	67	0.0625	62.5	456	500
t-c-h10	1:10	2	67	0.5	500	456	4000
t-c-h20	1:20	2	67	1	1000	456	8000
t-c-h40	1:40	2	67	2	2000	456	16000

[a]Calculated based on the degree of collagen modification measured by Ellman's assay.

Viscoelastic Properties of Thiol-Collagen Hydrogels

In order to investigate the tunability of the mechanical properties of the developed hydrogels, different thiol/maleimide ratios ranging from 1:1 to 1:40 were tested by varying the amount of added PEG-maleimide while keeping the thiol-collagen concentration constant (Table 4.1). The thiol/maleimide ratio of 1:0.5 failed to result in a hydrogel that could be demoulded. Gels were subjected to oscillatory rheology under varying frequency or amplitude. The storage modulus (G′) and loss modulus (G″) values indicating the elastic and viscous response of the hydrogels, respectively, were extracted from the frequency sweep measurements, whereas the LVR limits were calculated from the amplitude sweep experiments. Surprisingly, there were no significant differences in the G′ values of different hydrogels with different thiol/maleimide ratios up to 1:20, beyond which the hydrogels became significantly softer with low G′ value and high tan δ (Figure 4.2a,b). T-c-h20 hydrogels were found to have the highest storage modulus (6.4 ± 0.2 kPa) while G′ of t-c-h40 hydrogels was significantly lower (3.9 ± 0.5 kPa, $p < 0.05$). On the other hand, the t-c-h40 had the highest tan δ = 0.066 ± 0.004, while the tan δ of t-c-h20 was the lowest at 0.043 ± 0.007 ($p < 0.05$). The decrease in G′ and increase in tan δ of t-c-h40 hydrogels can be attributed to the decrease in crosslinks between collagen molecules because of increased grafting of PEG chains onto collagen. The LVR limit (indicating the elastic limit of the hydrogels) was determined from the measurement of G′ with increasing oscillation amplitude, defined as the oscillation amplitude value at which G′ is no longer constant. There were no significant differences observed among hydrogels of different formulations, with the overall average LVR limit of approximately 9 ± 2% oscillation strain (Figure 4.2c) and calculated average shear yield strength of 0.6 ± 0.1 kPa. All following experiments were performed using t-c-h20.

When considering potential tissue engineering applications, it may be important to design a hydrogel with viscoelastic properties that mimic the intended tissue because physical properties of the environment affect tissue regeneration and cellular responses[69,215–219]. Similar mechanical properties allow for more even stress distribution between the host tissue and the implant. One of the more extreme examples is the heart, which undergoes continuous expansions and contractions, experiencing global longitudinal strain of 16−20%[220] with segmental strain of 14−19%[221]. Therefore, we compared the mechanical properties of fully crosslinked hydrogels (stored in PBS for 6 months) with the passive properties of *ex vivo* mouse heart. The purpose of this experiment was to investigate whether the hydrogels self-heal and recover their original modulus (strain recovery) or undergo plastic deformation when subjected to a strain, which is outside the linear stress−strain region of the hydrogel. Overall, the measured G′ of the heart was comparable with that of the hydrogels developed here (Figure S4.3) (as well as in agreement with previously reported values)[222]. The mouse heart had a surprisingly low LVR limit (1%); however, it is important to note that these are the passive properties of *ex vivo* tissue and the properties of contracting heart would be different because of the active properties of cardiomyocytes. Most notably, both the heart and the hydrogel showed similar behavior in response to repeated conditions of low and high strain (Figure S4.3): G′ decreases when the strain is high (outside the linear stress−strain region for both the hydrogel and heart) but recovers when the strain is lowered (within the linear stress−strain region for both the hydrogel and heart). The difference in the heart G′ under the two conditions is almost 2-fold, while the G′ of the hydrogel is reduced by about 20% under high strain, compared to low strain.

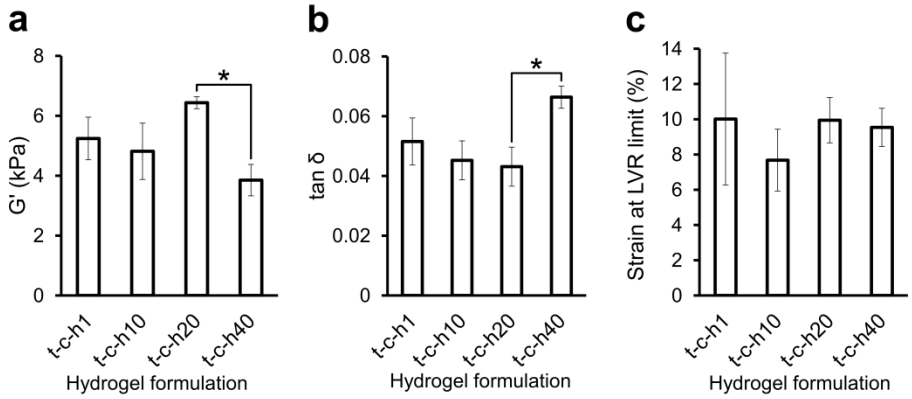

Figure 4.2. Characterization of the rheological properties of thiol-collagen hydrogels containing different amounts of 8-arm PEG-maleimide: (a) storage modulus (G′) at 1.1 Hz oscillation frequency; (b) tan δ at 1.1 Hz oscillation frequency; (c) oscillation strain at which the LVR limit is observed using 1.0 Hz oscillation frequency. All measurements were performed at 25 °C. Error bars = SD; *$p < 0.05$ (one-way ANOVA, followed by Tukey's test, n = 3 independent samples).

Injectability, Shear-Thinning, and Self-Healing Properties of Thiol-Collagen Hydrogels

Next, we examined the physical properties of the hydrogels that are relevant for cell delivery. Specifically, injectability and shear-thinning/self-healing properties were measured (Figure 4.3). First, to evaluate the injectability of the hydrogels, viscosity was measured with increasing shear rate, immediately after mixing the hydrogel components together (Figure 4.3a). The hydrogels exhibited a rapidly decreasing viscosity with an increasing shear rate, reaching approximately 6 Pa at 5 s^{-1}. Such shear-thinning indicates that the hydrogels are injectable, which was also confirmed practically by injecting the hydrogels through a 27-gauge needle. Second, viscosity was measured to assess the shear-thinning/self-healing properties of the hydrogels (i.e., their ability to undergo shear-thinning under high shear rate and recover the initial viscosity under low shear rate conditions repeatedly) (Figure 4.3b). The hydrogels were subjected to a continuous experiment of repeated intervals of low and high shear rate conditions of 0.01 and 10 s^{-1}, respectively. The hydrogels exhibited 99.8% reduction in viscosity at the change from low to high shear rate conditions. Initial viscosity was recovered to 98% at the return of low shear rate conditions. This behavior was not changed by raising the temperature to 37 °C (Figure S4.4).

Identical measurements were also carried out 5 h after mixing all the hydrogel components together. Hydrogels exhibited similar injectability and shear-thinning/self-healing properties as just-prepared hydrogels (Figure 4.3c,d).

Such shear-thinning/self-healing behavior, immediately and 5 h after mixing all the hydrogel components together, can be explained by taking into consideration the time required to achieve saturation in stiffness for thiol-collagen hydrogels, which is approximately 8 h (Figure S4.5). Before this time point, the newly formed thioether bonds in the hydrogel can reversibly

break under high shear rate conditions in a retro-Michael reaction and reform under low shear rate conditions in a Michael addition reaction. Such reversibility of thioether bonds in thiol/maleimide Michael addition reaction and exchange reaction have also been reported in the presence of excess thiols, prior to thiosuccinimide ring hydrolysis[99,223,224]. This is an important property when considering clinical applications because surgical procedures often require that the hydrogel be premixed and kept in a syringe or a catheter for 1 h or longer until injection[3].

Next, we investigated if the hydrogels maintain shear-thinning/self-healing properties only for a short time after hydrogel preparation, or if it persists even after the crosslinking reaction is complete. As the hydrogel requires 8 h to reach saturation in G′, identical experiments were performed 16 h after gel preparation at 25 and 37 °C. The hydrogels showed similar shear-thinning/self-healing properties as before (Figure S4.6). Moreover, the same measurements were also performed on 2-year-old hydrogels, which revealed that they maintained a similar shear-thinning/self-healing character as before (Figure S4.7).

Hence, it can be concluded that the reported thiol-collagen hydrogels have true shear-thinning/self-healing properties. This is unique as there are no other reports to date of shear-thinning/self-healing hydrogels that contain covalent crosslinks. Although the self-healing behavior in the first few hours after hydrogel preparation can be explained by the reversibility of Michael reaction, especially before the hydrolysis of the thiosuccinimide ring, this cannot be true for older hydrogels. Therefore, we hypothesize that because the degree of collagen thiol modification is low, covalent crosslinks (12 maximum crosslinks possible per collagen molecule) increase the propensity of interhelical assembly rather than significantly contribute toward increasing the storage modulus of the hydrogel. Under high shear rate, as in the shear-

thinning/self-healing experiment, or high strain, as in the strain recovery experiment, such assemblies can break and reform when the shear rate or strain is lowered.

The demonstrated shear-thinning/self-healing properties of injectable thiol-collagen hydrogels are relevant for regenerative medicine applications because they allow for hydrogel flow during injection followed by recovery of high viscosity, which prevents the hydrogel from escaping the site of injection. Conversely, if the hydrogel is injected into a contractile tissue, such as the heart, it will likely move along with the contraction and expansion of the tissue, while staying in place during periods of rest. Such behavior is advantageous because a nonmoving bolus of injected hydrogel may interfere with electric signals in the heart, causing arrhythmia[225].

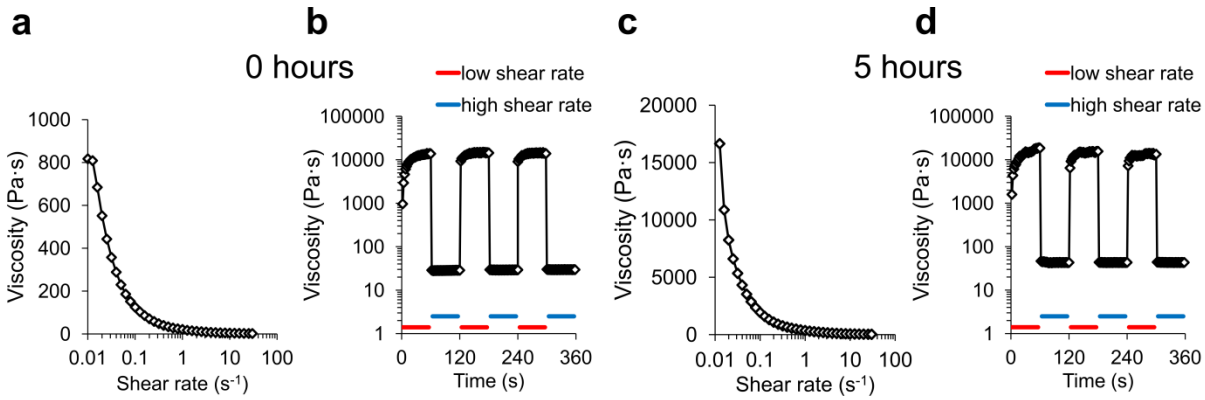

Figure 4.3. Injectability and shear-thinning/self-healing properties of thiol-collagen hydrogels: (a) viscosity at increasing shear rate measured immediately after hydrogel preparation; (b) viscosity measured at repeated low shear rate (0.01 s^{-1}) and high shear (10 s^{-1}) rate conditions immediately after hydrogel preparation; (c) viscosity at increasing shear rate measured 5 h after hydrogel preparation; (d) viscosity measured at repeated low shear rate (0.01 s^{-1}) and high shear rate (10 s^{-1}) conditions 5 h after hydrogel preparation. All measurements carried out on t-c-h20 hydrogels (Table 4.1) at 25 °C, shown are representative curves.

Thiol-Collagen Hydrogel Behavior in Aqueous Solutions

The injectable thiol-collagen hydrogels were evaluated to assess their swelling and shape changes when stored in an aqueous solution. Swelling tests were performed in PBS (pH 7.4) at 37 °C. Remarkably, for up to 30 days only 6% swelling was observed (Figure 4.4a). Furthermore, the hydrogels maintained their shape when stored in PBS at room temperature for 2 years (Figure 4.4b). Hence, it can be concluded that the correct balance between the hydrophilicity of the polymer chains and crosslink density in the hydrogel leads to higher elastic pressure of the hydrogel than its osmotic pressure, which is rarely observed in injectable hydrogels. The degree of material swelling is an important property to consider for *in vivo* applications because prolonged swelling (edema) is often harmful to tissues[211]. Thus, a material that undergoes minimal or no swelling may be preferable for injection into tissues sensitive to swelling.

Additionally, we noted that the stiffness of the hydrogels increases over time when stored in an aqueous solution (PBS, pH 7.4) at room temperature. Therefore, the initial storage modulus of the hydrogels (as prepared) was measured after allowing sufficient time to crosslink in a humid atmosphere; then the hydrogels were incubated in PBS and the changes in G′ were monitored (Figure 4.4c). The storage modulus of the hydrogels reached a plateau value within 3 days. After 3 days of incubation, the G′ of hydrogels was approximately 20% higher compared to initial measurement, a significant increase ($p < 0.05$). As the hydrogels were prepared in water, the observed increase in G′ is attributed to the Hofmeister effect of phosphate anions on protein gels[226].

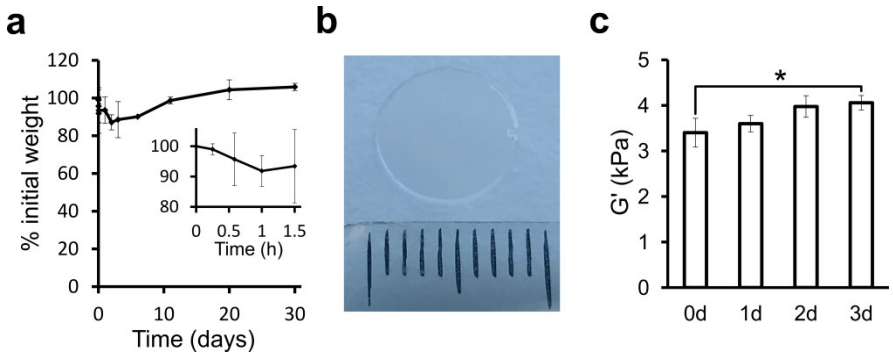

Figure 4.4. Properties of thiol-collagen hydrogels stored in aqueous conditions for prolonged periods of time: (a) swelling of thiol-collagen hydrogels stored in PBS at 37 °C for 30 days, expressed as percent of initial weight; inset: swelling over the first 1.5 h; (b) photograph of thiol-collagen hydrogel after being stored in PBS for 2 years (the original shape of 8-mm diameter disc), scale = 1 cm; (c) storage modulus (G′) of thiol-collagen hydrogels stored in PBS at room temperature over the first 3 days after hydrogel preparation. All experiments performed on t-c-h20 hydrogels (Table 4.1). Error bars = SD, $*p < 0.05$ (one-way ANOVA, followed by Tukey's test, n = 3 independent samples).

Degradation Properties of Thiol-Collagen Hydrogels

When designing hydrogels for various regenerative medicine and tissue engineering applications, it is crucial to consider their degradation properties, as it will affect the release of hydrogel load (cells or therapeutic compounds) and the replacement of the hydrogel with tissue[227,228]. To this end, degradation properties of thiol-collagen hydrogels were evaluated *in vitro* mimicking *in vivo* conditions: collagenase was used as a model of enzymatic degradation. The average overall rate of degradation by collagenase was 0.08 ± 0.01 mg/min, until the hydrogels were degraded to a degree that made it impossible to handle them after 6 h (Figure 4.5a).

Furthermore, the Michael addition product of thiol and maleimide functional groups has been reported to undergo exchange reaction in the presence of excess thiols, thus cleaving the crosslinking bonds[99]. A specific molecule of interest for *in vivo* hydrogel applications is glutathione, an intracellular and circulating reducing agent[229]. Hence, we have tested the degradation of these hydrogels in the presence of glutathione. The hydrogels were found to be dissolved slowly over a period of 1 month when treated with glutathione solution. Degradation was monitored using two different methods: measuring the weight and G′ of the hydrogels (Figures 4.5b and S4.8). The average rate of degradation in weight was 0.73 ± 0.14 mg/day, while G′ decreased by 97 ± 8 Pa/day. Given that the concentration of glutathione used in our experiments mimics the intracellular concentration (0.5−10 mM)[230], while the extracellular concentration of glutathione is much lower (2−20 μM)[231], it is likely that the degradation of thiol-collagen hydrogels *in vivo* would be dominated by enzymatic processes.

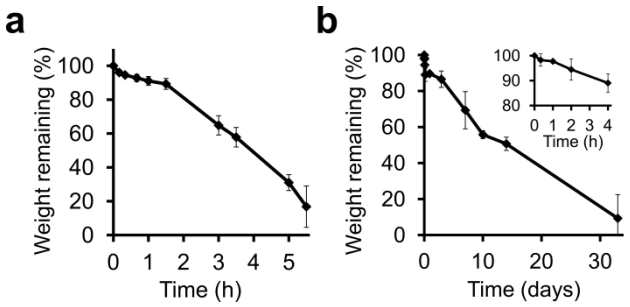

Figure 4.5. Degradation of thiol-collagen hydrogels under different *in vitro* conditions: (a) enzymatic degradation in collagenase solution (5 U/mL), expressed as percent of initial weight remaining; (b) degradation of hydrogels under reducing conditions in glutathione solution (10 mM), expressed as percent of initial weight remaining; inset: degradation of the hydrogels over the first 4 h. All experiments performed on t-c-h20 hydrogels (Table 4.1). Error bars = SD (n = 3).

Cell-Compatibility of Thiol-Collagen Hydrogels

Experiments were carried out to test the cell-compatibility of thiol-collagen hydrogel preparation and injection procedure and, subsequently, the ability of the hydrogels to sustain an encapsulated 3D cell culture *in vitro*. Mouse BMSCs and HUVECs were chosen as model cells for the experiments because mesenchymal stem cells and angiogenic cells are two common types of cells used in regenerative research[232].

First, we assessed the acute effect of encapsulating and injecting cells in a thiol-collagen hydrogel. Cells were encapsulated inside thiol-collagen hydrogels immediately after mixing the hydrogel components, injected through a fine-gauge needle and cell viability was assessed using live/dead assay 1 h post-injection (Figure 4.6). No significant differences were detected between hydrogel and PBS control for either BMSC or HUVEC viability. The viability of both cell types was ≥90%. Thus, thiol-Michael click reaction between thiol-collagen hydrogel components and subsequent injection is compatible with the tested cells.

Second, we investigated the ability of the hydrogels to sustain an embedded 3D cell culture *in vitro*. Hydrogels with encapsulated cells were prepared as above and following casting in cell culture plates, 3D cell cultures were carried out, and the viability of cells was evaluated using live/dead assay (Figure 4.7). The hydrogel sustained BMSC viability of ≥80% for up to 4 days. Approximately 70% HUVECs were viable for up to 4 days (Figures 4.7 and S4.9). Both types of cells exhibited good viability even further away from the outer layers of the hydrogel, indicating sufficient nutrient and oxygen diffusion.

Thus, our results are in agreement with previous research demonstrating that thiol-Michael click reaction is not toxic to encapsulated cells[26,64,104,209], although there are thiol functional groups present on the cell-surface proteins[233]. This is plausibly explained by the fact

that cell-surface thiol concentration is relatively low and the diffusion of cells and hydrogel components is limited because of their large size and the high viscosity of hydrogel precursor solution, reducing the possibility of cross-reaction.

While prolonged survival *in vitro* may not be crucial when considering therapeutic cell delivery immediately post-encapsulation, it is worth noting that the hydrogels maintained their shape for 4 days, in contrast to thiol-collagen hydrogel degradation using collagenase, which degraded the hydrogel within 6 h (although it is unclear to what degree the encapsulated cells may have replaced the hydrogel with secreted ECM). This suggests that under certain conditions (i.e., low external forces and low enzyme activity), the thiol-collagen hydrogels may remain at the site of injection for at least several days, allowing for slow cell release and native cell infiltration. Conversely, exposed to high enzymatic activity (e.g., at the site of myocardial infarction[234]), the hydrogels might be degraded and release encapsulated cells in a much shorter period of time. This is an important consideration for future research into *in vivo* application of thiol-collagen hydrogels for tissue engineering and regenerative medicine.

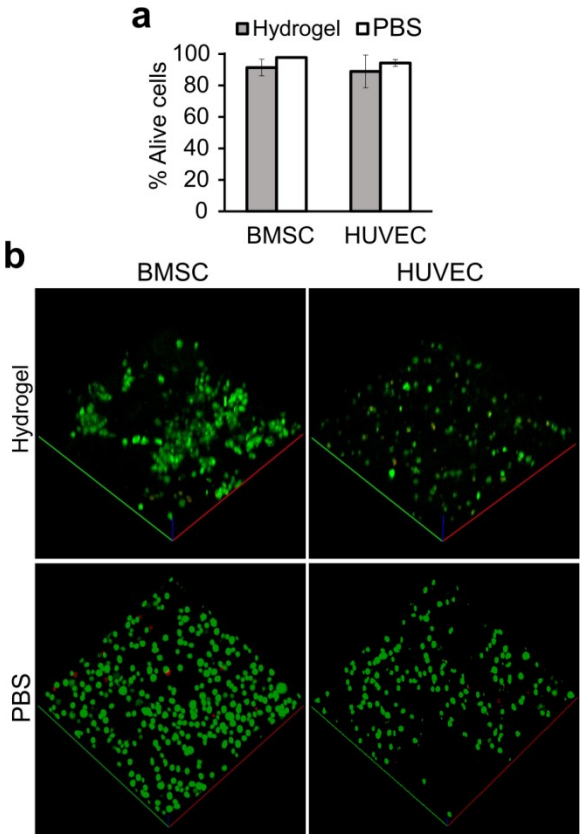

Figure 4.6. Cell viability 1 h after injection through a 27-gauge needle using thiol-collagen hydrogel or PBS as carriers, assessed using live/dead assay: (a) percentage of alive BMSCs and HUVECs; (b) representative 3D scans of BMSCs (left) and HUVECs (right) injected into a cell culture dish using thiol-collagen hydrogel or PBS as the carrier, after live/dead staining; green = live cells, red = dead cells. Error bars = SD (n = 4).

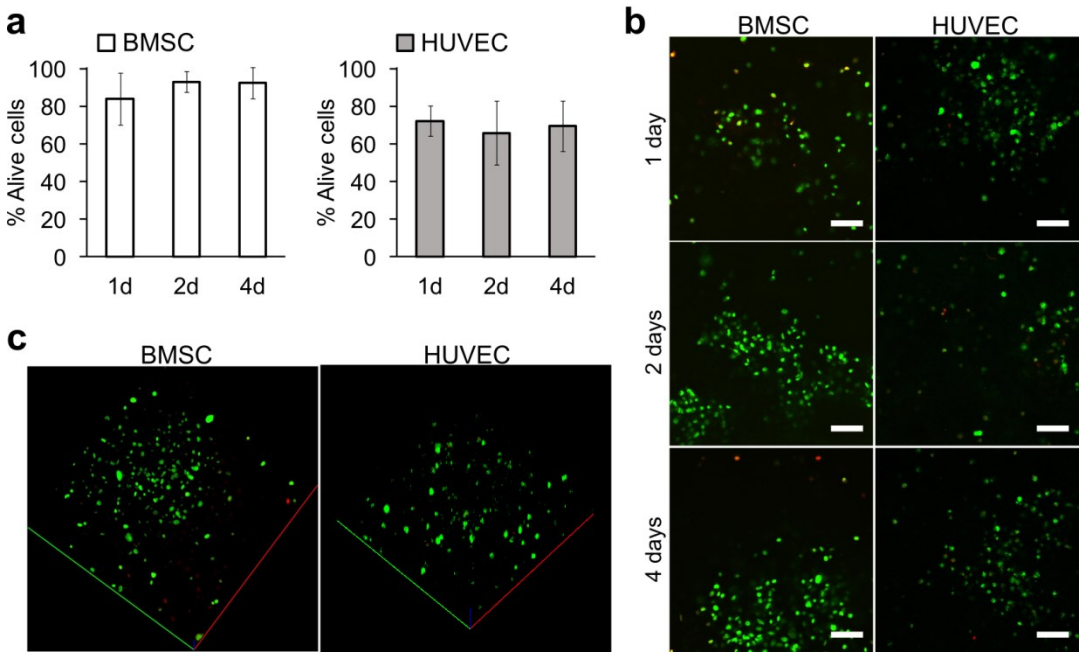

Figure 4.7. *In vitro* 3D cultures of BMSCs and HUVECs encapsulated in thiol-collagen hydrogels. Cell viability was assessed using live/dead assay: (a) percentage of alive BMSCs and HUVECs for up to 4 days in 3D culture; (b) representative images of BMSC and HUVEC cultures at different time points; (c) representative 3D scans of BMSC and HUVEC cultures after 4 days; green = alive cells, red = dead cells. Error bars = SD (n = 4). Scale bar = 100 μm.

Conclusions

In summary, this study demonstrates the modification of collagen to create thiol-collagen and its subsequent use in hydrogel preparation using thiol-Michael click reaction. The viscoelastic properties of the hydrogels were assessed using rheological measurements. Importantly, the hydrogels possess shear-thinning and self-healing properties, allowing hydrogel injection at 5 and 16 h after hydrogel preparation. This is of particular interest when considering clinical applications, where even minimally invasive surgery times may be an hour or longer. The hydrogels also demonstrate the ability to withstand repeated changes between low and high shear rate conditions showing excellent shear-thinning with minimal loss of initial viscosity when returned to low shear rate conditions. Moreover, the thiol-collagen hydrogels maintain their shape and show only minimal (6%) swelling when stored in an aqueous buffer for up to a month, which is relevant when considering clinical applications where pressure created by hydrogel swelling would be undesirable. Lastly, the thiol-collagen hydrogels are also suitable for cell delivery as demonstrated by more than 90% viability of encapsulated BMSCs and HUVECs after injection. The viability of encapsulated BMSCs and HUVECs is maintained at about 80 and 70%, respectively, for up to 4 days in the 3D culture *in vitro*. Thus, the hydrogels based on thiol-collagen and thiol-Michael addition click reaction demonstrate a combination of physical and biological properties highly desirable for tissue engineering and regenerative medicine applications.

Acknowledgements

The authors thank Professor Karl-Henrik Grinnemo for providing mouse heart samples and Julie Josso for experimental support.

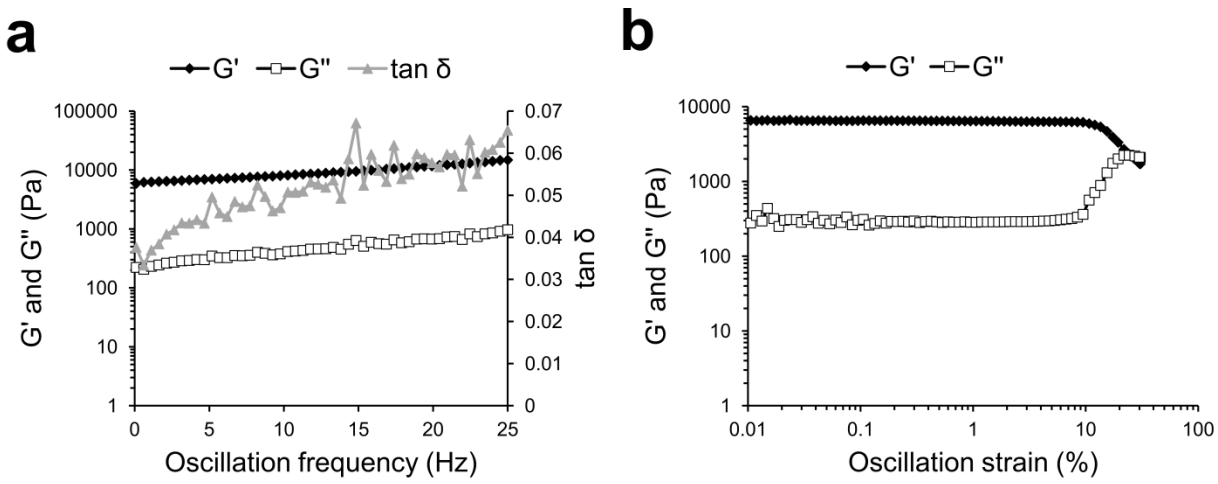

Figure S4.1. Representative graphs of the rheological property measurements of thiol-collagen hydrogels: a) storage modulus (G′), loss modulus (G″), and tan δ measured in a frequency sweep experiment with increasing frequency up to 25 Hz at 0.267% oscillation strain; b) G′ and G″ measured in an amplitude sweep experiment with increasing oscillation strain up to 30% at 1 Hz oscillation frequency in order to determine the linear viscoelastic region limit of the hydrogel. Hydrogel formulation t-c-h20.

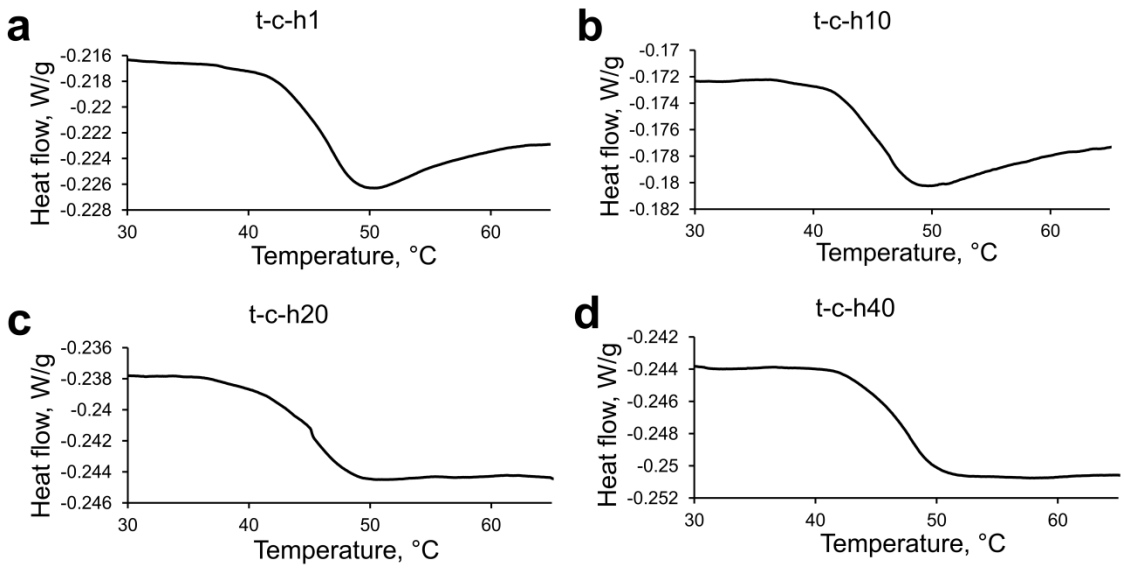

Figure S4.2. Representative graphs of differential scanning calorimetry measurements of the reported thiol-collagen hydrogel formulations: a) t-c-h1; b) t-c-h10; c) t-c-h20; d) t-c-h40.

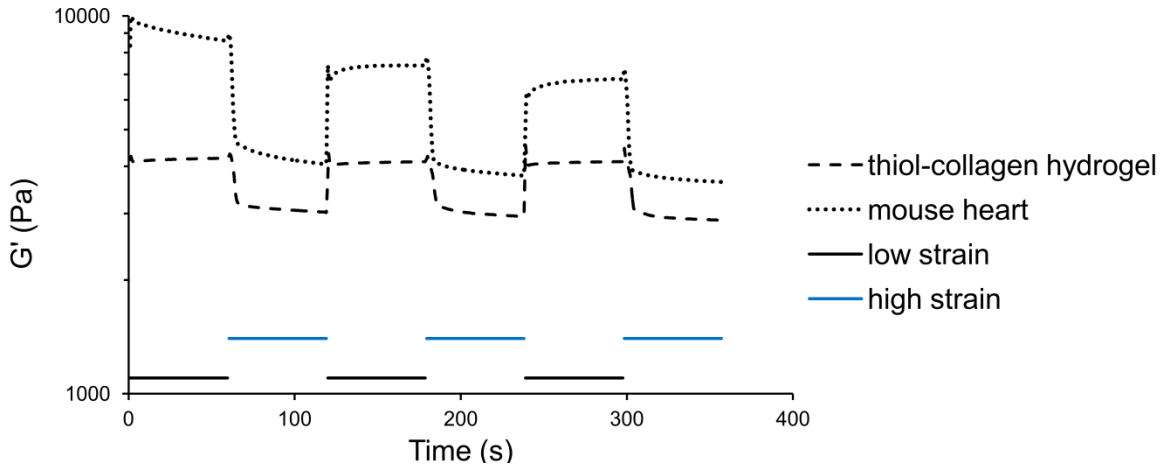

Figure S4.3. Strain recovery of fully crosslinked thiol-collagen hydrogels (stored for 6 months) and mouse heart: G′ measured under alternating low and high oscillation strain conditions (low strain = 1%, high strain = 12%). T-c-h20 hydrogels were cut in 8 mm-diameter discs. Healthy *ex vivo* mice hearts were dissected to remove the atria and right ventricle and to open up the left ventricle along to the long axis of the heart. Experiments performed at 25 °C at 1 Hz oscillation frequency using 8 mm-diameter stainless steel parallel plate geometry. Shown are representative graphs.

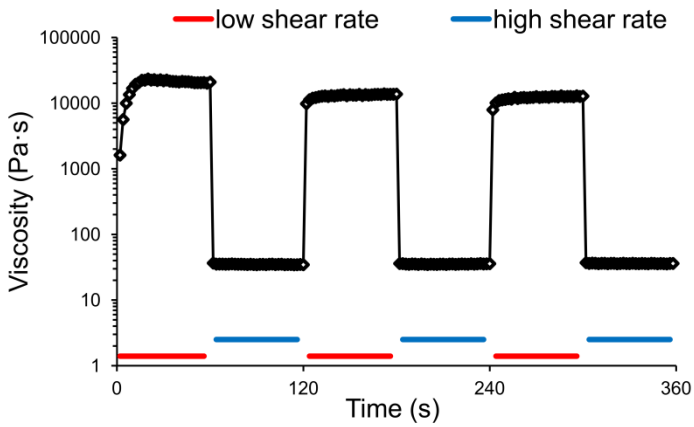

Figure S4.4. Shear-thinning/self-healing properties of thiol-collagen hydrogels at 37 °C: viscosity measured continuously at alternating low shear rate (0.01 s^{-1}) and high shear (10 s^{-1}) rate conditions 10 min after hydrogel preparation. Hydrogel formulation t-c-h20, representative graph.

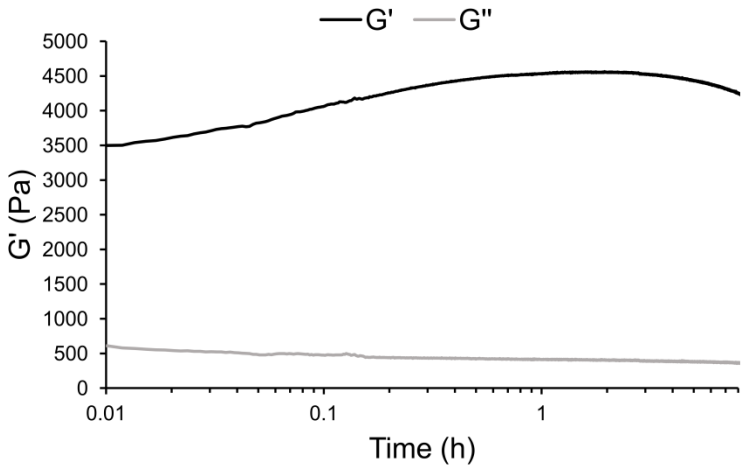

Figure S4.5. The changes in thiol-collagen hydrogel rheological properties with time immediately after mixing the hydrogel components. Hydrogel formulation t-c-h20, representative graph. Experiment carried out at 25 °C with 1% oscillation strain and 1 Hz oscillation frequency.

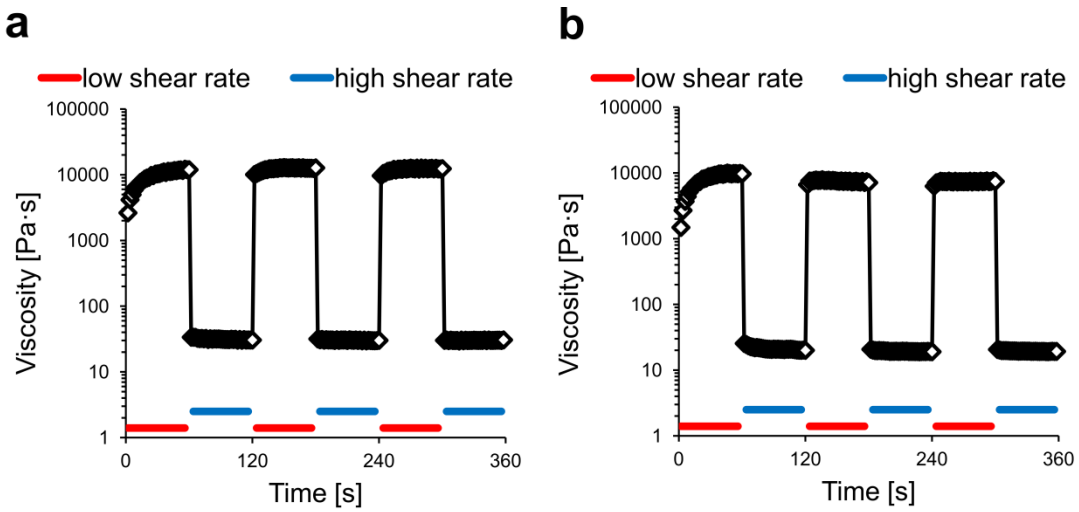

Figure S4.6. Shear-thinning/self-healing properties of thiol-collagen hydrogels extruded from syringe 16 h after hydrogel preparation: a) measured at 25 °C; b) measured at 37 °C. Viscosity was measured continuously at alternating low shear rate (0.01 s^{-1}) and high shear (10 s^{-1}) rate conditions. Hydrogel formulation t-c-h20, representative graph.

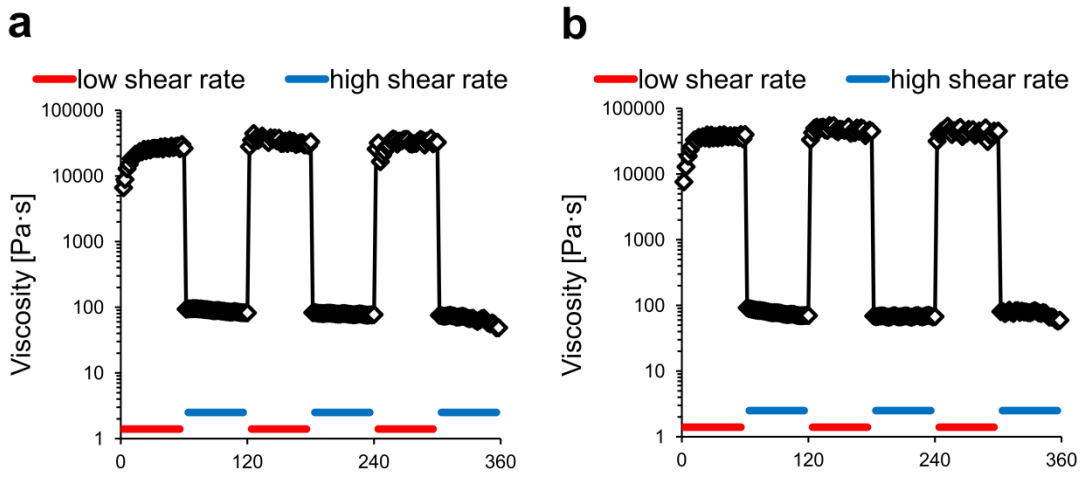

Figure S4.7. Shear-thinning/self-healing properties of two-year old gel measured at different temperatures: a) 25 °C; b) 37 °C. Viscosity was measured continuously at alternating low shear rate (0.01 s^{-1}) and high shear (10 s^{-1}) rate conditions. Hydrogel formulation t-c-h20, representative graph.

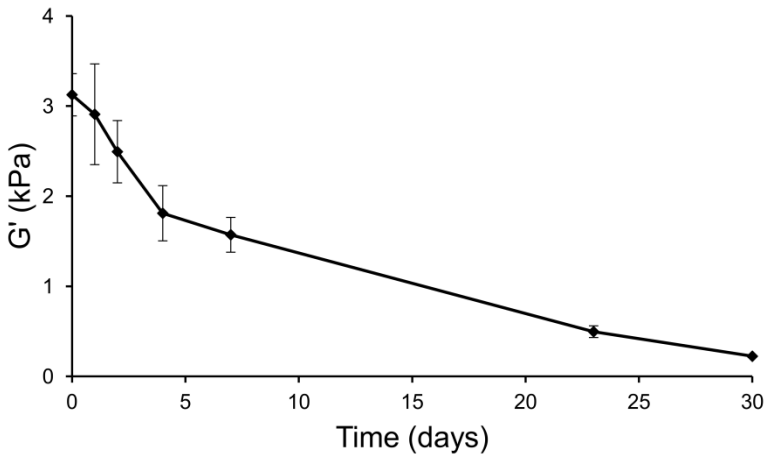

Figure S4.8. Degradation of thiol-collagen hydrogels under reducing conditions *in vitro* in glutathione solution (10 mM): reduction in G′ over time. The G′ value at 1.1 Hz was taken from frequency sweep experiment at an oscillation strain of 0.267%. Hydrogel formulation t-c-h20. Experiments performed at 37 °C. Error bars = SD (n = 3).

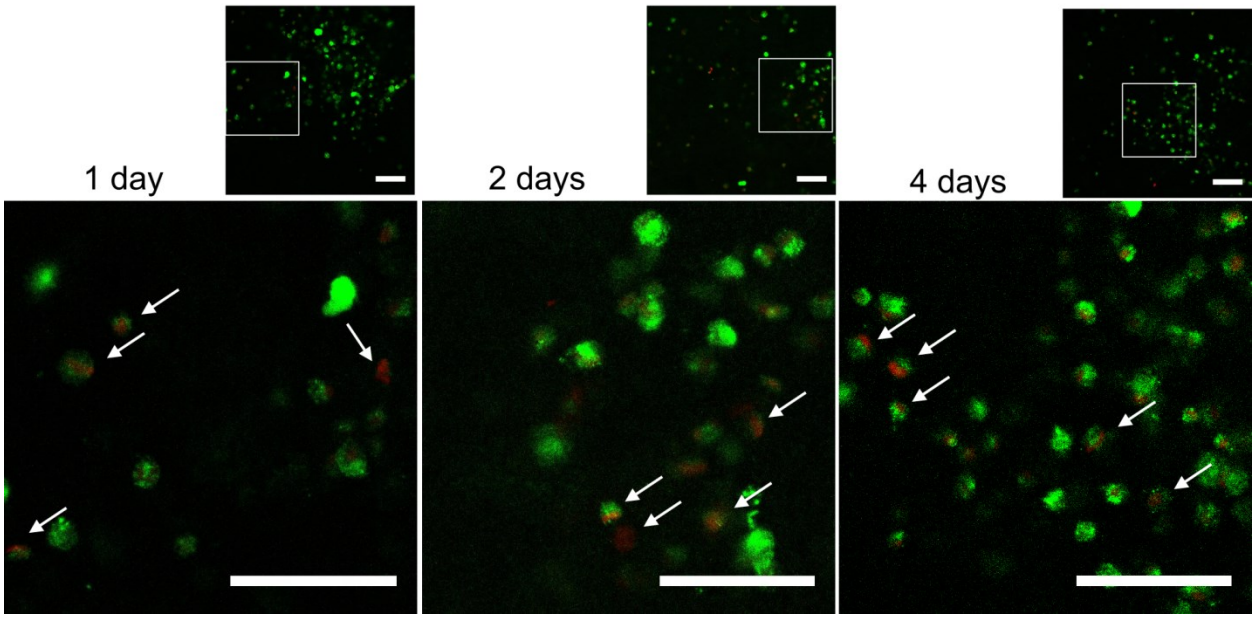

Figure S4.9. Enlarged sections of representative images of *in vitro* 3D cultures of human umbilical vein endothelial cells (HUVEC) encapsulated in thiol-collagen hydrogels after 1, 2, and 4 days in culture. Top row: full image as shown in Figure 4.7b; white squares show the enlarged sections shown in bottom row. Green = alive cells, red = dead cells (live/dead assay). White arrows point to red and double-stained cells. Double-stained cells were not counted as live cells when assessing the cell viability. Scale bar = 100 μm.

5 Paper III. Effect of Dose and Timing of Delivery in Human Recombinant Collagen III Hydrogel Therapy for Treating Myocardial Infarction

Manuscript:

J. Pupkaite*, V. Sedlakova*, C. Eren Cimenci, M. Ruel, E.I. Alarcon, E.J. Suuronen. Effect of dose and timing of delivery in human recombinant collagen III hydrogel therapy for treating myocardial infarction

*Authors contributed equally

Abstract

Injectable hydrogels are a promising method to enhance repair in the heart after myocardial infarction (MI). However, few studies have investigated the optimal delivery parameters of the biomaterial, such as timing and dosage. In this study human recombinant collagen III hydrogel was injected into the myocardium in a mouse MI model, varying its delivery parameters. Comparing hydrogel injection at a single early time point (3 h) and three time points (3 h, 1 and 2 weeks) post-MI revealed improved cardiac function, reduced scar size and inflammation, and increased vascularization in the single injection group. Additionally, omitting the 3 h hydrogel injection, followed by hydrogel injections at 1 and 2 weeks post-MI led to worsening of the cardiac function, further highlighting the importance of the early injection time point. Increasing the dose of collagen III from 1% to 2% in the hydrogel at a single early time point (3 h) injection did not confer any additional functional improvement compared to 1%, and resulted in scar size and vascular density comparable to control. This study highlights the importance of investigating the optimal delivery parameters of biomaterial therapy for myocardial infarction, and shows that, for collagen III hydrogel, more is not better.

Introduction

When the myocardium is damaged due to the occlusion of one or more coronary arteries (myocardial infarction, MI), its repair response involves three overlapping stages: the inflammatory, proliferative, and maturation phases. This leads to the formation of a collagenous scar to prevent cardiac rupture, but due to the heart's limited regenerative capacity, it fails to restore the myocardium. Even with the state-of-the-art treatment to reestablish blood flow to the damaged tissue, maladaptive remodeling may occur due to continuing pressure and volume load on the infarcted area and the inability of the non-contractile scar tissue to contribute to cardiac function[235]. This adverse ventricular remodeling is associated with chronic inflammation and can progress to heart failure[142,235]. A novel approach to limit adverse ventricular remodeling and prevent heart failure has been the development of biomaterial-based regenerative therapies. However, few reported studies have investigated the optimal biomaterial delivery strategy, including parameters such as timing and dosage, needed to reach the maximum efficacy of the treatment. Most studies on biomaterial therapies using rodent MI models report an improvement in cardiac function, but examine only a single time point for treatment, ranging from immediately after ligation surgery to 2 weeks post-MI[87,132,136,138–141,143]. Considering that both the cellular and extracellular matrix (ECM) components of the myocardium undergo a series of prominent changes through the inflammatory, proliferative, and maturation phases of repair[142,235,236], it is likely that the efficacy of a biomaterial therapy is dependent not only on the biomaterial itself but also on the timing of delivery and the dosage of the treatment.

We previously investigated the effects of treatment timing, in which a single collagen I hydrogel treatment was injected into the myocardium of mice at 3 hours, 7 days, or 14 days post-MI[130]. Our results revealed that the earliest hydrogel treatment (3 h) resulted in significantly

improved cardiac function, enhanced vascularity, and reduced fibrosis and cell death in the heart compared to later treatments. Collagen I, the most abundant protein in the cardiac ECM[237], has been well established in various animal models as a biomaterial that can improve cardiac function post-MI[95,125,130,210,238]. On the other hand, the second most abundant type of collagen in the heart, collagen III[237], has received much less attention for cardiac applications, despite the fact that it is largely responsible for the elasticity of the tissue[239,240]. We have previously reported that an injectable recombinant human collagen III (rHCIII) hydrogel was able to preserve cardiac function when delivered at 1 week post-MI in mice[241]. In other work, Dai et al. used the product Zyderm type 2 (composed of 95% collagen I and 5% collagen III) for post-MI therapy and observed improved cardiac function in rats[143]. In another approach, fibroblasts over-expressing collagen III were delivered into the infarct region of a mature scar (2 weeks post-MI in a rat model) and were able to prevent further deterioration of cardiac function[242].

Given this evidence, the aim of the present study was to investigate the effect of dosage and timing of delivery of a collagen III hydrogel treatment on cardiac function post-MI. Dosage was changed either by delivering the hydrogel multiple times (at the 3 healing phases of MI) or by increasing the material's collagen concentration. We show that the single injection of low dose material at an early time point (3 h post-MI) resulted in the greatest cardiac improvement; indicating that for this collagen III hydrogel, more is not better.

Materials and Methods

Preparation of rHCIII Hydrogels

Recombinant human collagen III (rHCIII) hydrogels were prepared according to our previously reported protocol[241]. Briefly, 1% and 2% collagen solutions were prepared by

dissolving 0.1 g and 0.2 g, respectively, of lyophilized recombinant human collagen III (Fibrogen, USA) in 10 ml of HyClone™ HyPure™ molecular biology grade water (GE Healthcare Life Sciences, USA). Chondroitin sulfate (CS) solution (40%) was prepared by dissolving 40 g of CS (Wako, USA) in 100 mL phosphate buffered saline (PBS, calcium and magnesium free). The rHCIII hydrogels were prepared on ice using an enclosed syringe mixing system. For 1% and 2% rHCIII hydrogels, chondroitin sulfate (CS), N-ethyl-N-(3-dimethylaminopropyl) carbodiimide (EDC) and N-hydroxysuccinimide (NHS) were added to produce a final mixture with a mass ratio of 1:4:0.5:0.3 and 2:4:0.5:0.3, respectively, for collagen:CS:NHS:EDC. The pH of hydrogels was adjusted to 7.4 by adding NaOH (1.0 N).

Mouse MI Model and Treatment

All procedures were approved by the University of Ottawa Animal Care Committee, and performed according to the National Institute of Health Guide for the Care and Use of Laboratory Animals. MI was induced in mice via left anterior descending (LAD) coronary artery ligation and hydrogel treatment was delivered as previously reported[95,130]. Briefly, 8-9-week old female C57BL/6 mice (Charles River, Canada) were anesthetized (3% isoflurane), intubated, and the heart was exposed via fourth intercostal thoracotomy. The LAD was then ligated just below its emergence from the left atrium. The surgeries were performed by the same technician who was blinded to the treatment group assignment. This procedure resulted in a large MI involving the anterolateral, posterior, and apical parts of the heart. Mice were randomly assigned to receive 3 separate treatments delivered at 3 h, 1 week, and 2 weeks post-MI via 5 equivolumetric intramyocardial injections (10 µl each site, 50 µl in total) through a 25G needle using an ultrasound-guided closed-chest procedure, under anesthesia. The experimental timeline

is summarized in Figure 5.1. The first study compared single vs. multiple injections of 1% rHCIII and consisted of the following groups:

	Time point injection		
Treatment group	3 h	1 wk	2 wk
PPP	PBS	PBS	PBS
1% CPP	1% rHCIII	PBS	PBS
1% CCC	1% rHCIII	1% rHCIII	1% rHCIII

To better understand the observations made from this first study, an additional set of mice received PBS at 3 h and 1% rHCIII at 1 and 2 weeks post-MI to examine the importance of the early delivery time-point in the triple injection group (1% PCC group). The second study compared 1% vs. 2% rHCIII delivered at 3h post-MI and consisted of the following groups:

	Time point injection		
Treatment group	3 h	1 wk	2 wk
PPP	PBS	PBS	PBS
1% CPP	1% rHCIII	PBS	PBS
2% CPP	2% rHCIII	PBS	PBS

Mice were sacrificed 4 weeks after the last injection. Hearts were collected for further analyses, which were performed in a blinded fashion.

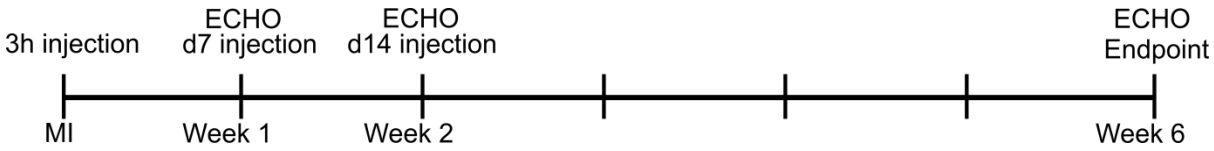

Figure 5.1. Study timeline.

Echocardiography and Cardiac Strain Analysis

Transthoracic echocardiography was performed on parasternal long-axis views using a Vevo3100 system in B mode with a MX400 series real-time microvisualization scanhead probe (VisualSonics, USA). The imaging was carried out at 1 week (right before 1 week treatment), 2 weeks (right before 2 weeks treatment injection), and 6 weeks post-MI (4 weeks after last injection). Left ventricular ejection fraction (LVEF), left ventricular end systolic volume (LVESV), end diastolic volume (LVEDV), and endocardial longitudinal strain of the anterior apical segment (corresponding to scar and border regions) at the time of aortic valve closure were determined using Vevo LAB 3.1.1 software (VisualSonics) by a researcher blinded to the treatment group assignment.

Histology and Immunohistochemistry

Hearts were harvested at 6 weeks post-MI (4 weeks after last injection), embedded in Optimal Cutting Temperature compound (Fisher Scientific, Canada), and snap frozen in liquid nitrogen. Sections (10 μm thick) were cut using a ThermoScientific HM550 Cryostat. To evaluate scar size, tissue sections were fixed in 4% PFA for 1 h and stained with Masson's trichrome stain (Sigma, Canada). Images were taken with a Celestron Handheld Digital Microscope Pro (USA). Scar size was measured using the mid-line arc method in ImageJ software[243]. For immunohistochemical staining, tissue sections were fixed in cold acetone for 20 min at 4 °C, washed with 0.05% Tween-20 in PBS, permeabilized with 0.1% Triton-X 100 in PBS for 10 min, washed again, and then blocked with 10% serum in PBS for 1 h at room temperature. Slides were incubated with primary antibodies in 10% serum in PBS overnight at 4 °C, then washed again and incubated with secondary antibodies for 1 h at room temperature,

protected from light. After washing, nuclei were stained with DAPI (1:500) and slides were mounted with ProLong™ Gold antifade reagent (Invitrogen, Canada).

Capillaries, arterioles and myofibroblasts were visualized using rat monoclonal anti-CD31 (PECAM-1, Santa Cruz Biotechnology, RM0032-1D12, 1:50, USA) and rabbit polyclonal anti-α-smooth muscle actin (α-SMA, Abcam, ab5694, 1:200, USA) antibodies, followed by detection with AlexaFluor-conjugated secondary antibodies: AF594 goat anti-rat (Invitrogen, A11007, 1:600, Canada) and AF488 goat anti-rabbit (Invitrogen, A11008, 1:600, Canada), respectively. M1 macrophages were visualized using rat monoclonal anti-CD86 antibody (Abcam, ab119857, 1:50, USA) and M2 macrophages using rabbit polyclonal anti-CD206 antibody (Abcam, ab64693, 1:200, USA), followed by detection with AF594 goat anti-rat (Invitrogen, A11007, 1:600, Canada) and AF488 goat anti-rabbit (Invitrogen, A11008, 1:600, Canada) secondary antibodies, respectively. Fluorescent images were taken with an Aperio Versa 8 microscope (Leica; Canada) and analyzed using ImageScope and ImageJ software.

Statistical Analysis

Statistical analysis was performed using R software. Outliers were identified using Tukey's fences (inter-quartile range) method for each measurement and removed from the statistical analysis of that measurement. One outlier in the 2% CPP group was identified at the baseline LVEF measurement (1 week post-MI) and removed from analysis altogether. Statistically significant differences among multiple groups were determined by one-way ANOVA followed by pair-wise comparisons using the Holm-Bonferroni procedure. To determine differences within a subject at two different time points, a paired t-test was performed. Significance was set at a $p < 0.05$. All data are presented as mean ± SEM.

Results

Comparison of Single and Multiple Time-Point Injection of 1% rHCIII Hydrogel Therapy

Mice underwent MI surgery (mortality rate = 4%), and were randomized to receive treatment of 1% rHCIII at 3 h only (1% CPP group) or at 3 h, 1 week, and 2 weeks (1% CCC group) post-MI. The control group received PBS at all 3 time points (PPP group). There was 0% mortality rate associated with the injection procedure.

At 2 weeks post-MI, both rHCIII treatment groups (1% CPP and 1% CCC) had greater LVEF compared to the PBS control group (43 ± 2% and 43 ± 3% vs. 31 ± 3%, respectively; Figure 5.2a). This improvement relative to control persisted up to 6 weeks post-MI (50 ± 1%, 41 ± 2%, and 30 ± 3% for 1% CPP, 1% CCC, and PPP, respectively). Notably, at 6 weeks post-MI, the LVEF of the single rHCIII treatment group was greater than that of triple treatment group. The single treatment group was also the only one to show an improvement in LVEF over time relative to its own baseline. No significant differences were observed in LVESV and LVEDV between the treatment groups, although there was a trend ($p \leq 0.1$) for reduced LVESV in the mice that received the single rHCIII injection (Figure 5.2b and c). Additionally, cardiac strain measurements showed increased strain (contraction) of the anterior apical segment (including scar and border zones) at the time of aortic valve closure for single rHCIII treatment group compared to control (Figure 5.2d). This indicates a better recovery of contractile function in the infarcted area after a single injection of rHCIII hydrogel.

Masson's Trichrome staining revealed that only the mice receiving the single rHCIII treatment had reduced scar size at 6 weeks post-MI compared to the PBS control (Figure 5.2e and f). Immunohistochemistry was performed using anti-αSMA and anti-CD31 antibodies to quantify the number of myofibroblasts (αSMA^+), capillaries ($CD31^+$), and arterioles ($CD31^+$

αSMA^{+} structures with characteristic vessel morphology) in the scar and border regions at 6 weeks post-MI (Figure 5.3a). Both the single and triple rHCIII treatment resulted in a reduced number of myofibroblasts in the border region compared to control (Figure 5.3b). The capillary density in the border region and arteriole density in the scar were increased in the single rHCIII treatment group compared to control and triple treatment groups, respectively (Figure 5.3c and d). To assess inflammation, the ratio between pro-inflammatory (CD86^{+} M1 cells) and pro-healing (CD206^{+} M2 cells) macrophages was determined in the scar and border zone at 6 weeks post-MI (Figure 5.3e and f). The triple rHCIII injection group had increased inflammation (i.e., greater M1/M2 ratio) compared to the single rHCIII injection group.

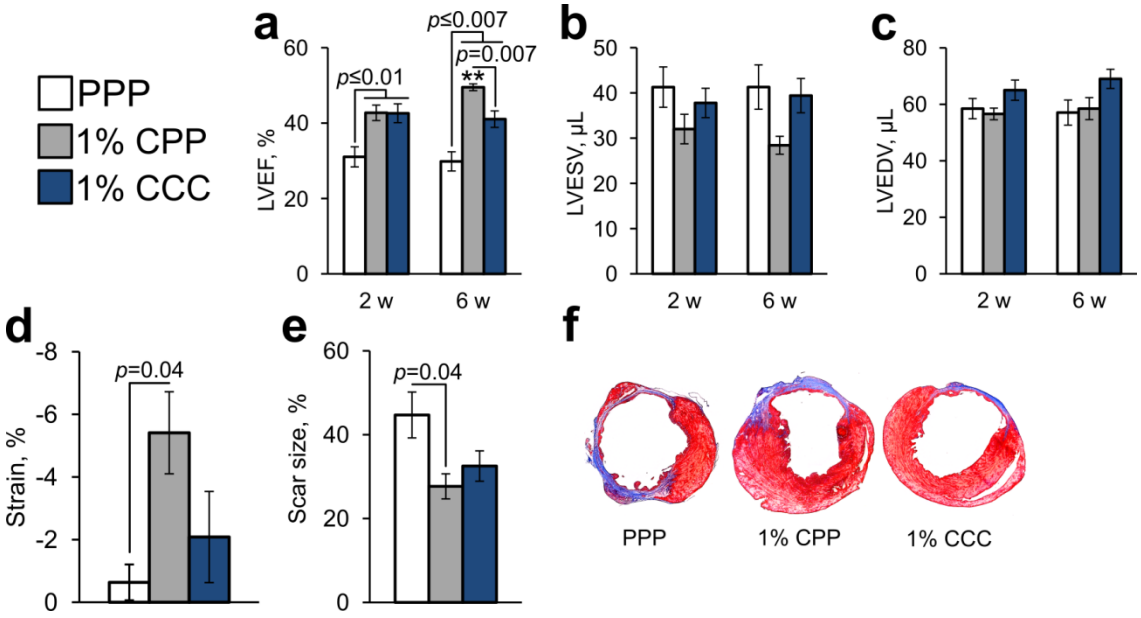

Figure 5.2. The effect of single (1% CPP) and triple (1% CCC) 1% rHCIII hydrogel treatment on cardiac function and fibrosis compared to control treatment (PPP): a) left ventricular ejection fraction (LVEF) at 2 and 6 weeks post-MI; b) left ventricular end-systolic volume (LVESV) at 2 and 6 weeks post-MI; c) left ventricular end-diastolic (LVEDV) volume at 2 and 6 weeks post-MI; d) endocardial longitudinal strain of the anterior apical segment (including scar and border zones) at aortic valve closure at 6 weeks post-MI; e) scar size (% circumference); f) representative images of tissue sections used for scar size evaluation (Masson's Trichrome stain). Error bars = SEM (n = 5 – 13), *p* values: one-way ANOVA comparing different treatment groups, followed by Holm-Bonferroni test, ** $p = 0.01$ (paired t-test compared to the group baseline).

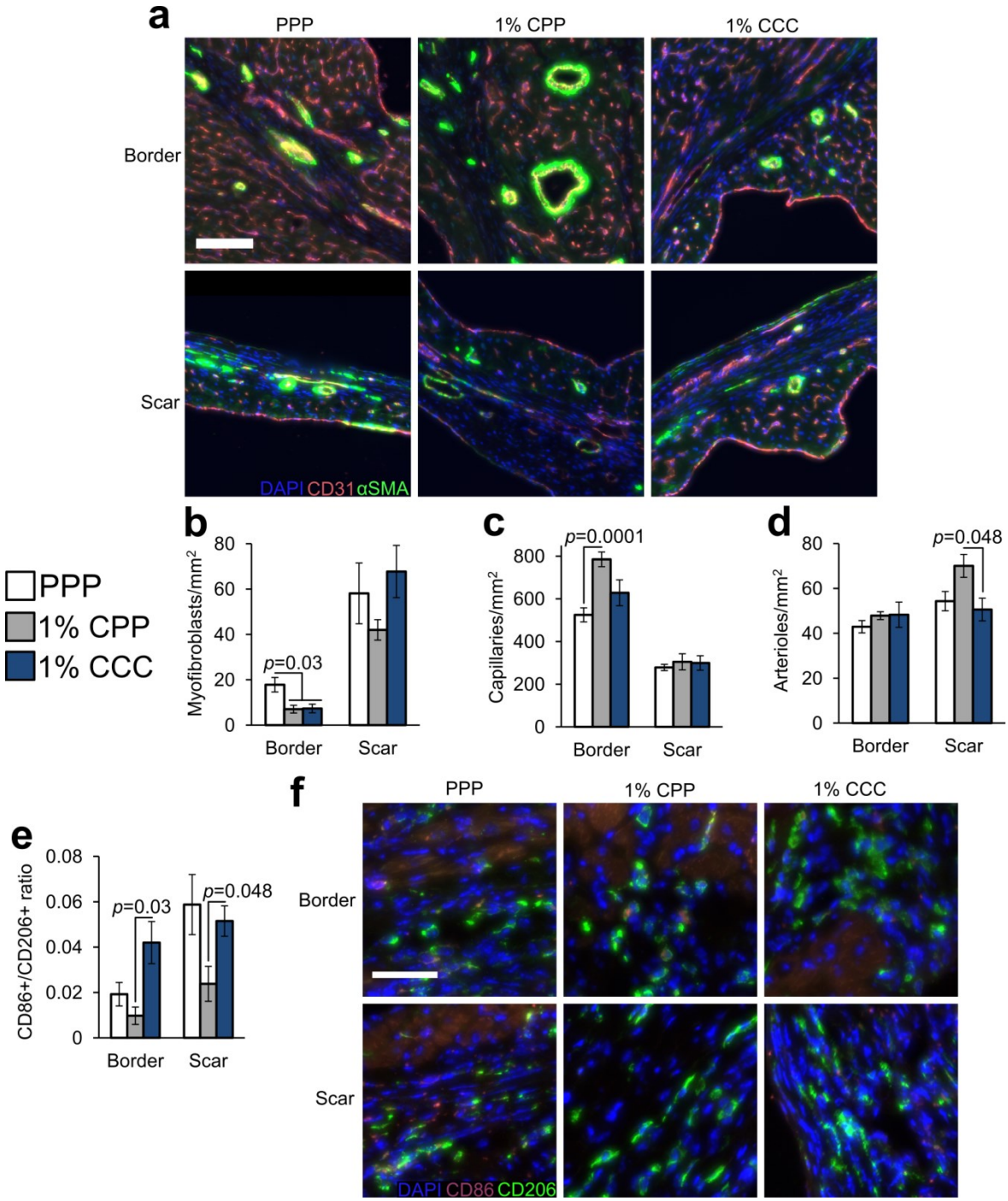

Figure 5.3. The effect of single (1% CPP) and multiple (1% CCC) 1% rHCIII hydrogel treatment on myocardial fibroblasts, vasculature, and inflammation compared to control treatment (PPP): a) representative images of tissues stained with anti-CD31 (red), anti-αSMA (green) antibodies, and DAPI (blue), scale bar = 100 μm; b) myofibroblast (αSMA^{+}) density in scar and border

regions; c) capillary ($CD31^+$) density in scar and border regions; d) arteriole density ($CD31^+$ αSMA^+) in scar and border regions; e) ratio of $CD86^+$ cells to $CD206^+$ cells in scar and border regions; f) representative images of border and scar regions stained with anti-CD86 (red), anti-CD206 (green) antibodies, and DAPI (blue), scale bar = 50 μm. Error bars = SEM (n = 5 – 13), *p* values: one-way ANOVA comparing different treatment groups, followed by Holm-Bonferroni test.

Removal of Early rHCIII Injection from the Triple Treatment Group

Given that a single rHCIII injection at 3 h post-MI was superior to the triple injection treatment (delivered at 3 h, 1 week, and 2 weeks post-MI), it appears that the initial 3 h treatment is critical for the therapeutic effect of rHCIII hydrogel therapy, and that adding more rHCIII over time reduces its efficacy. To investigate this further, another group of mice was treated with PBS at 3 h post-MI, followed by rHCIII injections at 1 and 2 weeks (the 1% PCC group) in order to eliminate the effect of the first rHCIII injection.

The LVEF of the 1% PCC treatment group was significantly reduced 2 weeks post-MI compared to triple treatment group (25 ± 1% and 43 ± 3%, respectively), with the difference persisting up to 6 weeks post-MI (21 ± 1% and 41 ± 2%, respectively, Figure 5.4a). Notably, the 1% PCC treatment group also showed reduced LVEF at 6 weeks post-MI compared to the PBS control, as well as to its own baseline (1 week post-MI). While there were no significant differences observed in LVESV and LVEDV among the three groups, there was a trend ($p \leq 0.1$) for increased LVESV in the 1% PCC group (Figure S5.1a). There were also no differences between treatment groups in the strain of the anterior apical segment measured at the time of aortic valve closure or scar size (Figure 5.4b, c).

Subsequent heart tissue analysis revealed greater myofibroblast density in the border region in the hearts of 1% PCC mice compared to 1% CCC group, and a trend ($p \leq 0.08$) for increased myofibroblast density in the scar of the 1% PCC mice compared to the other treatments (Figure 5.4d). There were no significant differences observed among the groups for the other parameters that were evaluated (capillary and arteriole density and the $CD86^+$ cell/ $CD206^+$ cell ratio in the scar and border regions, Figure 5.4e-i).

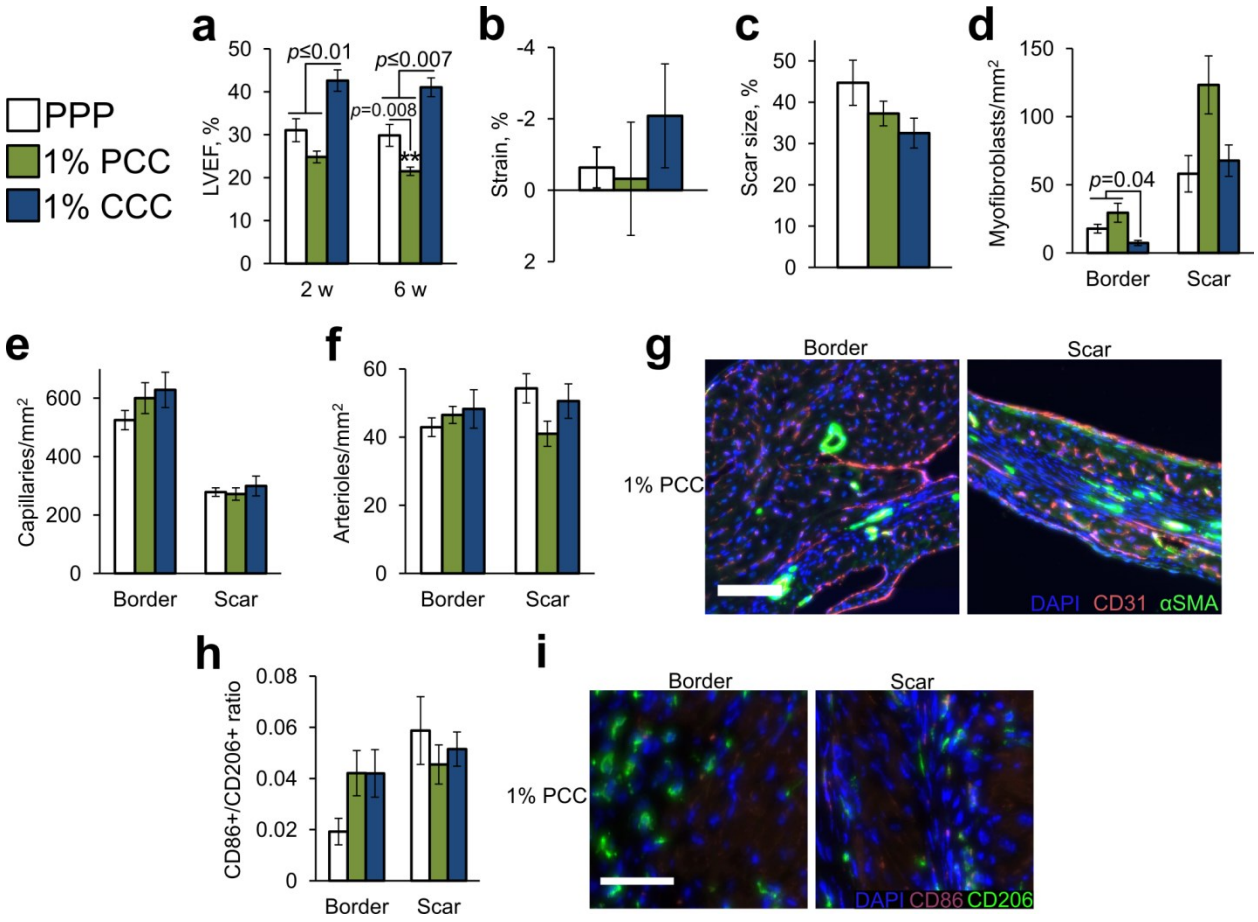

Figure 5.4. The effect of removing the early injection of 1% rHCIII hydrogel (1% PCC) on cardiac function and healing compared to triple injection rHCIII hydrogel or control treatment (1% CCC and PPP, respectively): a) left ventricular ejection fraction (LVEF) at 2 weeks and 6 weeks post-MI; b) endocardial longitudinal strain of the anterior apical segment (including scar and border zones) at aortic valve closure at 6 weeks post-MI; c) scar size (% circumference); (d-e) myofibroblast (αSMA^+), capillary ($CD31^+$), and arteriole density ($CD31^+$ αSMA^+) in scar and border regions; g) representative images of 1% PCC group border and scar regions stained with anti-CD31 (red), anti-αSMA (green) antibodies, and DAPI (blue), scale bar = 100 μm; h) ratio of $CD86^+$ cells and $CD206^+$ cells in scar and border regions; i) representative images of border and scar regions stained with anti-CD86 (red), anti-CD206 (green) antibodies, and DAPI (blue), scale

bar = 50 μm. Error bars = SEM (n = 7 – 13), *p* values: one-way ANOVA, followed by Holm-Bonferroni test, ** $p = 0.00003$ (paired t-test compared to the group baseline).

The Effect of Increasing Hydrogel rHCIII Concentration

Having determined that adding more rHCIII over time reduced the therapeutic effect of the single early time point rHCIII treatment, we next investigated the effect of raising the collagen dose for the single injection. The rHCIII concentration in the hydrogel was increased to 2% (2% CPP group) and compared to the 1% rHCIII group (1% CPP) when delivered at 3 h post-MI. The injection of 2% rHCIII resulted in 8% mortality rate, compared to 0% mortality for the 1% rHCIII hydrogel group.

At 2 weeks post-MI, only treatment with 1% rHCIII resulted in improved LVEF compared to the PBS control (Figure 5.5a). Both rHCIII groups had greater LVEF than the PBS group at 6 weeks post-MI (50 ± 1%, 44 ± 4%, and 30 ± 3% LVEF for the 1% rHCIII, 2% rHCIII, and control groups, respectively). There were no significant differences observed in LVESV and LVEDV between the treatment groups, although a trend ($p \leq 0.1$) for reduced LVESV in both the 1% and 2% hydrogel treatments compared to control was seen (Figure S5.1b).

Treatment with the 1% rHCIII hydrogel resulted in reduced scar size compared to both the PBS and 2% rHCIII groups (Figure 5.5b). In addition, myofibroblast density was reduced in the border regions of the 1% rHCIII treatment group compared to the PBS group, and there was a trend ($p \leq 0.1$) for reduced myofibroblast numbers in the scar of 1% rHCIII-treated mice compared to those receiving 2% rHCIII (Figure 5.5c). Furthermore, the 1% rHCIII group had greater capillary density in the border zone compared to the hearts treated with 2% rHCIII or PBS, but no differences in arteriole numbers were observed (Figure 5.5d-f).

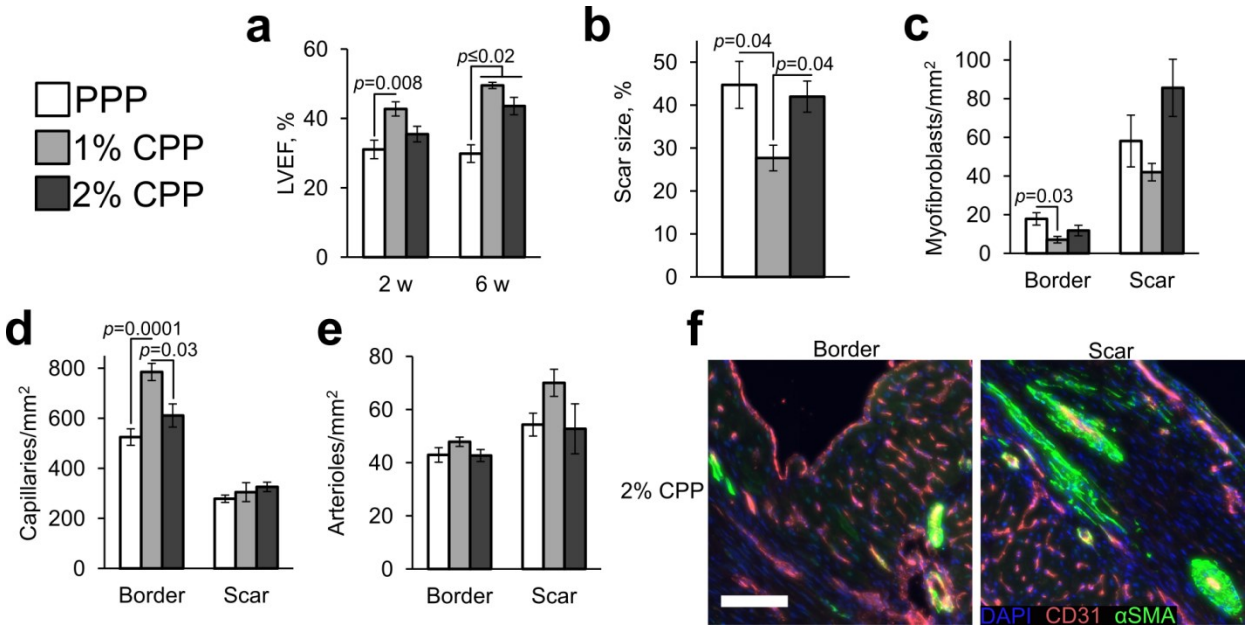

Figure 5.5. The effect of early 2% rHCIII hydrogel treatment (2% CPP) on cardiac function and histological changes compared to 1% rHCIII hydrogel or control treatment (1% CPP and PPP, respectively): a) left ventricular ejection fraction (LVEF) at 2 weeks and 6 weeks post-MI; b) scar size (% circumference); (c-e) myofibroblast (αSMA^+), capillary ($CD31^+$), and arteriole ($CD31^+$ αSMA^+) density in scar and border regions; f) representative images of 2% CPP group border and scar regions stained with anti-CD31 (red), anti-αSMA (green) antibodies, and DAPI (blue), scale bar = 100 μm; Error bars = SEM (n = 7 – 13), *p* values: one-way ANOVA, followed by Holm-Bonferroni test.

Discussion

Since our previous work showed that a single injection of rHCIII hydrogel at 1 week post-MI could preserve cardiac function[241], the aim of this work was to investigate if different rHCIII delivery strategies would improve its therapeutic efficacy. We hypothesized that increasing the rHCIII dosage either by delivering the hydrogel multiple times or by increasing the collagen concentration of the hydrogel would confer a greater benefit; however, the main finding was that increased collagen amount was not better, and that it could, in fact, be worse.

The multiple injection scheme delivered the hydrogel at 3 different time points, corresponding to the three healing phases of MI (3 h = inflammatory; 1 week = proliferative; 2 weeks = maturation). We found that a single early time point injection (3 h post-MI) resulted in superior improvement in cardiac function compared to the 3 sequential injections. Furthermore, we observed that omitting the first rHCIII injection (at 3 h) resulted in a significant decline in LVEF compared to the 3 injections, but surprisingly also to the control group. As the single early time point injection conferred the most benefit, we also investigated if increasing the dosage by increasing the collagen concentration would provide any additional advantage. However, a single injection of 2% rHCIII at 3 h post-MI proved to be overall inferior to the 1% rHCIII treatment, in addition to elevating the mortality risk.

This is the first study to investigate different delivery strategies for injectable collagen III hydrogel therapy with respect to timing and dosage. Previously, we investigated injectable collagen I hydrogel delivery at 3 h, 1 and 2 weeks post-MI[130], as well as compared single injection of collagen I versus collagen III hydrogel delivered at 1 week post-MI[241]. The present study looking at collagen III and that of Blackburn et al. (on collagen I) are in agreement that a single early time-point injection at 3 h post-MI leads to improved cardiac function compared to

later time-point delivery. Also, a single treatment delivery of rHCIII hydrogel at 1 wk post-MI was shown only to preserve cardiac function[241], and omitting the 3 h collagen III treatment from the triple injection procedure (1% PCC group of this study) resulted in significantly reduced LVEF compared to the untreated control. Taken together, this evidence indicates that early collagen treatment delivery is critical for conveying the best outcome.

Aside from our previous work, there have been a few other reports to date that investigated the timing effects of biomaterial therapy[105,106,144]. In contrast to our observation that early treatment (as soon as 3 h post-MI) was most effective in a mouse MI model, these other studies reported that the optimal delivery time for their materials was a few days post-MI (3-7 days). However, the biomaterials being tested were of non-protein origin: alginate[144], polyethylene glycol (PEG)[105], and poly(N-isopropylacrylamide) (NIPAAm)[106]. It is worth noting that the PEG-based biomaterial contained MMP-degradable peptide sequences and the NIPAAm-based material contained a polylactide component, making them degradable by the body. However, all three materials lack the bioactivity of collagen and its degradation products. Thus, the benefit of these materials is likely due to the bulking effect[129] and mechanical support that they provide to the scar (as was concluded by Yoshizumi et al.[106] as well). Therefore, if injected during the inflammatory phase, when MMPs and other ECM-degrading processes are highly activated, this type of biomaterial would be degraded quickly and thus may fail to provide support to the forming scar, whereas injecting them once inflammation is reduced would allow for slower degradation and thus prolonged effect.

The benefits of 3 h and 1 week treatment with a collagen hydrogel are likely mediated by the inherent bioactivity of the collagen and its interaction with cells[95,239,244], as well as its degradation fragments that are generated by MMPs. These breakdown products, termed

matricryptins, can then trigger complex signaling cascades involved in cell adhesion, migration, etc[245]. For example, there have been reports of collagen I and III and their degradation products acting as chemoattractants to fibroblasts[246] and blood monocytes but not neutrophils *in vitro*[247]. Also, Carragher et al. reported that collagen I fragments can result in focal adhesion disassembly in arterial smooth muscle cells *in vitro*, which in theory would increase migration and lead to enhanced neovascularization[248]. Furthermore, in a mouse MI model, treatment with an MMP-cleaved collagen Iα1 fragment (C-1158/59) resulted in improved wound healing and increased angiogenesis[249].

Although the mechanism through which the early rHCIII hydrogel treatment led to improved cardiac function is not altogether clear, our results show that it reduced fibrosis and myofibroblast density, while increasing vascularization (capillaries in the border zone and arterioles in the scar) and the pro-healing phenotype of the macrophage population. Similar effects were seen by Blackburn et al. when a type I collagen hydrogel treatment was applied to treat mice after MI[130]. Interestingly, Yoshimuzi et al. also reported increased vascularization after treatment with a NIPAAm-based biomaterial[106], suggesting that similar outcomes may be achieved through different materials and mechanisms, which is reminiscent of what is observed when comparing the effects of different types of cell therapy[250].

The failure of doubling the rHCIII concentration in the 3-hour injection to result in further improvement was surprising, as we expected that the increased bioactivity could result in greater cell-material interaction. However, it may be explained by different viscoelastic properties of 1% and 2% rHCIII hydrogels. Increasing the rHCIII concentration results in a more viscous solution, which is more challenging to inject, and which may also result in increased stiffness of the myocardium, thus impeding contraction. The greater viscosity may also prevent

spreading of the injected material resulting in a more bolus-like injection. Materials that have minimal interstitial distribution upon injection have been shown to be less effective at restoring cardiac function compared to those that spread throughout the myocardium[225]. So, the physical properties of the 2% rHCIII hydrogel may be responsible for its reduced therapeutic effect.

Conclusion

This study showed that the optimal delivery time-point for treating the infarcted mouse heart using a rHCIII hydrogel is in the first hours post-MI. Also, it was shown that increasing the amount of rHCIII being delivered did not lead to a superior therapeutic outcome, and in fact, could be detrimental depending on the timing of its administration. This highlights the importance of considering the dose and timing of delivery when developing biomaterial therapies for the treatment of myocardial infarction.

Supporting Information

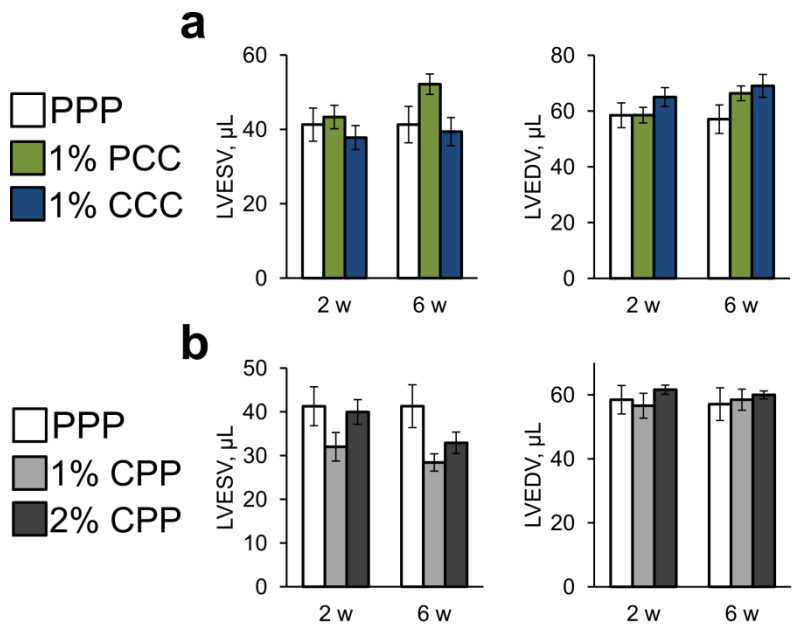

Figure S5.1. Left ventricular end-systolic (LVESV) and end-diastolic (LVEDV) volumes of treatment groups 2 weeks and 6 weeks post-MI: a) control, double (missing early injection), and triple rHCIII 1% hydrogel injection (PPP, 1% PCC, and 1% CCC, respectively); b) control, single 1%, and 2% rHCIII hydrogel injection (PPP, 1% CPP, and 2% CPP, respectively). Error bars = SEM, n = 7 – 13.

6 General Discussion

The aim of this dissertation was to develop collagen-based hydrogels for cardiovascular applications, addressing some of the challenges in collagen hydrogel-based strategies for tissue photobonding, cell delivery, and post-MI therapy.

The hydrogel presented in Paper I was crosslinked using rose Bengal and visible light, and its use as a tissue-bonding agent was demonstrated. In particular, the hydrogel could be used to close wounds whose edges are apart or uneven. This is difficult to achieve using an aqueous rose Bengal solution, which was proposed as a tissue-photobonding approach and was tested in a clinical trial with some success[168]. However, an aqueous solution cannot fill a gap in tissue and could be easily washed out of the wound. The approach reported here addressed this limitation.

The second hydrogel, described in Paper II, is a covalently crosslinked, non-swelling, shear-thinning, and self-healing collagen hydrogel – a combination of characteristics reported in the literature for the first time. Additionally, it is a two-component system based on click chemistry, which is shelf-stable (i.e., the crosslinked hydrogel kept in an aqueous solution at room temperature for 2 years maintained its shear-thinning character).

In Paper III, instead of focusing solely on hydrogel design, the scope was broadened to the other aspects of treatment, particularly, timing and dosage. Surprisingly, we found that for rHCIII hydrogel crosslinked with EDC and NHS, the best outcomes in post-MI therapy were achieved by delivering a single low dose at one early time-point post-MI. This shows that hydrogel composition is not the only factor which determines treatment outcome and that the hydrogel delivery strategy should be considered when developing biomaterials for specific therapies.

The papers presented in this thesis demonstrate three different collagen hydrogels designed for specific regenerative medicine applications: tissue bonding, cell delivery, and biomaterial therapy. Although all the described hydrogels are based on collagen, the hydrogel designs were developed with consideration for each intended application and potential for clinical translation.

6.1 Choosing Collagen

Different types of collagen are the main structural components of the ECM of many tissues. They influence cell behavior through interactions between adhesive motifs and cell surface proteins, such as integrins[93]. Additionally, collagen degradation fragments may act as signaling molecules to various cell types, particularly to cells involved in inflammatory responses[246,247]. As such, collagens can provide structural support to tissue, scaffolds for cell attachment, as well as affect healing processes. Additionally, many types of collagen (including type I and III) can self-assemble into supramolecular structures, induced by temperature, pH, or ionic environment[24]. This creates a 3D network (hydrogel) held via physical interactions. Therefore, collagen appears to be a great candidate for the development of hydrogels for regenerative medicine and tissue engineering applications.

However, despite the promising results using collagen hydrogels and the fact that various animal-sourced products are established in clinical practice[36], such materials do present certain concerns in their application for human use. For example, even with careful processing of animal tissue, there remains a risk of disease transmission, although such reports are very rare[251]. Additionally, due to the process of collagen extraction from tissue, the properties of extracted materials may differ depending on source species, extraction protocol, and individual

differences, resulting in batch-to-batch variation[252]. This presents difficulties in establishing Good Manufacturing Practice protocols required for clinical use. Cultural, religious, and ethical concerns may also prevent the use of animal-sourced collagen. Therefore, alternatives are being investigated, such as recombinant human collagen (also investigated in Paper III) and synthetic collagen-mimetic peptides, although these technologies need much further improvement to implement industrial yield and safety standards[24]. Thus, animal-sourced collagen is currently the most cost-effective option for pre-clinical hydrogel development.

Since collagen I is the main type of collagen in many tissues and organs, including skin, bone, and heart[24], in Papers I and II, it was chosen to design hydrogels for tissue photobonding and cell delivery. The use of collagen I allows these hydrogels to potentially be applied in regenerative applications of different tissues where collagen I is abundant. However, other types of collagen may be more suitable for the regeneration of certain other tissues. For example, in cartilage, collagen II is most prevalent, and it has been shown to be superior to collagen I in maintaining the phenotype of chondrocytes[27]. Collagen III is the second main structural component of the cardiac ECM, is more distensible compared to stiff collagen I structures and thus is responsible for the elasticity of the ECM[253]. The potential of collagen III for the use in regenerative medicine has not been widely investigated, but previous findings show that it can preserve cardiac function post-MI[241]. Thus, in Paper III, it was used to investigate how different delivery strategies may affect the therapeutic effect of a biomaterial.

Although physical collagen hydrogels have been used in regenerative medicine applications and indeed shown to convey a functional improvement in post-MI therapy[143], native ECM collagen structures *in vivo* are stabilized with additional covalent crosslinks, generated by enzymatic or glycation processes[24]. In contrast, physical collagen hydrogels produced in the lab

have relatively weak mechanical properties, are difficult to handle, and may be unable to provide the structural support for regenerating tissues. Thus, additional crosslinks need to be introduced into collagen hydrogels, which can be achieved through a variety of methods. Three different methods were chosen for the development of the hydrogels in this thesis, with consideration for the requirements of each intended application and the goals of each study.

6.2 Chemical Initiators, Photo-Crosslinking, or Click Chemistry?

Different covalent crosslinking methods were used to produce the hydrogels used in this thesis. As mentioned before, each crosslinking method has its advantages, which may be situation-specific; thus a universal optimal hydrogel design likely does not exist. Therefore, a different crosslinking method was chosen with consideration for the particular goals of each Paper.

Photo-crosslinking is a suitable *in situ* crosslinking strategy, as the onset of gelation can be controlled, thus allowing time to apply the hydrogel before exposing it to the light source. Additionally, wavelengths ranging from UV to IR have been showed to be biocompatible. UV irradiation is commonly used because it can produce a crosslinked hydrogel very quickly (30 s is usually enough)[145,149,150]. Nonetheless, certain concerns are associated with UV irradiation as it can cause DNA damage and its tissue penetration is very low. Therefore, in Paper I, rose Bengal was used to crosslink methacrylated collagen using visible light. It eliminates the use and potential harm of UV light, but 5–10 minutes of illumination with an LED was required to achieve optimal crosslinking. This presents a limiting factor for applications which require an immediate formation of a tight seal, although using a higher power illumination source, such as a laser, may reduce the crosslinking time. However, using an LED reduces the cost of the

treatment and the 5–10 min crosslinking time could be acceptable in some instances, such as the closure of skin wounds. This was demonstrated in a clinical trial that used an aqueous rose Bengal solution, where absorbable sutures were used for subcutaneous and dermal closure, and the epidermal layer was photobonded[168]. It reduced inflammation and scarring compared to a sutured epidermal layer, thus increasing patient well-being and satisfaction.

For a hydrogel designed for injection inside the body, especially if also intended for cell encapsulation, a cell-friendly crosslinking method which does not require any additional inputs (such as light) is desirable. Thus, thiol-Michael click reaction was chosen to design the hydrogel in Paper II. Additionally, the produced hydrogels showed excellent shear-thinning and self-healing properties, allowing for injection even after the crosslinking reaction was complete. Although click-crosslinked collagen hydrogels were reported before, none of them were reported to be shear-thinning (injectable) or self-healing[26,58,66,212].

Since different tissues have different mechanical properties, and cells may change their gene expression and behavior in response to these properties, mechanical properties that can be tuned by adjusting hydrogel composition or crosslinking parameters could help increase the utility of a hydrogel design. While the mechanical properties of the reported thiol-collagen hydrogels could be tuned by adjusting hydrogel composition, the achieved range was narrow. To improve these properties, acetyl-thiol-collagen hydrogel, crosslinked with multi-arm PEG-maleimide, was developed whose mechanical properties could be tuned with much greater control (manuscript, not included in this thesis).

Although in Paper II hydrogel formation was demonstrated using thiol-collagen and multi-arm PEG-maleimide, thiol-Michael addition reaction also occurs between thiols and vinyl sulfones, acrylates, and methacrylates, but maleimides and vinyl sulfones demonstrate the

highest reactivity[61]. Similarly, instead of PEG, other polymers might be used, such as maleilated chitosan[254] and vinyl sulfone-functionalized HA[255]. This would result in hydrogels composed entirely of natural polymers. The different polymers involved may affect the mechanical and shear-thinning properties of the hydrogels, which may be beneficial if it allows for better property control, but it may also be detrimental if the resulting hydrogels do not show shear-thinning properties. Nonetheless, the thiol-Michael addition is a very versatile method to produce biocompatible hydrogels, which can be crosslinked by simply mixing two solutions together.

Although the chemical crosslinking method involving EDC and NHS used in Paper III is arguably not as biocompatible as the other methods used in this thesis, its use has been demonstrated *in vitro* and *in vivo* before, with no adverse effects[43–45,130]. Importantly, it allows us to crosslink native rHCIII molecules, investigate its effects in a mouse MI model, make direct comparisons, and better understand other observations made in our lab using EDC and NHS crosslinked collagen hydrogels[130,241].

Thus, each crosslinking method has different characteristics that can be turned to advantages in specific situations and help prepare hydrogels with desired properties for each intended application, such as using photo-initiated reaction to control the onset of crosslinking, a slow click reaction to prepare injectable hydrogels, or chemical initiators to crosslink native collagen molecules.

6.3 Hydrogel Design for Clinical Use

Throughout all the work presented in this dissertation, its potential to contribute towards clinically translatable treatments was an important point of consideration. Rose Bengal was chosen as the photo-initiator in Paper I since its use in tissue photobonding was already

successfully tested in a clinical trial[168]. When developing the hydrogel in Paper II, a two-component system was developed based on biocompatible click chemistry, which is simple to prepare and is injectable even after crosslinking is complete, eliminating the need to match the gelation kinetics with the length of any possible procedures for which it may be used. In Paper III, rHCIII was used instead of animal-based products to avoid concerns associated with xenogeneic proteins.

These considerations are important because the field of biomaterials research is producing a lot of exciting hydrogel designs and pre-clinical results in small animals, but many proposed hydrogels are complex multi-component systems, and very few reported biomaterials have progressed to large animal models and even fewer to clinical testing. Only four clinical trials investigating hydrogel-based therapies for myocardial infarction and heart failure appear to have reported results so far. Two alginate-based hydrogels were tested in two trials using different delivery methods: intracoronary or intramyocardial injection, but only the latter demonstrated a positive outcome, highlighting the importance of the delivery strategy[256,257]. Additionally, two trials used cell-laden hydrogel patches made from either collagen I or fibrin, which were implanted during coronary artery bypass surgery[258,259]. Although the results of these studies appear encouraging, due to the complex treatment it is difficult to ascertain the role of each component.

Although the hydrogels presented in this thesis have only been tested *in vitro* and in small animal models, they have been designed with specific considerations toward possible clinical application, which may support their further development.

6.4 Further Research Directions

Cell – Biomaterial Interactions

During the development of the thiol-collagen hydrogel, encapsulated cell viability was investigated for 4 days in 3D culture *in vitro*. The cells showed viability of 70% and higher and maintained a rounded morphology throughout the study. Further testing of the interaction between the thiol-collagen hydrogel and different types of cells would be of interest for further material development, especially regarding any potential changes in gene expression and differentiation of mesenchymal stromal cells. Different aspects of the material could be affecting the cells, such as the mechanical properties, the availability of adhesive domains on modified and crosslinked collagen molecules, the presence of any unreacted thiol and maleimide functional groups, and the presence of PEG, which does not provide any cell attachment points and is known to prevent protein adsorption[260].

Tissue Photo-Bonding Models

Rose Bengal mediated photo-crosslinking of methacrylated collagen was demonstrated in a mouse skin wound model. While it is a suitable initial model, further research could be conducted using animal models whose skin and wound healing more closely mimics that of humans[261,262]. Additionally, an *ex vivo* or a biomimetic model could be designed to test the depth of tissue defect that may be crosslinked using this method. Although light required for rose Bengal excitation may not penetrate the tissue and hydrogel through the entire depth of the wound, there may be enough radical and reactive oxygen species generated to allow crosslinking of the deeper regions.

Body's Response to Collagen Hydrogels

Surprising effects of different collagen III treatment strategies were observed in a mouse MI model. Further studies could be performed to elucidate the mechanisms leading to the observed functional and histological changes and how the myocardial environment at a particular time point after MI affects the outcome of the therapy. Since the best functional outcome was observed when the hydrogel was injected at the earliest time point, during the inflammatory phase, the hydrogel may be affecting the cells present in the myocardium at that time differently than the cells present at the later healing phases.

Additionally, the thiol-collagen hydrogels could be further investigated using *in vivo* models. Even though the hydrogel was designed with the intention to use it for cell delivery in post-MI therapy, it may also be used as an acellular injectable treatment and could be augmented by encapsulating growth factors or extracellular vesicles[263,264]. Alternatively, since collagen I is a common ECM component, the thiol-collagen hydrogel may be used for cell delivery for the regeneration of other organs where cell engraftment is also an issue[1]. Since the hydrogel includes a synthetic multi-arm PEG component, its clearance from the body requires special attention. Although molecules whose molecular weight is less 40 kDa are generally cleared by the kidneys, their shape and any conjugates (such as collagen fragments) may affect their filtration from blood[265,266].

7 Conclusions

The work presented in this thesis demonstrates that:

(Paper I) Tissue-bonding hydrogel based on collagen crosslinked using visible light can improve skin wound healing compared to sutures;

(Paper II) Collagen hydrogel crosslinked using thiol-Michael addition reaction has excellent shear-thinning properties and is suitable for cell encapsulation and delivery;

(Paper III) Single early intramyocardial injection of collagen III results in improved cardiac function compared to repeated injections in a mouse MI model.

Taken together, these studies reflect the versatility of collagen-based hydrogels and contribute new knowledge to collagen hydrogel designs and application strategies for tissue bonding, cell delivery, and post-MI therapy in the field of regenerative medicine.

8 Lay Summary in Swedish (Populärvetenskaplig Sammanfattning)

Det har gjorts många forskningsframsteg under de senaste åren för att öka möjligheter att behandla skadad vävnad. Men det finns fortfarande stora utmaningar i att hitta nya metoder för att reparera eller byta ut skadade organ eller vävnader. Ett exempel på när en vävnadsskada kan uppkomma är då ett blodkärl blir blockerat vid en hjärtinfarkt. En operation kan oftast återställa blodflödet, men ofta kvarstår skador på hjärtat som gör att patienten behöver en hjärttransplantation. Eftersom världens befolkning blir äldre och antalet tillgängliga givare är begränsat, behövs forskning för att hitta alternativa sätt att reparera eller regenerera skadade organ som hjärtat.

Ett sätt är att använda sig av stamceller och hydrogeler. Hydrogeler är tredimensionella polymera geler som kan absorbera stora mängder vatten på samma sätt som tvättsvampar. Hydrogeler kan framställas av samma material som redan finns i våra kroppar, som tex. kollagen. Genom att tillföra hydrogeler till skadade områden kan dessa påverka läkningsprocessen och få de egna cellerna eller tillförda stamceller att växa och reparera skadad vävnad. Men det är fortfarande en utmaning att tillverka hydrogeler med rätt egenskaper för att göra dem säkra och användbara i kliniska situationer.

Denna avhandling beskriver utveckling och användning av hydrogeler för tre olika applikationer: som hjälp vid sårläkning, möjlighet att göra hydrogeler som innehåller stamceller, och användning av hydrogeler vid reparation av hjärtvävnad efter hjärtattack.

I första studien användes kollagen-hydrogel för att laga hudskador utan att sy ihop huden. Hydrogelerna tillverkades av kollagen som kan bilda nätverksstrukturer då det aktiveras av ljus tillsammans med en aktivator. Vi kunde visa att såren läkte med mindre ärrbildning då man använde dessa hydrogeler jämfört med om man använde suturer.

I den andra studien utvecklades ett nytt sätt att tillverka hydrogeler. Genom att använda en modifierad form av kollagen kunde vi få kollagenet att bilda nätverk utan tillsats av aktivator (vilket annars oftast behövs för att skapa hydrogeler). En stor fördel var att denna hydrogel hade egenskaper som gjorde att den kunde injiceras efter att nätverket var färdigbildat. Denna egenskap kan vara värdefull för att kunna innesluta stamceller i hydrogelen och ökar möjligheten för stamcellerna att överleva då de tillförs till skadad vävnad.

I den tredje studien undersökte vi olika sätt att använda hydrogeler för att skydda hjärtvävnad vid en hjärtattack. Vi inducerade hjärtattack hos möss och injicerade sedan kollagen-baserade hydrogeler vid olika tider efter hjärtattacken. Vi jämförde möss som endast fick en injektion direkt efter hjärtattacken med möss som fick flera injektioner, både direkt efter och sedan även en och två veckor efter hjärtattacken. Vi fann till vår förvåning att mössen som endast fick en injektion läkte bättre än möss som fick upprepade injektioner. Detta visar att det är viktigt att undersöka tidsfönstret för optimal behandling.

Sammanfattningsvis bidrar denna avhandling till kunskap om hur kollagen-hydrogeler kan utvecklas och potentiellt användas för reparation och regeneration av skadad vävnad. Vi har visat på möjligheten att använda hydrogeler vid sårläkning, injektion av stamceller och för att förbättra hjärtfunktion efter en hjärtattack.

9 References

1. Ashammakhi, N., Ahadian, S., Darabi, M. A., Tahchi, M. E., Lee, J., Suthiwanich, K., Sheikhi, A., Dokmeci, M. R., Oklu, R. & Khademhosseini, A. Minimally Invasive and Regenerative Therapeutics. *Adv. Mater.* **31,** 1804041 (2018).
2. Flégeau, K., Pace, R., Gautier, H., Rethore, G., Guicheux, J., Le Visage, C. & Weiss, P. Toward the development of biomimetic injectable and macroporous biohydrogels for regenerative medicine. *Adv. Colloid Interface Sci.* **247,** 589–609 (2017).
3. Johnson, T. D. & Christman, K. L. Injectable hydrogel therapies and their delivery strategies for treating myocardial infarction. *Expert Opin. Drug Deliv.* **10,** 59–72 (2013).
4. Dimatteo, R., Darling, N. J. & Segura, T. In situ forming injectable hydrogels for drug delivery and wound repair. *Adv. Drug Deliv. Rev.* **127,** 167–184 (2018).
5. Brunette, I., Roberts, C. J., Vidal, F., Harissi-Dagher, M., Lachaine, J., Sheardown, H., Durr, G. M., Proulx, S. & Griffith, M. Alternatives to eye bank native tissue for corneal stromal replacement. *Prog. Retin. Eye Res.* **59,** 97–130 (2017).
6. Toh, W. S. & Loh, X. J. Advances in hydrogel delivery systems for tissue regeneration. *Mater. Sci. Eng. C* **45,** 690–697 (2014).
7. Drury, J. L. & Mooney, D. J. Hydrogels for tissue engineering: scaffold design variables and applications. *Biomaterials* **24,** 4337–4351 (2003).
8. Zhu, J. Bioactive modification of poly(ethylene glycol) hydrogels for tissue engineering. *Biomaterials* **31,** 4639–4656 (2010).
9. Daviran, M., Longwill, S. M., Casella, J. F. & Schultz, K. M. Rheological characterization of dynamic remodeling of the pericellular region by human mesenchymal stem cell-secreted enzymes in well-defined synthetic hydrogel scaffolds. *Soft Matter* **14,** 3078–3089 (2018).
10. Zustiak, S. P. & Leach, J. B. Hydrolytically Degradable Poly(Ethylene Glycol) Hydrogel Scaffolds with Tunable Degradation and Mechanical Properties. *Biomacromolecules* **11,** 1348–1357 (2010).
11. Naahidi, S., Jafari, M., Logan, M., Wang, Y., Yuan, Y., Bae, H., Dixon, B. & Chen, P. Biocompatibility of hydrogel-based scaffolds for tissue engineering applications. *Biotechnol. Adv.* **35,** 530–544 (2017).
12. He, Y. J., Young, D. A., Mededovic, M., Li, K., Li, C., Tichauer, K., Venerus, D. & Papavasiliou, G. Protease-Sensitive Hydrogel Biomaterials with Tunable Modulus and Adhesion Ligand Gradients for 3D Vascular Sprouting. *Biomacromolecules* **19,** 4168–4181 (2018).
13. Kraehenbuehl, T. P., Ferreira, L. S., Hayward, A. M., Nahrendorf, M., van der Vlies, A. J., Vasile, E., Weissleder, R., Langer, R. & Hubbell, J. A. Human embryonic stem cell-derived microvascular grafts for cardiac tissue preservation after myocardial infarction. *Biomaterials* **32,** 1102–1109 (2011).
14. Lin, K., Zhang, D., Macedo, M. H., Cui, W., Sarmento, B. & Shen, G. Advanced Collagen-Based Biomaterials for Regenerative Biomedicine. *Adv. Funct. Mater.* **29,** 1804943 (2019).

15. Janmey, P. A., Winer, J. P. & Weisel, J. W. Fibrin gels and their clinical and bioengineering applications. *J. R. Soc. Interface* **6,** 1–10 (2009).

16. Highley, C. B., Prestwich, G. D. & Burdick, J. A. Recent advances in hyaluronic acid hydrogels for biomedical applications. *Curr. Opin. Biotechnol.* **40,** 35–40 (2016).

17. Ruvinov, E. & Cohen, S. Alginate biomaterial for the treatment of myocardial infarction: Progress, translational strategies, and clinical outlook: From ocean algae to patient bedside. *Adv. Drug Deliv. Rev.* **96,** 54–76 (2016).

18. Pellá, M. C. G., Lima-Tenório, M. K., Tenório-Neto, E. T., Guilherme, M. R., Muniz, E. C. & Rubira, A. F. Chitosan-based hydrogels: From preparation to biomedical applications. *Carbohydr. Polym.* **196,** 233–245 (2018).

19. Ponta, H., Sherman, L. & Herrlich, P. A. CD44: From adhesion molecules to signalling regulators. *Nat. Rev. Mol. Cell Biol.* **4,** 33–45 (2003).

20. Lynn, A. K., Yannas, I. V. & Bonfield, W. Antigenicity and immunogenicity of collagen. *J. Biomed. Mater. Res. B Appl. Biomater.* **71B,** 343–354 (2004).

21. Anderson, J. M., Rodriguez, A. & Chang, D. T. Foreign body reaction to biomaterials. *Semin. Immunol.* **20,** 86–100 (2008).

22. Kaiser, N. J. & Coulombe, K. L. K. Physiologically inspired cardiac scaffolds for tailored in vivo function and heart regeneration. *Biomed. Mater.* **10,** 034003 (2015).

23. Corradetti, B., Taraballi, F., Corbo, C., Cabrera, F., Pandolfi, L., Minardi, S., Wang, X., Eps, J. V., Bauza, G., Weiner, B. & Tasciotti, E. Immune tuning scaffold for the local induction of a pro-regenerative environment. *Sci. Rep.* **7,** 1–13 (2017).

24. Sorushanova, A., Delgado, L. M., Wu, Z., Shologu, N., Kshirsagar, A., Raghunath, R., Mullen, A. M., Bayon, Y., Pandit, A., Raghunath, M. & Zeugolis, D. I. The Collagen Suprafamily: From Biosynthesis to Advanced Biomaterial Development. *Adv. Mater.* **31,** 1801651 (2019).

25. Yue, K., Trujillo-de Santiago, G., Alvarez, M. M., Tamayol, A., Annabi, N. & Khademhosseini, A. Synthesis, properties, and biomedical applications of gelatin methacryloyl (GelMA) hydrogels. *Biomaterials* **73,** 254–271 (2015).

26. Ravichandran, R., Islam, M. M., Alarcon, E., Samanta, A., Wang, S., Lundström, P., Hilborn, J., Griffith, M. & Phopase, J. Functionalised type-I collagen as hydrogel building block for bio-orthogonal tissue engineering applications. *J. Mater. Chem. B* **4,** 318–326 (2016).

27. Yang, K., Sun, J., Wei, D., Yuan, L., Yang, J., Guo, L., Fan, H. & Zhang, X. Photo-crosslinked mono-component type II collagen hydrogel as a matrix to induce chondrogenic differentiation of bone marrow mesenchymal stem cells. *J. Mater. Chem. B* **5,** 8707–8718 (2017).

28. Nimmo, C. M., Owen, S. C. & Shoichet, M. S. Diels−Alder Click Cross-Linked Hyaluronic Acid Hydrogels for Tissue Engineering. *Biomacromolecules* **12,** 824–830 (2011).

29. Fu, S., Dong, H., Deng, X., Zhuo, R. & Zhong, Z. Injectable hyaluronic acid/poly(ethylene glycol) hydrogels crosslinked via strain-promoted azide-alkyne cycloaddition click reaction. *Carbohydr. Polym.* **169,** 332–340 (2017).

30. Wang, L., Neumann, M., Fu, T., Li, W., Cheng, X. & Su, B.-L. Porous and responsive hydrogels for cell therapy. *Curr. Opin. Colloid Interface Sci.* **38,** 135–157 (2018).

31. Hartwell, R., Chan, B., Elliott, K., Alnojeidi, H. & Ghahary, A. Polyvinyl alcohol-graft-polyethylene glycol hydrogels improve utility and biofunctionality of injectable collagen biomaterials. *Biomed. Mater.* **11,** 035013 (2016).

32. Tseng, T.-C., Tao, L., Hsieh, F.-Y., Wei, Y., Chiu, I.-M. & Hsu, S. An Injectable, Self-Healing Hydrogel to Repair the Central Nervous System. *Adv. Mater.* **27,** 3518–3524 (2015).

33. Yu, L. & Ding, J. Injectable hydrogels as unique biomedical materials. *Chem. Soc. Rev.* **37,** 1473–1481 (2008).

34. Mantooth, S. M., Munoz-Robles, B. G. & Webber, M. J. Dynamic Hydrogels from Host–Guest Supramolecular Interactions. *Macromol. Biosci.* **19,** 1800281 (2019).

35. Malcor, J.-D., Juskaite, V., Gavriilidou, D., Hunter, E. J., Davidenko, N., Hamaia, S., Sinha, S., Cameron, R. E., Best, S. M., Leitinger, B. & Farndale, R. W. Coupling of a specific photoreactive triple-helical peptide to crosslinked collagen films restores binding and activation of DDR2 and VWF. *Biomaterials* **182,** 21–34 (2018).

36. Tam, H., Zhang, W., Infante, D., Parchment, N., Sacks, M. & Vyavahare, N. Fixation of Bovine Pericardium-Based Tissue Biomaterial with Irreversible Chemistry Improves Biochemical and Biomechanical Properties. *J Cardiovasc. Transl. Res.* **10,** 194–205 (2017).

37. Yang, Y., Ritchie, A. C. & Everitt, N. M. Comparison of glutaraldehyde and procyanidin cross-linked scaffolds for soft tissue engineering. *Mater. Sci. Eng. C* **80,** 263–273 (2017).

38. Casali Dominic M., Yost Michael J. & Matthews Michael A. Eliminating glutaraldehyde from crosslinked collagen films using supercritical CO2. *J. Biomed. Mater. Res. A* **106,** 86–94 (2017).

39. Umashankar, P. R., Mohanan, P. V. & Kumari, T. V. Glutaraldehyde Treatment Elicits Toxic Response Compared to Decellularization in Bovine Pericardium. *Toxicol. Int.* **19,** 51–58 (2012).

40. Davidenko, N., Schuster, C. F., Bax, D. V., Raynal, N., Farndale, R. W., Best, S. M. & Cameron, R. E. Control of crosslinking for tailoring collagen-based scaffolds stability and mechanics. *Acta Biomater.* **25,** 131–142 (2015).

41. Moshnikova, A. B., Afanasyev, V. N., Proussakova, O. V., Chernyshov, S., Gogvadze, V. & Beletsky, I. P. Cytotoxic activity of 1-ethyl-3-(3-dimethylaminopropyl)-carbodiimide is underlain by DNA interchain cross-linking. *Cell. Mol. Life Sci. CMLS* **63,** 229–234 (2006).

42. Gilles, M. A., Hudson, A. Q. & Borders, C. L. Stability of water-soluble carbodiimides in aqueous solution. *Anal. Biochem.* **184,** 244–248 (1990).

43. Omobono, M. A., Zhao, X., Furlong, M. A., Kwon, C.-H., Gill, T. J., Randolph, M. A. & Redmond, R. W. Enhancing the stiffness of collagen hydrogels for delivery of encapsulated

chondrocytes to articular lesions for cartilage regeneration. *J. Biomed. Mater. Res. A* **103,** 1332–1338 (2015).

44. Yang, G., Xiao, Z., Long, H., Ma, K., Zhang, J., Ren, X. & Zhang, J. Assessment of the characteristics and biocompatibility of gelatin sponge scaffolds prepared by various crosslinking methods. *Sci. Rep.* **8,** 1616 (2018).

45. Lin, Y.-L., Chen, C.-P., Lo, C.-M. & Wang, H.-S. Stiffness-controlled three-dimensional collagen scaffolds for differentiation of human Wharton's jelly mesenchymal stem cells into cardiac progenitor cells. *J. Biomed. Mater. Res. A* **104A,** 2234– 2242 (2016).

46. Ibusuki, S., Halbesma, G. J., Randolph, M. A., Redmond, R. W., Kochevar, I. E. & Gill, T. J. Photochemically Cross-Linked Collagen Gels as Three-Dimensional Scaffolds for Tissue Engineering. *Tissue Eng.* **13,** 1995–2001 (2007).

47. Chan, B. p., Hui, T. y., Chan, O. c. m., So, K.-F., Lu, W., Cheung, K. m. c., Salomatina, E. & Yaroslavsky, A. Photochemical Cross-Linking for Collagen-Based Scaffolds: A Study on Optical Properties, Mechanical Properties, Stability, and Hematocompatibility. *Tissue Eng.* **13,** 73–85 (2007).

48. Yue, K., Liu, Y., Byambaa, B., Singh, V., Liu, W., Li, X., Sun, Y., Zhang, Y. S., Tamayol, A., Zhang, P., Ng, K. W., Annabi, N. & Khademhosseini, A. Visible light crosslinkable human hair keratin hydrogels. *Bioeng. Transl. Med.* **3,** 37–48 (2018).

49. Zhou, Y., Zhao, S., Zhang, C., Liang, K., Li, J., Yang, H., Gu, S., Bai, Z., Ye, D. & Xu, W. Photopolymerized maleilated chitosan/thiol-terminated poly (vinyl alcohol) hydrogels as potential tissue engineering scaffolds. *Carbohydr. Polym.* **184,** 383–389 (2018).

50. Shih, H. & Lin, C.-C. Visible-Light-Mediated Thiol-Ene Hydrogelation Using Eosin-Y as the Only Photoinitiator. *Macromol. Rapid Commun.* **34,** 269–273 (2013).

51. Han, S., Hwang, B. W., Jeon, E. Y., Jung, D., Lee, G. H., Keum, D. H., Kim, K. S., Yun, S. H., Cha, H. J. & Hahn, S. K. Upconversion Nanoparticles/Hyaluronate-Rose Bengal Conjugate Complex for Noninvasive Photochemical Tissue Bonding. *ACS Nano* **11,** 9979–9988 (2017).

52. Qin, X.-H., Wang, X., Rottmar, M., Nelson, B. J. & Maniura-Weber, K. Near-Infrared Light-Sensitive Polyvinyl Alcohol Hydrogel Photoresist for Spatiotemporal Control of Cell-Instructive 3D Microenvironments. *Adv. Mater.* **30,** 1705564 (2018).

53. Kolb, H. C., Finn, M. G. & Sharpless, K. B. Click Chemistry: Diverse Chemical Function from a Few Good Reactions. *Angew. Chem. Int. Ed.* **40,** 2004–2021 (2001).

54. Nimmo, C. M. & Shoichet, M. S. Regenerative Biomaterials that "Click": Simple, Aqueous-Based Protocols for Hydrogel Synthesis, Surface Immobilization, and 3D Patterning. *Bioconjug. Chem.* **22,** 2199–2209 (2011).

55. Zou, Y., Zhang, L., Yang, L., Zhu, F., Ding, M., Lin, F., Wang, Z. & Li, Y. "Click" chemistry in polymeric scaffolds: Bioactive materials for tissue engineering. *J. Controlled Release* **273,** 160–179 (2018).

56. Jiang, Y., Chen, J., Deng, C., Suuronen, E. J. & Zhong, Z. Click hydrogels, microgels and nanogels: Emerging platforms for drug delivery and tissue engineering. *Biomaterials* **35,** 4969–4985 (2014).

57. Ryan, E. J., Ryan, A. J., González-Vázquez, A., Philippart, A., Ciraldo, F. E., Hobbs, C., Nicolosi, V., Boccaccini, A. R., Kearney, C. J. & O'Brien, F. J. Collagen scaffolds functionalised with copper-eluting bioactive glass reduce infection and enhance osteogenesis and angiogenesis both in vitro and in vivo. *Biomaterials* **197,** 405–416 (2019).

58. Madl, C. M., Katz, L. M. & Heilshorn, S. C. Bio-Orthogonally Crosslinked, Engineered Protein Hydrogels with Tunable Mechanics and Biochemistry for Cell Encapsulation. *Adv. Funct. Mater.* **26,** 3612–3620 (2016).

59. DeForest, C. A., Polizzotti, B. D. & Anseth, K. S. Sequential click reactions for synthesizing and patterning three-dimensional cell microenvironments. *Nat. Mater.* **8,** 659–664 (2009).

60. Han, S.-S., Yoon, H. Y., Yhee, J. Y., Cho, M. O., Shim, H.-E., Jeong, J.-E., Lee, D.-E., Kim, K., Guim, H., Lee, J. H., Huh, K. M. & Kang, S.-W. In situ cross-linkable hyaluronic acid hydrogels using copper free click chemistry for cartilage tissue engineering. *Polym. Chem.* **9,** 20–27 (2017).

61. Nair, D. P., Podgórski, M., Chatani, S., Gong, T., Xi, W., Fenoli, C. R. & Bowman, C. N. The Thiol-Michael Addition Click Reaction: A Powerful and Widely Used Tool in Materials Chemistry. *Chem. Mater.* **26,** 724–744 (2014).

62. Chatani, S., Nair, D. P. & Bowman, C. N. Relative reactivity and selectivity of vinyl sulfones and acrylates towards the thiol–Michael addition reaction and polymerization. *Polym. Chem.* **4,** 1048–1055 (2013).

63. Chawla, K., Yu, T., Liao, S. W. & Guan, Z. Biodegradable and Biocompatible Synthetic Saccharide−Peptide Hydrogels for Three-Dimensional Stem Cell Culture. *Biomacromolecules* **12,** 560–567 (2011).

64. Liu, Z. Q., Wei, Z., Zhu, X. L., Huang, G. Y., Xu, F., Yang, J. H., Osada, Y., Zrínyi, M., Li, J. H. & Chen, Y. M. Dextran-based hydrogel formed by thiol-Michael addition reaction for 3D cell encapsulation. *Colloids Surf. B Biointerfaces* **128,** 140–148 (2015).

65. Qiu, B., Stefanos, S., Ma, J., Lalloo, A., Perry, B. A., Leibowitz, M. J., Sinko, P. J. & Stein, S. A hydrogel prepared by in situ cross-linking of a thiol-containing poly(ethylene glycol)-based copolymer: a new biomaterial for protein drug delivery. *Biomaterials* **24,** 11–18 (2003).

66. Li, R., Cai, Z., Li, Z., Zhang, Q., Zhang, S., Deng, L., Lu, L., Li, L. & Zhou, C. Synthesis of in-situ formable hydrogels with collagen and hyaluronan through facile Michael addition. *Mater. Sci. Eng. C* **77,** 1035–1043 (2017).

67. Lutolf, M. P., Lauer-Fields, J. L., Schmoekel, H. G., Metters, A. T., Weber, F. E., Fields, G. B. & Hubbell, J. A. Synthetic matrix metalloproteinase-sensitive hydrogels for the conduction of tissue regeneration: Engineering cell-invasion characteristics. *Proc. Natl. Acad. Sci.* **100,** 5413–5418 (2003).

68. Anderson, J. M. Future challenges in the in vitro and in vivo evaluation of biomaterial biocompatibility. *Regen. Biomater.* **3,** 73–77 (2016).

69. Engler, A. J., Carag-Krieger, C., Johnson, C. P., Raab, M., Tang, H.-Y., Speicher, D. W., Sanger, J. W., Sanger, J. M. & Discher, D. E. Embryonic cardiomyocytes beat best on a

matrix with heart-like elasticity: scar-like rigidity inhibits beating. *J. Cell Sci.* **121,** 3794–3802 (2008).

70. Engler, A. J., Sen, S., Sweeney, H. L. & Discher, D. E. Matrix Elasticity Directs Stem Cell Lineage Specification. *Cell* **126,** 677–689 (2006).

71. Floren, M., Bonani, W., Dharmarajan, A., Motta, A., Migliaresi, C. & Tan, W. Human mesenchymal stem cells cultured on silk hydrogels with variable stiffness and growth factor differentiate into mature smooth muscle cell phenotype. *Acta Biomater.* **31,** 156–166 (2016).

72. Zhang, S., Ma, X., Guo, J., Yao, K., Wang, C., Dong, Z., Zhu, H., Fan, F., Huang, Z., Yang, X., Qian, J., Zou, Y., Sun, A. & Ge, J. Bone marrow CD34+ cell subset under induction of moderate stiffness of extracellular matrix after myocardial infarction facilitated endothelial lineage commitment in vitro. *Stem Cell Res. Ther.* **8,** 280 (2017).

73. Seidlits, S. K., Khaing, Z. Z., Petersen, R. R., Nickels, J. D., Vanscoy, J. E., Shear, J. B. & Schmidt, C. E. The effects of hyaluronic acid hydrogels with tunable mechanical properties on neural progenitor cell differentiation. *Biomaterials* **31,** 3930–3940 (2010).

74. Banerjee, A., Arha, M., Choudhary, S., Ashton, R. S., Bhatia, S. R., Schaffer, D. V. & Kane, R. S. The influence of hydrogel modulus on the proliferation and differentiation of encapsulated neural stem cells. *Biomaterials* **30,** 4695–4699 (2009).

75. Fan, L., Liu, C., Chen, X., Zou, Y., Zhou, Z., Lin, C., Tan, G., Zhou, L., Ning, C. & Wang, Q. Directing Induced Pluripotent Stem Cell Derived Neural Stem Cell Fate with a Three-Dimensional Biomimetic Hydrogel for Spinal Cord Injury Repair. *ACS Appl. Mater. Interfaces* **10,** 17742–17755 (2018).

76. Alarcon, E. I., Vulesevic, B., Argawal, A., Ross, A., Bejjani, P., Podrebarac, J., Ravichandran, R., Phopase, J., Suuronen, E. J. & Griffith, M. Coloured cornea replacements with anti-infective properties: expanding the safe use of silver nanoparticles in regenerative medicine. *Nanoscale* **8,** 6484–6489 (2016).

77. Cha, B.-H., Shin, S. R., Leijten, J., Li, Y.-C., Singh, S., Liu, J. C., Annabi, N., Abdi, R., Dokmeci, M. R., Vrana, N. E., Ghaemmaghami, A. M. & Khademhosseini, A. Integrin-Mediated Interactions Control Macrophage Polarization in 3D Hydrogels. *Adv. Healthc. Mater.* **6,** 1700289 (2017).

78. Sun, G., Zhang, X., Shen, Y.-I., Sebastian, R., Dickinson, L. E., Fox-Talbot, K., Reinblatt, M., Steenbergen, C., Harmon, J. W. & Gerecht, S. Dextran hydrogel scaffolds enhance angiogenic responses and promote complete skin regeneration during burn wound healing. *Proc. Natl. Acad. Sci.* **108,** 20976–20981 (2011).

79. Özkaya, N., Leger, D., Goldsheyder, D. & Nordin, M. Mechanical Properties of Biological Tissues. In: *Fundamentals of Biomechanics.* 361–387 (Springer International Publishing, 2017).

80. Cameron, A. R., Frith, J. E., Gomez, G. A., Yap, A. S. & Cooper-White, J. J. The effect of time-dependent deformation of viscoelastic hydrogels on myogenic induction and Rac1 activity in mesenchymal stem cells. *Biomaterials* **35,** 1857–1868 (2014).

81. Chaudhuri, O., Gu, L., Klumpers, D., Darnell, M., Bencherif, S. A., Weaver, J. C., Huebsch, N., Lee, H., Lippens, E., Duda, G. N. & Mooney, D. J. Hydrogels with tunable stress relaxation regulate stem cell fate and activity. *Nat. Mater.* **15,** 326–334 (2016).

82. Darnell, M., Young, S., Gu, L., Shah, N., Lippens, E., Weaver, J., Duda, G. & Mooney, D. Substrate Stress-Relaxation Regulates Scaffold Remodeling and Bone Formation In Vivo. *Adv. Healthc. Mater.* **6,** 1601185 (2017).

83. Mirazul Islam, M., Ravichandran, R., Olsen, D., K. Ljunggren, M., Fagerholm, P., J. Lee, C., Griffith, M. & Phopase, J. Self-assembled collagen-like-peptide implants as alternatives to human donor corneal transplantation. *RSC Adv.* **6,** 55745–55749 (2016).

84. Buznyk, O., Pasyechnikova, N., Islam, M. M., Iakymenko, S., Fagerholm, P. & Griffith, M. Bioengineered Corneas Grafted as Alternatives to Human Donor Corneas in Three High-Risk Patients. *Clin. Transl. Sci.* **8,** 558–562 (2015).

85. Cornelison, R. C., Gonzalez-Rothi, E. J., Porvasnik, S. L., Wellman, S. M., Park, J. H., Fuller, D. D. & Schmidt, C. E. Injectable hydrogels of optimized acellular nerve for injection in the injured spinal cord. *Biomed. Mater.* **13,** 034110 (2018).

86. Breen, B. A., Kraskiewicz, H., Ronan, R., Kshiragar, A., Patar, A., Sargeant, T., Pandit, A. & McMahon, S. S. Therapeutic Effect of Neurotrophin-3 Treatment in an Injectable Collagen Scaffold Following Rat Spinal Cord Hemisection Injury. *ACS Biomater. Sci. Eng.* **3,** 1287–1295 (2017).

87. Rodell, C. B., MacArthur, J. W., Dorsey, S. M., Wade, R. J., Wang, L. L., Woo, Y. J. & Burdick, J. A. Shear-Thinning Supramolecular Hydrogels with Secondary Autonomous Covalent Crosslinking to Modulate Viscoelastic Properties In Vivo. *Adv. Funct. Mater.* **25,** 636–644 (2015).

88. Liu, Y. & Hsu, S. Synthesis and Biomedical Applications of Self-healing Hydrogels. *Front. Chem.* **6,** 449 (2018).

89. Loh, Q. L. & Choong, C. Three-Dimensional Scaffolds for Tissue Engineering Applications: Role of Porosity and Pore Size. *Tissue Eng. Part B Rev.* **19,** 485–502 (2013).

90. Zidek, J., Vojtova, L., Abdel-Mohsen, A. M., Chmelik, J., Zikmund, T., Brtnikova, J., Jakubicek, R., Zubal, L., Jan, J. & Kaiser, J. Accurate micro-computed tomography imaging of pore spaces in collagen-based scaffold. *J. Mater. Sci. Mater. Med.* **27,** 110 (2016).

91. Bartoš, M., Suchý, T. & Foltán, R. Note on the use of different approaches to determine the pore sizes of tissue engineering scaffolds: what do we measure? *Biomed. Eng. OnLine* **17,** 110 (2018).

92. Murphy, C. M. & O'Brien, F. J. Understanding the effect of mean pore size on cell activity in collagen-glycosaminoglycan scaffolds. *Cell Adhes. Migr.* **4,** 377–381 (2010).

93. Barczyk, M., Carracedo, S. & Gullberg, D. Integrins. *Cell Tissue Res.* **339,** 269–280 (2010).

94. Lian, C., Wang, X., Qiu, X., Wu, Z., Gao, B., Liu, L., Liang, G., Zhou, H., Yang, X., Peng, Y., Liang, A., Xu, C., Huang, D. & Su, P. Collagen type II suppresses articular chondrocyte hypertrophy and osteoarthritis progression by promoting integrin β1−SMAD1 interaction. *Bone Res.* **7,** 8 (2019).

95. Ahmadi, A., McNeill, B., Vulesevic, B., Kordos, M., Mesana, L., Thorn, S., Renaud, J. M., Manthorp, E., Kuraitis, D., Toeg, H., Mesana, T. G., Davis, D. R., Beanlands, R. S., DaSilva, J. N., deKemp, R. A., Ruel, M. & Suuronen, E. J. The role of integrin α2 in cell and matrix therapy that improves perfusion, viability and function of infarcted myocardium. *Biomaterials* **35,** 4749–4758 (2014).

96. Arya, N., Forget, A., Sarem, M. & Shastri, V. P. RGDSP functionalized carboxylated agarose as extrudable carriers for chondrocyte delivery. *Mater. Sci. Eng. C* **99,** 103–111 (2019).

97. Li, X. & Fan, D. Smart Collagen Hydrogels Based on 1-Ethyl-3-methylimidazolium Acetate and Microbial Transglutaminase for Potential Applications in Tissue Engineering and Cancer Therapy. *ACS Biomater. Sci. Eng.* **5,** 3523–3536 (2019).

98. Liu, Y., Yang, J., Luo, Z., Li, D., Lu, J., Wang, Q., Xiao, Y. & Zhang, X. Development of an injectable thiolated icariin functionalized collagen/hyaluronic hydrogel to promote cartilage formation in vitro and in vivo. *J. Mater. Chem. B* **7,** 2845–2854 (2019).

99. D. Baldwin, A. & L. Kiick, K. Reversible maleimide – thiol adducts yield glutathione-sensitive poly(ethylene glycol)– heparin hydrogels. *Polym. Chem.* **4,** 133–143 (2013).

100. Wu, D., Wang, W., Diaz-Dussan, D., Peng, Y.-Y., Chen, Y., Narain, R. & Hall, D. G. In Situ Forming, Dual-Crosslink Network, Self-Healing Hydrogel Enabled by a Bioorthogonal Nopoldiol–Benzoxaborolate Click Reaction with a Wide pH Range. *Chem. Mater.* **31,** 4092–4102 (2019).

101. Zhang, M., Song, C.-C., Du, F.-S. & Li, Z.-C. Supersensitive Oxidation-Responsive Biodegradable PEG Hydrogels for Glucose-Triggered Insulin Delivery. *ACS Appl. Mater. Interfaces* **9,** 25905–25914 (2017).

102. Shahriari, D., Koffler, J., Lynam, D. A., Tuszynski, M. H. & Sakamoto, J. S. Characterizing the degradation of alginate hydrogel for use in multilumen scaffolds for spinal cord repair. *J. Biomed. Mater. Res. A* **104,** 611–619 (2016).

103. Ghuman, H., Mauney, C., Donnelly, J., Massensini, A. R., Badylak, S. F. & Modo, M. Biodegradation of ECM hydrogel promotes endogenous brain tissue restoration in a rat model of stroke. *Acta Biomater.* **80,** 66–84 (2018).

104. Speidel, A. T., Stuckey, D. J., Chow, L. W., Jackson, L. H., Noseda, M., Abreu Paiva, M., Schneider, M. D. & Stevens, M. M. Multimodal Hydrogel-Based Platform To Deliver and Monitor Cardiac Progenitor/Stem Cell Engraftment. *ACS Cent. Sci.* **3,** 338–348 (2017).

105. Kadner, K., Dobner, S., Franz, T., Bezuidenhout, D., Sirry, M. S., Zilla, P. & Davies, N. H. The beneficial effects of deferred delivery on the efficiency of hydrogel therapy post myocardial infarction. *Biomaterials* **33,** 2060–2066 (2012).

106. Yoshizumi, T., Zhu, Y., Jiang, H., D'Amore, A., Sakaguchi, H., Tchao, J., Tobita, K. & Wagner, W. R. Timing effect of intramyocardial hydrogel injection for positively impacting left ventricular remodeling after myocardial infarction. *Biomaterials* **83,** 182–193 (2016).

107. Jha, A. K., Tharp, K. M., Browne, S., Ye, J., Stahl, A., Yeghiazarians, Y. & Healy, K. E. Matrix metalloproteinase-13 mediated degradation of hyaluronic acid-based matrices

orchestrates stem cell engraftment through vascular integration. *Biomaterials* **89,** 136–147 (2016).

108. Malliaras, K., Cheng, K., Smith, R. R., Wu, E., Bonow, R., Mendizabal, A., Gerstenblith, G., Johnston, P. V., Schuleri, K., Lardo, A. C., Marbán, L., Makkar, R. & Marbán, E. Intracoronary Cardiosphere-Derived Cells After Myocardial Infarction: Magnetic Resonance Imaging Analysis of Regeneration and Determinants of Efficacy in the Final 1-year Results of the CADUCEUS Trial. *J. Am. Coll. Cardiol.* **61,** E104 (2013).
109. Delewi, R., Andriessen, A., Tijssen, J. G. P., Zijlstra, F., Piek, J. J. & Hirsch, A. Impact of intracoronary cell therapy on left ventricular function in the setting of acute myocardial infarction: a meta-analysis of randomised controlled clinical trials. *Heart* **99,** 225–232 (2013).
110. Wang, C., Han, X., Li, Y. & Zhang, B. Impact of bone marrow mononuclear cells therapy on left ventricular function in patients with ST-elevated myocardial infarction. *Medicine (Baltimore)* **97,** e0359 (2018).
111. Karantalis, V. & Hare, J. M. Use of Mesenchymal Stem Cells for Therapy of Cardiac Disease. *Circ. Res.* **116,** 1413–1430 (2015).
112. Bagno, L., Hatzistergos, K. E., Balkan, W. & Hare, J. M. Mesenchymal Stem Cell-Based Therapy for Cardiovascular Disease: Progress and Challenges. *Mol. Ther.* **26,** 1610–1623 (2018).
113. Rojas, S. V., Martens, A., Zweigerdt, R., Baraki, H., Rathert, C., Schecker, N., Rojas-Hernandez, S., Schwanke, K., Martin, U., Haverich, A. & Kutschka, I. Transplantation Effectiveness of Induced Pluripotent Stem Cells Is Improved by a Fibrinogen Biomatrix in an Experimental Model of Ischemic Heart Failure. *Tissue Eng. Part A* **21,** 1991–2000 (2015).
114. Ban, K., Park, H.-J., Kim, S., Andukuri, A., Cho, K.-W., Hwang, J. W., Cha, H. J., Kim, S. Y., Kim, W.-S., Jun, H.-W. & Yoon, Y.-S. Cell Therapy with Embryonic Stem Cell-Derived Cardiomyocytes Encapsulated in Injectable Nanomatrix Gel Enhances Cell Engraftment and Promotes Cardiac Repair. *ACS Nano* **8,** 10815–10825 (2014).
115. Matsushita, S., Forrester, J. S., Li, C., Sato, M., Li, Z., Guo, X., Guan, J. & Amano, A. Administration of cells with thermosensitive hydrogel enhances the functional recovery in ischemic rat heart. *J. Tissue Eng.* **7,** 1–8 (2016).
116. Ciuffreda, M. C., Malpasso, G., Chokoza, C., Bezuidenhout, D., Goetsch, K. P., Mura, M., Pisano, F., Davies, N. H. & Gnecchi, M. Synthetic extracellular matrix mimic hydrogel improves efficacy of mesenchymal stromal cell therapy for ischemic cardiomyopathy. *Acta Biomater.* **70,** 71–83 (2018).
117. Lee, A. S., Inayathullah, M., Lijkwan, M. A., Zhao, X., Sun, W., Park, S., Hong, W. X., Parekh, M. B., Malkovskiy, A. V., Lau, E., Qin, X., Pothineni, V. R., Sanchez-Freire, V., Zhang, W. Y., Kooreman, N. G., Ebert, A. D., Chan, C. K. F., Nguyen, P. K., Rajadas, J. & Wu, J. C. Prolonged survival of transplanted stem cells after ischaemic injury via the slow release of pro-survival peptides from a collagen matrix. *Nat. Biomed. Eng.* **2,** 104–113 (2018).

118. Ketabat, F., Khorshidi, S. & Karkhaneh, A. Application of minimally invasive injectable conductive hydrogels as stimulating scaffolds for myocardial tissue engineering. *Polym. Int.* **67,** 975–982 (2018).

119. Tong, X. & Yang, F. Recent Progress in Developing Injectable Matrices for Enhancing Cell Delivery and Tissue Regeneration. *Adv. Healthc. Mater.* **7,** 1701065 (2018).

120. Aguado, B. A., Mulyasasmita, W., Su, J., Lampe, K. J. & Heilshorn, S. C. Improving Viability of Stem Cells During Syringe Needle Flow Through the Design of Hydrogel Cell Carriers. *Tissue Eng. Part A* **18,** 806–815 (2012).

121. Gaffey, A. C., Chen, M. H., Trubelja, A., Venkataraman, C. M., Chen, C. W., Chung, J. J., Schultz, S., Sehgal, C. M., Burdick, J. A. & Atluri, P. Delivery of progenitor cells with injectable shear-thinning hydrogel maintains geometry and normalizes strain to stabilize cardiac function after ischemia. *J. Thorac. Cardiovasc. Surg.* **157,** 1479–1490 (2019).

122. Huang, P., Tian, X., Li, Q. & Yang, Y. New strategies for improving stem cell therapy in ischemic heart disease. *Heart Fail. Rev.* **21,** 737–752 (2016).

123. Spadaccio, C., Nappi, F., Marco, F. D., Sedati, P., Taffon, C., Nenna, A., Crescenzi, A., Chello, M., Trombetta, M., Gambardella, I. & Rainer, A. Implantation of a Poly-l-Lactide GCSF-Functionalized Scaffold in a Model of Chronic Myocardial Infarction. *J Cardiovasc. Transl. Res.* **10,** 47–65 (2017).

124. Hosoyama, K., Ahumada, M., McTiernan, C. D., Davis, D. R., Variola, F., Ruel, M., Liang, W., Suuronen, E. J. & Alarcon, E. I. Nanoengineered Electroconductive Collagen-Based Cardiac Patch for Infarcted Myocardium Repair. *ACS Appl. Mater. Interfaces* **10,** 44668–44677 (2018).

125. Serpooshan, V., Zhao, M., Metzler, S. A., Wei, K., Shah, P. B., Wang, A., Mahmoudi, M., Malkovskiy, A. V., Rajadas, J., Butte, M. J., Bernstein, D. & Ruiz-Lozano, P. The effect of bioengineered acellular collagen patch on cardiac remodeling and ventricular function post myocardial infarction. *Biomaterials* **34,** 9048–9055 (2013).

126. Stelzle, D., Shah, A. S. V., Anand, A., Strachan, F. E., Chapman, A. R., Denvir, M. A., Mills, N. L. & McAllister, D. A. High-sensitivity cardiac troponin I and risk of heart failure in patients with suspected acute coronary syndrome: a cohort study. *Eur. Heart J. - Qual. Care Clin. Outcomes* **4,** 36–42 (2018).

127. Gorman, R. C. & Gorman, J. H. A Clinical Commentary on the Article "Injectable Acellular Hydrogels for Cardiac Repair". *J Cardiovasc. Transl. Res.* **4,** 543–544 (2011).

128. Christman, K. L., Fok, H. H., Sievers, R. E., Fang, Q. & Lee, R. J. Fibrin Glue Alone and Skeletal Myoblasts in a Fibrin Scaffold Preserve Cardiac Function after Myocardial Infarction. *Tissue Eng.* **10,** 403–409 (2004).

129. Tous, E., Purcell, B., Ifkovits, J. L. & Burdick, J. A. Injectable Acellular Hydrogels for Cardiac Repair. *J Cardiovasc. Transl. Res.* **4,** 528–542 (2011).

130. Blackburn, N. J. R., Sofrenovic, T., Kuraitis, D., Ahmadi, A., McNeill, B., Deng, C., Rayner, K. J., Zhong, Z., Ruel, M. & Suuronen, E. J. Timing underpins the benefits associated with injectable collagen biomaterial therapy for the treatment of myocardial infarction. *Biomaterials* **39,** 182–192 (2015).

131. Li, Z., Masumoto, H., Jo, J., Yamazaki, K., Ikeda, T., Tabata, Y. & Minatoya, K. Sustained release of basic fibroblast growth factor using gelatin hydrogel improved left ventricular function through the alteration of collagen subtype in a rat chronic myocardial infarction model. *Gen. Thorac. Cardiovasc. Surg.* **66,** 641–647 (2018).

132. Wassenaar, J. W., Gaetani, R., Garcia, J. J., Braden, R. L., Luo, C. G., Huang, D., DeMaria, A. N., Omens, J. H. & Christman, K. L. Evidence for Mechanisms Underlying the Functional Benefits of a Myocardial Matrix Hydrogel for Post-MI Treatment. *J. Am. Coll. Cardiol.* **67,** 1074–1086 (2016).

133. Leor, J., Tuvia, S., Guetta, V., Manczur, F., Castel, D., Willenz, U., Petneházy, Ö., Landa, N., Feinberg, M. S., Konen, E., Goitein, O., Tsur-Gang, O., Shaul, M., Klapper, L. & Cohen, S. Intracoronary Injection of In Situ Forming Alginate Hydrogel Reverses Left Ventricular Remodeling After Myocardial Infarction in Swine. *J. Am. Coll. Cardiol.* **54,** 1014–1023 (2009).

134. Choy, J. S., Leng, S., Acevedo-Bolton, G., Shaul, S., Fu, L., Guo, X., Zhong, L., Guccione, J. M. & Kassab, G. S. Efficacy of intramyocardial injection of Algisyl-LVR for the treatment of ischemic heart failure in swine. *Int. J. Cardiol.* **255,** 129–135 (2018).

135. Wang, L. L., Liu, Y., Chung, J. J., Wang, T., Gaffey, A. C., Lu, M., Cavanaugh, C. A., Zhou, S., Kanade, R., Atluri, P., Morrisey, E. E. & Burdick, J. A. Sustained miRNA delivery from an injectable hydrogel promotes cardiomyocyte proliferation and functional regeneration after ischaemic injury. *Nat. Biomed. Eng.* **1,** 983–992 (2017).

136. Purcell, B. P., Elser, J. A., Mu, A., Margulies, K. B. & Burdick, J. A. Synergistic effects of SDF-1α chemokine and hyaluronic acid release from degradable hydrogels on directing bone marrow derived cell homing to the myocardium. *Biomaterials* **33,** 7849–7857 (2012).

137. Fan, Z., Fu, M., Xu, Z., Zhang, B., Li, Z., Li, H., Zhou, X., Liu, X., Duan, Y., Lin, P.-H., Duann, P., Xie, X., Ma, J., Liu, Z. & Guan, J. Sustained Release of a Peptide-Based Matrix Metalloproteinase-2 Inhibitor to Attenuate Adverse Cardiac Remodeling and Improve Cardiac Function Following Myocardial Infarction. *Biomacromolecules* **18,** 2820–2829 (2017).

138. Yoon, S. J., Hong, S., Fang, Y. H., Song, M., Son, K. H., Son, H. S., Kim, S. K., Sun, K. & Park, Y. Differential regeneration of myocardial infarction depending on the progression of disease and the composition of biomimetic hydrogel. *J. Biosci. Bioeng.* **118,** 461–468 (2014).

139. Monaghan, M. G., Holeiter, M., Brauchle, E., Layland, S. L., Lu, Y., Deb, A., Pandit, A., Nsair, A. & Schenke-Layland, K. Exogenous miR-29B Delivery Through a Hyaluronan-Based Injectable System Yields Functional Maintenance of the Infarcted Myocardium. *Tissue Eng. Part A* **24,** 57–67 (2017).

140. Plotkin, M., Vaibavi, S. R., Rufaihah, A. J., Nithya, V., Wang, J., Shachaf, Y., Kofidis, T. & Seliktar, D. The effect of matrix stiffness of injectable hydrogels on the preservation of cardiac function after a heart attack. *Biomaterials* **35,** 1429–1438 (2014).

141. Rufaihah, A. J., Johari, N. A., Vaibavi, S. R., Plotkin, M., Di Thien, D. T., Kofidis, T. & Seliktar, D. Dual delivery of VEGF and ANG-1 in ischemic hearts using an injectable hydrogel. *Acta Biomater.* **48,** 58–67 (2017).

142. Prabhu Sumanth D. & Frangogiannis Nikolaos G. The Biological Basis for Cardiac Repair After Myocardial Infarction. *Circ. Res.* **119,** 91–112 (2016).

143. Dai, W., Wold, L. E., Dow, J. S. & Kloner, R. A. Thickening of the Infarcted Wall by Collagen Injection Improves Left Ventricular Function in RatsA Novel Approach to Preserve Cardiac Function After Myocardial Infarction. *J. Am. Coll. Cardiol.* **46,** 714–719 (2005).

144. Landa, N., Miller, L., Feinberg, M. S., Holbova, R., Shachar, M., Freeman, I., Cohen, S. & Leor, J. Effect of Injectable Alginate Implant on Cardiac Remodeling and Function After Recent and Old Infarcts in Rat. *Circulation* **117,** 1388–1396 (2008).

145. Annabi, N., Zhang, Y.-N., Assmann, A., Sani, E. S., Cheng, G., Lassaletta, A. D., Vegh, A., Dehghani, B., Ruiz-Esparza, G. U., Wang, X., Gangadharan, S., Weiss, A. S. & Khademhosseini, A. Engineering a highly elastic human protein–based sealant for surgical applications. *Sci. Transl. Med.* **9,** eaai7466 (2017).

146. Annabi, N., Yue, K., Tamayol, A. & Khademhosseini, A. Elastic sealants for surgical applications. *Eur. J. Pharm. Biopharm.* **95,** 27–39 (2015).

147. Korde, J. M. & Kandasubramanian, B. Biocompatible alkyl cyanoacrylates and their derivatives as bio-adhesives. *Biomater. Sci.* **6,** 1691–1711 (2018).

148. Rahimnejad, M. & Zhong, W. Mussel-inspired hydrogel tissue adhesives for wound closure. *RSC Adv.* **7,** 47380–47396 (2017).

149. Liu, Y., Cheong NG, S., Yu, J. & Tsai, W.-B. Modification and crosslinking of gelatin-based biomaterials as tissue adhesives. *Colloids Surf. B Biointerfaces* **174,** 316–323 (2019).

150. Lu, M., Liu, Y., Huang, Y.-C., Huang, C.-J. & Tsai, W.-B. Fabrication of photo-crosslinkable glycol chitosan hydrogel as a tissue adhesive. *Carbohydr. Polym.* **181,** 668–674 (2018).

151. Matsumoto, M., Udomsinprasert, W., Laengee, P., Honsawek, S., Patarakul, K. & Chirachanchai, S. A Water-Based Chitosan–Maleimide Precursor for Bioconjugation: An Example of a Rapid Pathway for an In Situ Injectable Adhesive Gel. *Macromol. Rapid Commun.* **37,** 1618–1622 (2016).

152. Chen, T., Chen, Y., Rehman, H. U., Chen, Z., Yang, Z., Wang, M., Li, H. & Liu, H. Ultratough, Self-Healing, and Tissue-Adhesive Hydrogel for Wound Dressing. *ACS Appl. Mater. Interfaces* **10,** 33523–33531 (2018).

153. Bai, Z., Dan, W., Yu, G., Wang, Y., Chen, Y., Huang, Y., Yang, C. & Dan, N. Tough and tissue-adhesive polyacrylamide/collagen hydrogel with dopamine-grafted oxidized sodium alginate as crosslinker for cutaneous wound healing. *RSC Adv.* **8,** 42123–42132 (2018).

154. Fan, C., Fu, J., Zhu, W. & Wang, D.-A. A mussel-inspired double-crosslinked tissue adhesive intended for internal medical use. *Acta Biomater.* **33,** 51–63 (2016).

155. Pinnaratip, R., Bhuiyan, M. S. A., Meyers, K., Rajachar, R. M. & Lee, B. P. Multifunctional Biomedical Adhesives. *Adv. Healthc. Mater.* **8,** 1801568 (2019).

156. Ahadian, S., Sadeghian, R. B., Salehi, S., Ostrovidov, S., Bae, H., Ramalingam, M. & Khademhosseini, A. Bioconjugated Hydrogels for Tissue Engineering and Regenerative Medicine. *Bioconjug. Chem.* **26,** 1984–2001 (2015).

157. Baino, F., Perero, S., Ferraris, S., Miola, M., Balagna, C., Verné, E., Vitale-Brovarone, C., Coggiola, A., Dolcino, D. & Ferraris, M. Biomaterials for orbital implants and ocular prostheses: Overview and future prospects. *Acta Biomater.* **10,** 1064–1087 (2014).

158. Pashuck, E. T. & Stevens, M. M. Designing Regenerative Biomaterial Therapies for the Clinic. *Sci. Transl. Med.* **4,** 160sr4 (2012).

159. Sculean, A., Nikolidakis, D., Nikou, G., Ivanovic, A., Chapple, I. L. C. & Stavropoulos, A. Biomaterials for promoting periodontal regeneration in human intrabony defects: a systematic review. *Periodontol. 2000* **68,** 182–216 (2015).

160. Hocwald, E., Sichel, J.-Y., Dano, I., Meir, K. & Eliashar, R. Adverse reaction to surgical sutures in thyroid surgery. *Head Neck* **25,** 77–81 (2003).

161. Kumar, M. S., Natta, S., Shankar, G., Reddy, S. H. K., Visalakshi, D. & Seshiah, G. V. Comparison between Silk Sutures and Cyanoacrylate Adhesive in Human Mucosa- A Clinical and Histological Study. *J. Int. Oral Health JIOH* **5,** 95–100 (2013).

162. Mackenzie, D. The History of Sutures. *Med. Hist.* **17,** 158–168 (1973).

163. Niessen, F., Spauwen, P. & Kon, M. The Role of Suture Material in Hypertrophic Scar Formation: Monocryl vs. Vicryl-rapide. *Ann. Plast. Surg.* **39,** 254–260 (1997).

164. Lauto, A., Mawad, D. & Foster, L. J. R. Adhesive biomaterials for tissue reconstruction. *J. Chem. Technol. Biotechnol.* **83,** 464–472 (2008).

165. Forsch, R. T. Essentials of Skin Laceration Repair. *Am. Fam. Physician* **78,** 945–951 (2008).

166. Ricci, N. A. & Rizzolo, D. Laceration repair: Avoid infection, optimize healing, minimize scarring. *J. Am. Acad. PAs* **24,** 28–33 (2011).

167. Kamegaya, Y., Farinelli, W. A., Vila Echague, A. V., Akita, H., Gallagher, J., Flotte, T. J., Anderson, R. R., Redmond, R. W. & Kochevar, I. E. Evaluation of photochemical tissue bonding for closure of skin incisions and excisions. *Lasers Surg. Med.* **37,** 264–270 (2005).

168. Tsao, S., Yao, M., Tsao, H., Henry, F. P., Zhao, Y., Kochevar, J. J., Redmond, R. W. & Kochevar, I. E. Light-activated tissue bonding for excisional wound closure: a split-lesion clinical trial. *Br. J. Dermatol.* **166,** 555–563 (2012).

169. Cherfan, D., Verter, E. E., Melki, S., Gisel, T. E., Doyle, F. J., Scarcelli, G., Yun, S. H., Redmond, R. W. & Kochevar, I. E. Collagen Cross-Linking Using Rose Bengal and Green Light to Increase Corneal Stiffness. *Invest. Ophthalmol. Vis. Sci.* **54,** 3426–3433 (2013).

170. Xu, N., Yao, M., Farinelli, W., Hajjarian, Z., Wang, Y., Redmond, R. W. & Kochevar, I. E. Light-activated sealing of skin wounds. *Lasers Surg. Med.* **47,** 17–29 (2015).

171. Alarcón, E., Edwards, A. M., Aspée, A., Borsarelli, C. D. & Lissi, E. A. Photophysics and photochemistry of rose bengal bound to human serum albumin. *Photochem. Photobiol. Sci.* **8,** 933–943 (2009).

172. Simpson, M. J., Poblete, H., Griffith, M., Alarcon, E. I. & Scaiano, J. C. Impact of Dye-Protein Interaction and Silver Nanoparticles on Rose Bengal Photophysical Behavior and Protein Photocrosslinking. *Photochem. Photobiol.* **89,** 1433–1441 (2013).

173. Hu, J., Wang, J., Nguyen, T. H. & Zheng, N. The chemistry of amine radical cations produced by visible light photoredox catalysis. *Beilstein J. Org. Chem.* **9,** 1977–2001 (2013).

174. Binazadeh, M., Faghihnejad, A., Unsworth, L. D. & Zeng, H. Understanding the Effect of Secondary Structure on Molecular Interactions of Poly-l-lysine with Different Substrates by SFA. *Biomacromolecules* **14,** 3498–3508 (2013).

175. Koh, L. B., Islam, M. M., Mitra, D., Noel, C. W., Merrett, K., Odorcic, S., Fagerholm, P., Jackson, W. B., Liedberg, B., Phopase, J. & Griffith, M. Epoxy Cross-Linked Collagen and Collagen-Laminin Peptide Hydrogels as Corneal Substitutes. *J. Funct. Biomater.* **4,** 162–177 (2013).

176. Liu, Y., Gan, L., Carlsson, D. J., Fagerholm, P., Lagali, N., Watsky, M. A., Munger, R., Hodge, W. G., Priest, D. & Griffith, M. A Simple, Cross-linked Collagen Tissue Substitute for Corneal Implantation. *Invest. Ophthalmol. Vis. Sci.* **47,** 1869–1875 (2006).

177. Alarcon, E., Noel, C., Udekwu, K., Gagnon, L. B.-P., Taylor, P., Vulesevic, B., Simpson, M. J., Gkotzis, S., Islam, M., Lee, C.-J., Richter-Dahlfors, A., Mah, T.-F., Suuronen, E., Scaiano, T. & Griffith, M. Safety and Efficacy of Composite Collagen-Silver Nanoparticle Hydrogels as Tissue Engineering Scaffolds. *Nanoscale* **7,** 18789–18798 (2015).

178. Tan, H. & Marra, K. G. Injectable, Biodegradable Hydrogels for Tissue Engineering Applications. *Materials* **3,** 1746–1767 (2010).

179. Hilborn, J. In vivo injectable gels for tissue repair. *Wiley Interdiscip. Rev. Nanomed. Nanobiotechnol.* **3,** 589–606 (2011).

180. Guvendiren, M., Lu, H. D. & Burdick, J. A. Shear-thinning hydrogels for biomedical applications. *Soft Matter* **8,** 260–272 (2011).

181. Nguyen, Q. V., Huynh, D. P., Park, J. H. & Lee, D. S. Injectable polymeric hydrogels for the delivery of therapeutic agents: A review. *Eur. Polym. J.* **72,** 602–619 (2015).

182. Reis, L. A., Chiu, L. L. Y., Feric, N., Fu, L. & Radisic, M. Biomaterials in myocardial tissue engineering. *J. Tissue Eng. Regen. Med.* **10,** 11–28 (2016).

183. Bergman, K., Engstrand, T., Hilborn, J., Ossipov, D., Piskounova, S. & Bowden, T. Injectable cell-free template for bone-tissue formation. *J. Biomed. Mater. Res. A* **91A,** 1111–1118 (2009).

184. Docherty-Skogh, A.-C., Bergman, K., Waern, M. J., Ekman, S., Hultenby, K., Ossipov, D., Hilborn, J., Bowden, T. & Engstrand, T. Bone Morphogenetic Protein-2 Delivered by Hyaluronan-Based Hydrogel Induces Massive Bone Formation and Healing of Cranial Defects in Minipigs. *Plast. Reconstr. Surg.* **125,** 1383–1392 (2010).

185. Martínez-Sanz, E., Ossipov, D. A., Hilborn, J., Larsson, S., Jonsson, K. B. & Varghese, O. P. Bone reservoir: Injectable hyaluronic acid hydrogel for minimal invasive bone augmentation. *J. Controlled Release* **152,** 232–240 (2011).

186. Oommen, O. P., Wang, S., Kisiel, M., Sloff, M., Hilborn, J. & Varghese, O. P. Smart Design of Stable Extracellular Matrix Mimetic Hydrogel: Synthesis, Characterization, and In Vitro and In Vivo Evaluation for Tissue Engineering. *Adv. Funct. Mater.* **23,** 1273–1280 (2013).

187. Piskounova, S., Rojas, R., Bergman, K. & Hilborn, J. The Effect of Mixing on the Mechanical Properties of Hyaluronan-Based Injectable Hydrogels. *Macromol. Mater. Eng.* **296,** 944–951 (2011).

188. Shi, L., Wang, F., Zhu, W., Xu, Z., Fuchs, S., Hilborn, J., Zhu, L., Ma, Q., Wang, Y., Weng, X. & Ossipov, D. A. Self-Healing Silk Fibroin-Based Hydrogel for Bone Regeneration: Dynamic Metal-Ligand Self-Assembly Approach. *Adv. Funct. Mater.* **27,** 1700591 (2017).

189. Shi, L., Carstensen, H., Hölzl, K., Lunzer, M., Li, H., Hilborn, J., Ovsianikov, A. & Ossipov, D. A. Dynamic Coordination Chemistry Enables Free Directional Printing of Biopolymer Hydrogel. *Chem. Mater.* **29,** 5816–5823 (2017).

190. Loebel, C., Rodell, C. B., Chen, M. H. & Burdick, J. A. Shear-thinning and self-healing hydrogels as injectable therapeutics and for 3D-printing. *Nat. Protoc.* **12,** 1521–1541 (2017).

191. Rodell, C. B., Kaminski, A. L. & Burdick, J. A. Rational Design of Network Properties in Guest–Host Assembled and Shear-Thinning Hyaluronic Acid Hydrogels. *Biomacromolecules* **14,** 4125–4134 (2013).

192. Highley, C. B., Rodell, C. B. & Burdick, J. A. Direct 3D Printing of Shear-Thinning Hydrogels into Self-Healing Hydrogels. *Adv. Mater.* **27,** 5075–5079 (2015).

193. Neovius, E., Lemberger, M., Docherty Skogh, AC., Hilborn, J. & Engstrand, T. Alveolar bone healing accompanied by severe swelling in cleft children treated with bone morphogenetic protein-2 delivered by hydrogel. *J. Plast. Reconstr. Aesthet. Surg.* **66,** 37–42 (2013).

194. Tu, Y., Mithieux, S. M., Annabi, N., Boughton, E. A. & Weiss, A. S. Synthetic elastin hydrogels that are coblended with heparin display substantial swelling, increased porosity, and improved cell penetration. *J. Biomed. Mater. Res. A* **95A,** 1215–1222 (2010).

195. Führmann, T., Obermeyer, J., Tator, C. H. & Shoichet, M. S. Click-crosslinked injectable hyaluronic acid hydrogel is safe and biocompatible in the intrathecal space for ultimate use in regenerative strategies of the injured spinal cord. *Methods* **84,** 60–69 (2015).

196. Shu, X. Z., Ghosh, K., Liu, Y., Palumbo, F. S., Luo, Y., Clark, R. A. & Prestwich, G. D. Attachment and spreading of fibroblasts on an RGD peptide–modified injectable hyaluronan hydrogel. *J. Biomed. Mater. Res. A* **68A,** 365–375 (2004).

197. Khetan, S. & Burdick, J. A. Patterning network structure to spatially control cellular remodeling and stem cell fate within 3-dimensional hydrogels. *Biomaterials* **31,** 8228–8234 (2010).

198. Khetan, S., Katz, J. S. & Burdick, J. A. Sequential crosslinking to control cellular spreading in 3-dimensional hydrogels. *Soft Matter* **5,** 1601–1606 (2009).

199. Ranga, A., Lutolf, M. P., Hilborn, J. & Ossipov, D. A. Hyaluronic Acid Hydrogels Formed in Situ by Transglutaminase-Catalyzed Reaction. *Biomacromolecules* **17,** 1553–1560 (2016).

200. Samarawickrama, C., Samanta, A., Liszka, A., Fagerholm, P., Buznyk, O., Griffith, M. & Allan, B. Collagen-Based Fillers as Alternatives to Cyanoacrylate Glue for the Sealing of Large Corneal Perforations. *Cornea* **37,** 609–616 (2018).

201. Jangamreddy, J. R., Haagdorens, M. K. C., Mirazul Islam, M., Lewis, P., Samanta, A., Fagerholm, P., Liszka, A., Ljunggren, M. K., Buznyk, O., Alarcon, E. I., Zakaria, N., Meek, K. M. & Griffith, M. Short Peptide Analogs as Alternatives to Collagen in Pro-Regenerative Corneal Implants. *Acta Biomater.* **69,** 120–130 (2018).

202. Nazir, R., Bruyneel, A., Carr, C. & Czernuszka, J. Collagen type I and hyaluronic acid based hybrid scaffolds for heart valve tissue engineering. *Biopolymers* **110,** e23278 (2019).

203. Li, X., Xue, W., Zhu, C., Fan, D., Liu, Y. & XiaoxuanMa. Novel hydrogels based on carboxyl pullulan and collagen crosslinking with 1, 4-butanediol diglycidylether for use as a dermal filler: initial in vitro and in vivo investigations. *Mater. Sci. Eng. C* **57,** 189–196 (2015).

204. Olde Damink, L. H. H., Dijkstra, P. J., Van Luyn, M. J. A., Van Wachem, P. B., Nieuwenhuis, P. & Feijen, J. Glutaraldehyde as a crosslinking agent for collagen-based biomaterials. *J. Mater. Sci. Mater. Med.* **6,** 460–472 (1995).

205. Zhao, L., Li, X., Zhao, J., Ma, S., Ma, X., Fan, D., Zhu, C. & Liu, Y. A novel smart injectable hydrogel prepared by microbial transglutaminase and human-like collagen: Its characterization and biocompatibility. *Mater. Sci. Eng. C* **68,** 317–326 (2016).

206. Khanmohammadi, M., Dastjerdi, M. B., Ai, A., Ahmadi, A., Godarzi, A., Rahimi, A. & Ai, J. Horseradish peroxidase-catalyzed hydrogelation for biomedical applications. *Biomater. Sci.* **6,** 1286–1298 (2018).

207. Nguyen, T.-U., Watkins, K. E. & Kishore, V. Photochemically crosslinked cell-laden methacrylated collagen hydrogels with high cell viability and functionality. *J. Biomed. Mater. Res. A* **107,** 1541–1550 (2019).

208. Gaudet, I. D. & Shreiber, D. I. Characterization of Methacrylated Type-I Collagen as a Dynamic, Photoactive Hydrogel. *Biointerphases* **7,** 25 (2012).

209. Elia, R., Fuegy, P. W., VanDelden, A., Firpo, M. A., Prestwich, G. D. & Peattie, R. A. Stimulation of in vivo angiogenesis by in situ crosslinked, dual growth factor-loaded, glycosaminoglycan hydrogels. *Biomaterials* **31,** 4630–4638 (2010).

210. Xu, G., Wang, X., Deng, C., Teng, X., Suuronen, E. J., Shen, Z. & Zhong, Z. Injectable biodegradable hybrid hydrogels based on thiolated collagen and oligo(acryloyl carbonate)–poly(ethylene glycol)–oligo(acryloyl carbonate) copolymer for functional cardiac regeneration. *Acta Biomater.* **15,** 55–64 (2015).

211. Tran, A. P., Warren, P. M. & Silver, J. The Biology of Regeneration Failure and Success After Spinal Cord Injury. *Physiol. Rev.* **98,** 881–917 (2018).

212. Holmes, R., Yang, X.-B., Dunne, A., Florea, L., Wood, D. & Tronci, G. Thiol-Ene Photo-Click Collagen-PEG Hydrogels: Impact of Water-Soluble Photoinitiators on Cell Viability, Gelation Kinetics and Rheological Properties. *Polymers* **9,** 226 (2017).

213. Kommareddy, S. & Amiji, M. Preparation and Evaluation of Thiol-Modified Gelatin Nanoparticles for Intracellular DNA Delivery in Response to Glutathione. *Bioconjug. Chem.* **16,** 1423–1432 (2005).

214. Zhang, Z. K., Li, G. Y. & Shi, B. Physicochemical properties of collagen, gelatin and collagen hydrolysate derived from bovine limed split wastes. *J. Soc. Leather Technol. Chem.* **90,** 23–28 (2006).

215. Engler, A. J., Griffin, M. A., Sen, S., Bönnemann, C. G., Sweeney, H. L. & Discher, D. E. Myotubes differentiate optimally on substrates with tissue-like stiffness: pathological implications for soft or stiff microenvironments. *J. Cell Biol.* **166,** 877–887 (2004).

216. Flanagan, L., Ju, Y.-E., Marg, B., Osterfield, M. & Janmey, P. Neurite branching on deformable substrates. *Neuroreport* **13,** 2411–2415 (2002).

217. Moeendarbary, E., Weber, I. P., Sheridan, G. K., Koser, D. E., Soleman, S., Haenzi, B., Bradbury, E. J., Fawcett, J. & Franze, K. The soft mechanical signature of glial scars in the central nervous system. *Nat. Commun.* **8,** 14787 (2017).

218. Rodriguez, M. L., Beussman, K. M., Chun, K. S., Walzer, M. S., Yang, X., Murry, C. E. & Sniadecki, N. J. Substrate Stiffness, Cell Anisotropy, and Cell–Cell Contact Contribute to Enhanced Structural and Calcium Handling Properties of Human Embryonic Stem Cell-Derived Cardiomyocytes. *ACS Biomater. Sci. Eng.* **5,** 3876–3888 (2019).

219. Leiva, O., Leon, C., Ng, S. K., Mangin, P., Gachet, C. & Ravid, K. The role of extracellular matrix stiffness in megakaryocyte and platelet development and function. *Am. J. Hematol.* **93,** 430–441 (2018).

220. Pedrizzetti, G., Mangual, J. & Tonti, G. On the geometrical relationship between global longitudinal strain and ejection fraction in the evaluation of cardiac contraction. *J. Biomech.* **47,** 746–749 (2014).

221. Tee, M., Noble, J. A. & Bluemke, D. A. Imaging techniques for cardiac strain and deformation: comparison of echocardiography, cardiac magnetic resonance and cardiac computed tomography. *Expert Rev. Cardiovasc. Ther.* **11,** 221–231 (2013).

222. Berry, M. F., Engler, A. J., Woo, Y. J., Pirolli, T. J., Bish, L. T., Jayasankar, V., Morine, K. J., Gardner, T. J., Discher, D. E. & Sweeney, H. L. Mesenchymal stem cell injection after myocardial infarction improves myocardial compliance. *Am. J. Physiol. - Heart Circ. Physiol.* **290,** H2196–H2203 (2006).

223. Fontaine, S. D., Reid, R., Robinson, L., Ashley, G. W. & Santi, D. V. Long-term stabilization of maleimide-thiol conjugates. *Bioconjug. Chem.* **26,** 145–152 (2015).

224. Lyon, R. P., Setter, J. R., Bovee, T. D., Doronina, S. O., Hunter, J. H., Anderson, M. E., Balasubramanian, C. L., Duniho, S. M., Leiske, C. I., Li, F. & Senter, P. D. Self-hydrolyzing maleimides improve the stability and pharmacological properties of antibody-drug conjugates. *Nat. Biotechnol.* **32,** 1059–1062 (2014).

225. Suarez, S. L., Rane, A. A., Muñoz, A., Wright, A. T., Zhang, S. X., Braden, R. L., Almutairi, A., McCulloch, A. D. & Christman, K. L. Intramyocardial injection of hydrogel with high interstitial spread does not impact action potential propagation. *Acta Biomater.* **26,** 13–22 (2015).

226. Tadeo, X., López-Méndez, B., Castaño, D., Trigueros, T. & Millet, O. Protein Stabilization and the Hofmeister Effect: The Role of Hydrophobic Solvation. *Biophys. J.* **97,** 2595–2603 (2009).

227. Mak, W. C., Magne, B., Cheung, K. Y., Atanasova, D. & Griffith, M. Thermo-rheological responsive microcapsules for time-dependent controlled release of human mesenchymal stromal cells. *Biomater. Sci.* **5,** 2241–2250 (2017).

228. Nicodemus, G. D. & Bryant, S. J. Cell Encapsulation in Biodegradable Hydrogels for Tissue Engineering Applications. *Tissue Eng. Part B Rev.* **14,** 149–165 (2008).

229. Saito, G., Swanson, J. A. & Lee, K.-D. Drug delivery strategy utilizing conjugation via reversible disulfide linkages: role and site of cellular reducing activities. *Adv. Drug Deliv. Rev.* **55,** 199–215 (2003).

230. Wu, G., Fang, Y.-Z., Yang, S., Lupton, J. R. & Turner, N. D. Glutathione Metabolism and Its Implications for Health. *J. Nutr.* **134,** 489–492 (2004).

231. Jones, D. P., Carlson, J. L., Samiec, P. S., Sternberg, P., Mody, V. C., Reed, R. L. & Brown, L. A. S. Glutathione measurement in human plasma: Evaluation of sample collection, storage and derivatization conditions for analysis of dansyl derivatives by HPLC. *Clin. Chim. Acta* **275,** 175–184 (1998).

232. Hou, L., Kim, J. J., Woo, Y. J. & Huang, N. F. Stem cell-based therapies to promote angiogenesis in ischemic cardiovascular disease. *Am. J. Physiol.-Heart Circ. Physiol.* **310,** H455–H465 (2016).

233. Gao, W., Li, T., Wang, J., Zhao, Y. & Wu, C. Thioether-Bonded Fluorescent Probes for Deciphering Thiol-Mediated Exchange Reactions on the Cell Surface. *Anal. Chem.* **89,** 937–944 (2017).

234. Lindsey, M. L., Iyer, R. P., Jung, M., DeLeon-Pennell, K. Y. & Ma, Y. Matrix metalloproteinases as input and output signals for post-myocardial infarction remodeling. *J. Mol. Cell. Cardiol.* **91,** 134–140 (2016).

235. Steenbergen, C. & Frangogiannis, N. G. Ischemic heart disease. In: *Muscle* (eds. Hill, J. A. & Olson, E. N.) 495–521 (Academic Press, 2012).

236. Dobaczewski, M., Gonzalez-Quesada, C. & Frangogiannis, N. G. The extracellular matrix as a modulator of the inflammatory and reparative response following myocardial infarction. *J. Mol. Cell. Cardiol.* **48,** 504–511 (2010).

237. Horn, M. A. & Trafford, A. W. Aging and the cardiac collagen matrix: Novel mediators of fibrotic remodelling. *J. Mol. Cell. Cardiol.* **93,** 175–185 (2016).

238. Giordano, C., Thorn, S. L., Renaud, J. M., Al-Atassi, T., Boodhwani, M., Klein, R., Kuraitis, D., Dwivedi, G., Zhang, P., DaSilva, J. N., Ascah, K. J., deKemp, R. A., Suuronen, E. J., Beanlands, R. S. B. & Ruel, M. Preclinical Evaluation of Biopolymer-

Delivered Circulating Angiogenic Cells in a Swine Model of Hibernating Myocardium. *Circ. Cardiovasc. Imaging* **6,** 982–991 (2013).

239. Shamhart, P. E. & Meszaros, J. G. Non-fibrillar collagens: Key mediators of post-infarction cardiac remodeling? *J. Mol. Cell. Cardiol.* **48,** 530–537 (2010).

240. LeGrice, I., Pope, A. & Smaill, B. The Architecture of the Heart: Myocyte Organization and the Cardiac Extracellular Matrix. In: *Interstitial Fibrosis in Heart Failure* (ed. Villarreal, F. J.) 3–21 (Springer New York, 2005).

241. McLaughlin, S., McNeill, B., Podrebarac, J., Hosoyama, K., Sedlakova, V., Cron, G., Smith, D., Seymour, R., Goel, K., Liang, L., Rayner, K. J., Ruel, M., Suuronen, E. J. & Alarcon, E. I. Injectable human recombinant collagen matrices limit adverse remodeling and improve cardiac function after myocardial infarction. *Nat. Commun.* accepted (2019).

242. Uchinaka, A., Yoshida, M., Tanaka, K., Hamada, Y., Mori, S., Maeno, Y., Miyagawa, S., Sawa, Y., Nagata, K., Yamamoto, H. & Kawaguchi, N. Overexpression of collagen type III in injured myocardium prevents cardiac systolic dysfunction by changing the balance of collagen distribution. *J. Thorac. Cardiovasc. Surg.* **156,** 217-226.e3 (2018).

243. Takagawa, J., Zhang, Y., Wong, M. L., Sievers, R. E., Kapasi, N. K., Wang, Y., Yeghiazarians, Y., Lee, R. J., Grossman, W. & Springer, M. L. Myocardial infarct size measurement in the mouse chronic infarction model: comparison of area- and length-based approaches. *J. Appl. Physiol.* **102,** 2104–2111 (2007).

244. Civitarese, R. A., Kapus, A., McCulloch, C. A. & Connelly, K. A. Role of integrins in mediating cardiac fibroblast–cardiomyocyte cross talk: a dynamic relationship in cardiac biology and pathophysiology. *Basic Res. Cardiol.* **112,** 6 (2016).

245. Davis, G. E., Bayless, K. J., Davis, M. J. & Meininger, G. A. Regulation of Tissue Injury Responses by the Exposure of Matricryptic Sites within Extracellular Matrix Molecules. *Am. J. Pathol.* **156,** 1489–1498 (2000).

246. Postlethwaite, A. E., Seyer, J. M. & Kang, A. H. Chemotactic attraction of human fibroblasts to type I, II, and III collagens and collagen-derived peptides. *Proc. Natl. Acad. Sci.* **75,** 871–875 (1978).

247. Postlethwaite, A. E. & Kang, A. H. Collagen-and collagen peptide-induced chemotaxis of human blood monocytes. *J. Exp. Med.* **143,** 1299–1307 (1976).

248. Carragher, N. O., Levkau, B., Ross, R. & Raines, E. W. Degraded Collagen Fragments Promote Rapid Disassembly of Smooth Muscle Focal Adhesions That Correlates with Cleavage of Pp125FAK, Paxillin, and Talin. *J. Cell Biol.* **147,** 619–630 (1999).

249. Lindsey, M. L., Iyer, R. P., Zamilpa, R., Yabluchanskiy, A., DeLeon-Pennell, K. Y., Hall, M. E., Kaplan, A., Zouein, F. A., Bratton, D., Flynn, E. R., Cannon, P. L., Tian, Y., Jin, Y.-F., Lange, R. A., Tokmina-Roszyk, D., Fields, G. B. & de Castro Brás, L. E. A Novel Collagen Matricryptin Reduces Left Ventricular Dilation Post-Myocardial Infarction by Promoting Scar Formation and Angiogenesis. *J. Am. Coll. Cardiol.* **66,** 1364–1374 (2015).

250. Shintani, Y., Fukushima, S., Varela-Carver, A., Lee, J., Coppen, S. R., Takahashi, K., Brouilette, S. W., Yashiro, K., Terracciano, C. M. N., Yacoub, M. H. & Suzuki, K. Donor

cell-type specific paracrine effects of cell transplantation for post-infarction heart failure. *J. Mol. Cell. Cardiol.* **47,** 288–295 (2009).

251. Hashoul, J., Saliba, W., Bloch, I. & Jabaly-Habib, H. Heidenhain variant of Creutzfeldt–Jakob disease in a patient who had bovine bioprosthetic valve implantation. *Indian J. Ophthalmol.* **64,** 767–769 (2016).

252. Antoine, E. E., Vlachos, P. P. & Rylander, M. N. Review of Collagen I Hydrogels for Bioengineered Tissue Microenvironments: Characterization of Mechanics, Structure, and Transport. *Tissue Eng. Part B Rev.* **20,** 683–696 (2014).

253. Graham, H. K., Horn, M. & Trafford, A. W. Extracellular matrix profiles in the progression to heart failure. *Acta Physiol.* **194,** 3–21 (2008).

254. Ye, B., Meng, L., Li, Z., Li, R., Li, L., Lu, L., Ding, S., Tian, J. & Zhou, C. A facile method to prepare polysaccharide-based in-situ formable hydrogels with antibacterial ability. *Mater. Lett.* **183,** 81–84 (2016).

255. Shendi, D., Dede, A., Yin, Y., Wang, C., Valmikinathan, C. & Jain, A. Tunable, bioactive protein conjugated hyaluronic acid hydrogel for neural engineering applications. *J. Mater. Chem. B* **4,** 2803–2818 (2016).

256. McCune, C., McKavanagh, P. & Menown, I. B. A. A Review of the Key Clinical Trials of 2015: Results and Implications. *Cardiol. Ther.* **5,** 109–132 (2016).

257. Mann, D. L., Lee, R. J., Coats, A. J. S., Neagoe, G., Dragomir, D., Pusineri, E., Piredda, M., Bettari, L., Kirwan, B.-A., Dowling, R., Volterrani, M., Solomon, S. D., Sabbah, H. N., Hinson, A. & Anker, S. D. One-year follow-up results from AUGMENT-HF: a multicentre randomized controlled clinical trial of the efficacy of left ventricular augmentation with Algisyl in the treatment of heart failure. *Eur. J. Heart Fail.* **18,** 314–325 (2016).

258. Chachques, J. C., Trainini, J. C., Lago, N., Masoli, O. H., Barisani, J. L., Cortes-Morichetti, M., Schussler, O. & Carpentier, A. Myocardial Assistance by Grafting a New Bioartificial Upgraded Myocardium (MAGNUM Clinical Trial): One Year Follow-Up. *Cell Transplant.* **16,** 927–934 (2007).

259. Menasché, P., Vanneaux, V., Hagège, A., Bel, A., Cholley, B., Parouchev, A., Cacciapuoti, I., Al-Daccak, R., Benhamouda, N., Blons, H., Agbulut, O., Tosca, L., Trouvin, J.-H., Fabreguettes, J.-R., Bellamy, V., Charron, D., Tartour, E., Tachdjian, G., Desnos, M. & Larghero, J. Transplantation of Human Embryonic Stem Cell–Derived Cardiovascular Progenitors for Severe Ischemic Left Ventricular Dysfunction. *J. Am. Coll. Cardiol.* **71,** 429–438 (2018).

260. Prime, K. L. & Whitesides, G. M. Self-assembled organic monolayers: model systems for studying adsorption of proteins at surfaces. *Science* **252,** 1164–1167 (1991).

261. Seaton, M., Hocking, A. & Gibran, N. S. Porcine Models of Cutaneous Wound Healing. *ILAR J.* **56,** 127–138 (2015).

262. Davidson, J. M., Yu, F. & Opalenik, S. R. Splinting Strategies to Overcome Confounding Wound Contraction in Experimental Animal Models. *Adv. Wound Care* **2,** 142–148 (2013).

263. Potz, B. A., Scrimgeour, L. A., Pavlov, V. I., Sodha, N. R., Abid, M. R. & Sellke, F. W. Extracellular Vesicle Injection Improves Myocardial Function and Increases Angiogenesis in a Swine Model of Chronic Ischemia. *J. Am. Heart Assoc.* **7,** e008344 (2018).

264. Zhang, K., Zhao, X., Chen, X., Wei, Y., Du, W., Wang, Y., Liu, L., Zhao, W., Han, Z., Kong, D., Zhao, Q., Guo, Z., Han, Z., Liu, N., Ma, F. & Li, Z. Enhanced Therapeutic Effects of Mesenchymal Stem Cell-Derived Exosomes with an Injectable Hydrogel for Hindlimb Ischemia Treatment. *ACS Appl. Mater. Interfaces* **10,** 30081–30091 (2018).

265. Caliceti, P. & Veronese, F. M. Pharmacokinetic and biodistribution properties of poly(ethylene glycol)–protein conjugates. *Adv. Drug Deliv. Rev.* **55,** 1261–1277 (2003).

266. Deshmukh, M., Kutscher, H. L., Gao, D., Sunil, V. R., Malaviya, R., Vayas, K., Stein, S., Laskin, J. D., Laskin, D. L. & Sinko, P. J. Biodistribution and renal clearance of biocompatible lung targeted poly(ethylene glycol) (PEG) nanogel aggregates. *J. Controlled Release* **164,** 65–73 (2012).